IANCAS Bulletin

Ion Beam Analysis for Materials Characterization

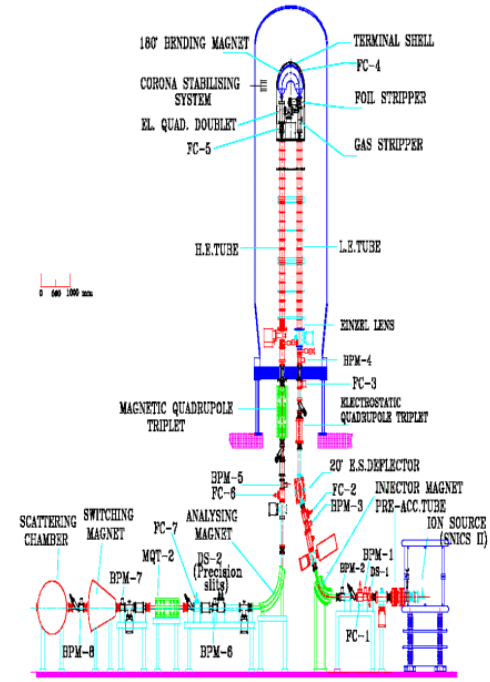

Editor : Y. K. Bhardwaj

Guest Editors : R. Acharya and Sanjiv Kumar

Volume : XVI, No.1 March 2021

Editor : Y. K. Bhardwaj
Editorial

Energetic ion beams are employed for synthesis, modification, and analysis of materials. Interaction of ion beams with material is accompanied by complex specific effects owing to several channels of interactions. These channels can be used for the nondestructive quantitative analysis of studied target element composition and some features of its structure. Ion beam analysis (IBA) covers a broad field of characterization techniques applicable to wide spectrum of materials where the interest is in thesurface or near-surface region up to a fraction of few mm thickness. Thin film elemental depth profiling being very-sensitive, absolute and non-destructive is of critical importance to a wide range of modern science and technologies which includes coatings, sensors, forensics, heritage, semi-conductors, magnetics, environmental monitoring, biological & medical field and cultural heritage. Use of various established IBA based techniques have provided key insights into many material systems and it is expected that this ever evolving analysis technique in hyphenation with others like focused ion beam (FIB) with scanning electron microscope (SEM) or ion beams focused to sub-micron sizes would be able to map and provide exact 3D images of the structural and elemental/molecular distributions of a target material and thus providing further insight into complex matrices to sub-atomic levels.

I am sure this bulletin, guest edited by Dr. R. Acharya and Dr. Sanjiv Kumar, both very accomplished names in their respective fields will cover various aspects of Ion Beam Analysis for Materials Characterization.

I sincerely thank Dr. R. Acharya and Dr. Sanjiv Kumar, for agreeing to be the guest editor of this bulletin. It is because of their efforts that this bulletin has been possible.

CONTENTS

About IANCAS

(Web: www.iancas.org.in)

The Indian Association of Nuclear Chemists and Allied Scientists (IANCAS) was founded in 1981 with an objective of popularizing nuclear sciences among the scientific community in the country. Under its mandate, IANCAS is continuously promoting the subject of nuclear and radiochemistry, and use of radioisotopes & radiation sources in education, research, agriculture, medicine and industry by organizing seminars, workshops and publishing periodical thematic bulletins. With its enthusiastic 1869 Life Members from all over the country and overseas (till March 2021) and 20 Corporate Members, IANCAS has become one of the popular platforms for popularizing the subject of nuclear and radiochemistry across the country.

IANCAS brings out quarterly thematic bulletins on the topic of relevance to the nuclear science and technology with the financial support from BRNS. So far it has published 65 such bulletins which are distributed free to all its members and are freely available for download. The Association's popular book on "*Fundamentals of Nuclear and Radiochemistry*" is widely sought amongst the academia, researchers and students of DAE, non-DAE units and Universities. These workshops play paramount role in motivating the young researchers and encourage them to accept the subject of radiochemistry and applications of radioisotopes. It is mater of proud and immense satisfaction to share that IANCAS has successfully conducted 100thNational Workshop on "*Radiochemistry and Applications of Radioisotopes*" at the Department of Chemistry, University of Kerala during December 9 – 14, 2019. With the support from BRNS,) a set of G.M. Counter and / or NaI(Tl) detector are donated to the host institute of each National Workshops for their academic use. Similarly, IANCAS is also conducting one-day school Workshops to encourage and popularize the nuclear and radiochemistry subject amongst the young students. These workshops are conducted by the IANCAS main body and its four regional chapters (Southern Regional Chapter at Kalpakkam, Tarapur Chapter, Northern Regional Chapter at Amritsar, and Eastern Regional Chapter Bhubaneswar) covering the entire nation. IANCAS has set up a module of lecture cum demonstration Programme for the school/college students.

Through its various outreach programs, IANCAS endeavors to motivate the researchers and scientists to achieve excellence in the field of nuclear and allied sciences. To encourage scientists / researchers actively pursuing activities in this discipline, IANCAS has instituted several awards. ***Dr. M.V. Ramaniah Memorial Award*** is conferred annually to an outstanding scientist for their significant contributions and lifetime achievements in the field of nuclear and radiochemistry. The award, introduced in 1999, carries a medal, citation and Rs.25,000/- in cash. **Dr. *Tarun Datta Memorial Award*** is given annually to a young scientist (below 45 years of age) with minimum 5 years of research experience in the field of nuclear and radiochemistry and applications of radioisotopes. This award was instituted in 1997 and carries a medal, citation and Rs.15,000/- cash. IANCAS also gives ***Prof. H.J. Arnikar Best Thesis Award*** annually for the Ph.D. research in the nuclear and radiochemistry area. This award carries a medal, citation and Rs.10,000/- in cash. Apart from this, IANCAS has instituted***Dr. K.S. Venkateswarlu Memorial Endowment Lecture*** which is biannually bestowed during NUCAR symposium to the scientists / academics in recognition of their contributions in the area of water chemistry & related field. In addition, IANCAS also gives cash awards and merit certificates to young researchers as Best Presentation Award for their work presented in biennial NUCAR symposium.

To achieve the excellent in its cause for popularizing the nuclear sciences through electronic media, IANCAS has its own website (www.iancas.org.in) which is updated from regularly. Information about the workshops, Awards and various activities of IANCAS are available on the website. All the publications of IANCAS including bulletins and books are available in free downloadable form.

Secretary, IANCAS

Executive Committee of IANCAS

Previous Executive Committee
(April 2018 – March 2021)

President
Dr. B.S. Tomar
Ex-Dir., RC&I Group, BARC, Mumbai

Vice-President (Head Quarter)
Dr. P.K. Pujari
Dir. RC & I Group, BARC, Mumbai

Vice-President (Out Side HQ)
Prof. Alok Srivastava
Punjab University, Chandigarh

General Secretary
Dr. R. Tripathi
RCD, BARC, Mumbai

Joint Secretary
Dr. S.A. Ansari
RCD, BARC, Mumbai

Treasurer
Dr. Ashok Kumar
FCD, BARC, Mumbai

Joint Treasurer
Dr. A.C. Deb
FCD, BARC, Mumbai

Editor
Dr. Y.K. Bhardwaj
RTDD, BARC, Mumbai

Members
Dr. A.V.R. Reddy *(Ex-President)*
Ex-Head, ACD, BARC, Mumbai

Dr. R. Acharya (Ex-Secretary)
RCD, BARC, Mumbai

Dr. P.C. Kalsi
RCD, BARC, Mumbai

Dr. N. L. Mishra
FCD, BARC, Mumbai

Dr. S. Kannan
Head, FCD, BARC, Mumbai

Dr. V. Venugopal
Ex-Director, RC&I Group, BARC

Dr. Vijayalaxmi Adya
RCD, BARC, Mumbai

Dr. Pradeep Kumar
IFFF, BARC, Mumbai

Dr. Arnab Sarkar
FCD, BARC, Mumbai

Prof. N. Laxman Das
GITAM University

New Executive Committee
(April 2021 – March 2024)

President
Dr. P.K. Pujari
Dir., RC&I Group, BARC, Mumbai

Vice-President (Head Quarter)
Dr. S. Kannan
Head, FCD, BARC, Mumbai

Vice-President (Out Side HQ)
Prof. G.A. Ramarao
GITAM University, Hyderabad

General Secretary
Dr. Seraj A. Ansari
RCD, BARC, Mumbai

Joint Secretary
Dr. Pranaw Kumar
FCD, BARC, Mumbai

Treasurer
Dr. M.B. Mallia
RPhD, BARC, Mumbai

Joint Treasurer
Dr. Arnab Sarkar
FCD, BARC, Mumbai

Editor
Dr. S.K. Gupta
RCD, BARC, Mumbai

Members
Dr. B.S. Tomar *(Ex-President)*
Ex-Dir., RC&I Group, BARC, Mumbai

Dr. Rahul Tripathi (Ex-Secretary)
RCD, BARC, Mumbai

Dr. A.V.R. Reddy
Ex-Head, ACD, BARC, Mumbai

Dr. P.C. Kalsi
Ex-RCD, BARC, Mumbai

Dr. P.K. Mohapatra
RCD, BARC, Mumbai

Dr. Rajesh V. Pai
FCD, BARC

Dr. A.C. Deb
FCD, BARC, Mumbai

Dr. Y.K. Bhardwaj
RTDD, BARC, Mumbai

Dr. Tapas Das
RPhD, BARC, Mumbai

Dr. (Mrs.) Aparna Banerjee
FCD, BARC

FOCUS

Dr. B.S. Tomar
President, IANCAS
Raja Ramana Fellow-DAE & Institute Chair Professor, HBNI

Ever since the pioneering experiment by A.L. Turkevich on analysis of composition of moon's surface by Rutherford Backscattering Spectrometry (RBS) in 1967 as a part of Surveyor V mission, Ion beam analysis (IBA) techniques have found numerous applications in solving important and difficult problems in high technology areas, not to mention about the routine application of techniques such as proton induced X-ray emission (PIXE) and Particle Induced Gamma-ray Emission (PIGE) in environmental, geological, glass and ceramics, chemical sciences etc. The underlying principles behind these are based on the fundamentals of nuclear reactions, including elastic scattering, involving low energy light charged particles. Thus, while RBS and elastic recoil detection analysis (ERDA) are based on the kinematic relations between the energy of the outgoing particle and the angle of scattering, nuclear reaction analysis (NRA) is based on the sharp resonances in excitation functions involving emission of high energy gamma rays, and which is unique in its ability to determine the depth profile of hydrogen an element not amenable to many spectroscopic and other analytical techniques. What is important that these techniques, not only provide concentrations, but also their depth profile, which provides valuable information about the processes occurring at interfaces or bulk, viz., diffusion. The classic example being determination of interdiffusion between Na^+ and H_3O^+ during the leaching of sodium from borosilicate glass matrix containing the vitrified high-level waste, and diffusion of hydrogen in Zr based alloys used as pressure tube materials in pressurized heavy water reactors.

In this context the present bulletin assumes great relevance when we look for solutions to the problems being faced by the technologists in high technology areas, such as nuclear space and microelectronics.Chapters 1 and 2 are devoted to PIXE and PIGE which are being routinely used compositional characterization of materials used in various fields. Chapters 3 and 4 deal with the two most important IBA techniques, namely RBS and NRA which find applications in solving important technological problems in high technology areas. Chapter 5 deals with another important IBA technique, namely channeling which is mused in studying the defects/imperfections in crystalline matrices used in high-end technology areas. The other two chapters cover the review of the literature on IBA and the facilities for such studies in India. I compliment the Editor, Guest Editors and Authors for bringing out this Bulletin on **"Ion Beam Analysis for Materials Characterization"** which will provide valuable inputs not only to those researchers who are staring their carrier in nuclear analytical techniques, but also to those scientists and engineers who might find this helpful in finding solutions to the problems being faced by them.

B. S. Tomar

From Secretary's Desk

Accelerator based analytical techniques (IBA) play a very important role in material characterization due to their advantages such as capability to analyze as received samples for wide range of elements with elemental and isotopic identification and possibility of depth profiling. IBA techniques for elemental information include particle induced X-ray emission (PIXE), particle induced gamma-ray emission (PIGE), Rutherford Backscattering spectrometry (RBS), Elastic Recoil detection Analysis (ERDA) and Nuclear Reaction Analysis (NRA). In addition, ion channeling technique can provide information about lattice atom displacements and presence on impurity atoms. Selection of a specific IBA technique depends on the type of application. These techniques find applications in a wide range of areas such as material science, chemical science, geology, forensic science, food and agriculture and many other areas.

The present bulletin includes articles on PIXE, PIGE, RBS, NRA and Ion Channeling describing their basic principles and unique applications. A separate article fully dedicated to applications of IBA techniques in wide range of areas has also been included in this bulletin. Towards the end of the bulletin, details of the various ion beam facilities in India are given for information current and new researchers in this area. On behalf of IANCAS, I would like to thank Dr. R. Acharya and Dr Sanjiv Kumar, Guest Editors, for bringing out this bulletin on IBA techniques with a comprehensive coverage. I would also like to thank all the authors who have contributed to this bulletin. I am sure this bulletin would be very useful to readers in getting an overview of the IBA techniques and their applications.

Rahul Tripathi

Preface

Ion Beam Analysis for Materials Characterization

Ion Beam Analysis (IBA) is an important modern analytical technique involving the use of MeV ion beams to probe the composition and obtain elemental depth profiles in the near-surface layer of solids. It is unique among surface analytical techniques by virtue of its sensitivity towards several elementsacross the periodic table (from H to U) and non-destructive depth perception capability. It has been used extensively for elemental and stoichiometric analyses, determination of depth profiles and diffusion parameters, defect analysis and micro area elemental distributions in materials that find applications in fields ranging from Geology, Biology, Food, environmental science, archaeology, Forensic Science, Material Sciences, Energy and Nuclear Technology.

IBA is performed using energetic beams of protons, a-particles or heavy ions as probes. The energetic ion beams are produced by a particle accelerator which is usually a DC machine based commercial accelerators are tandem type which produce ion beams of energies (n+1)*V*MeV where n is charge state of the beam and *V* the terminal voltage. The terminal voltages of the machines range from a few hundred kilovolt to several million volts while their stability is usually about or better than 0.1 %. IBA, in fact, is an array of techniques which are classified on the basis of the nature of the interaction of ions beams with matter. Particle Induced X-ray Emission (PIXE), Particle Induced Gamma-ray Emission (PIGE) Rutherford Backscattering Spectrometry (RBS), Nuclear Reaction Analysis (NRA), Elastic Recoil Detection Analysis (ERDA) and Channeling are the prominent IBA techniques. These techniques have their own advantages and are often complementary. IBA experiments are performed in a scattering (interaction) chamber at ~ $10^{\prime}10^{-6}$ Torr pressure wherein a well-collimated beam of charged particles (mm to μm) strikes the specimens/targets. In addition to detectors to detect the reaction products, the chamber is equipped with several gadgets. Typical beam (particle) current in an IBA experiment is a few tens of nA though in some cases, currents as high as 500 nA become a requisite.

Among IBA techniques NRA is suitable for the isotopic analysis & depth profiling of light elements. It utilizes a nuclear reaction, preferably with a high Q-value, and involves *prompt* measurement of one of the reaction products. Resonances in the excitation functions of the reactions are used for depth profiling. Such analyses are referred to as nuclear resonance reaction analysis (NRRA). The sensitivity and depth resolution of the measurement depend on the cross-section and width of the resonance. In favorable cases the detection sensitivity is in ppm levels while depth resolution, in nanometers. However, low detection sensitivity and high-depth resolution are seldom realized. The determination and depth profiling of hydrogen in materials is one of the prominent applications of NRRA in view of the facts that the element has a profound affect on the electrical, chemical and structural properties of materials and is analytically intractable. $^{1}H(^{15}N,ag)^{12}C$ (E_R = 6.385 MeV) or $^{1}H(^{19}F,ag)^{16}O$ (E_R = 6.385 MeV) resonance reactions have been used extensively for depth profiling hydrogen in various materials. In

hydrogen storage. In addition to hydrogen, NRA or NRRA is used for the analysis of several elements which include boron, nitrogen, oxygen, fluorine, magnesium and aluminum.

RBS is considered to the backbone of IBA. Based on the detection of backscattered particles, RBS is an experimentally simple technique without any complexity in quantification. Rapidity, simultaneous multielement detection and depth perception capabilities are the major hallmarks of the technique. RBS is essentially sensitive to mid and high Z elements. However such important low Z elements as C, B, N and O can be sensitively analyzed and depth profiled by nuclear backscattering spectrometry (NBS), a variant of the technique (RBS). RBS is eminently suitable for the analysis of multilayered coatings. It provides information on the composition, thickness and position of individual layers in such coatings. RBS is used to determine diffusion coefficients from extracted depth profiles and provides information on interfacial reactions and the formation of resulting phases. It is also used in the characterization of defects in association with channeling.

NRA and RBS are essentially useful in the development of materials as these provide analytical support which is crucial for process optimization. But for trace level detection elements are accomplished by PIXE and PIGE techniques The principles underlying PIXE is well known; so is the area of its applications. It involves high (energy) resolution measurement of characteristic X-rays emanating from the target following its irradiation with charged particles. It is well suited for the analysis of elements with Z> 18 and is performed in thin target and thick target variants with the later generally referred to as thick-target PIXE (TT-PIXE). Thin target PIXE is amenable to quantification but the preparation of suitable targets is tedious. TT-PIXE, on the other hand, is performed on thick targets which can be prepared rather easily; related quantification, however, is complex. PIXE is generally performed by 2-2.5 MeV proton beam. Álpha particles or other heavy ions beams can also be used as projectiles but their energies should be significantly higher in order to achieve comparable sensitivity. Attempts have been made to explore the depth profiling capability of PIXE but these have met limited success.

PIGE is complementary to PIXE and facilitates the determination of light elements (like Li, B, F, Na, Mg, Al and Si) due to use of low energy, mostly, proton beam and higher gamma-ray yield. It is based on high resolution ã-ray spectroscopy of prompt ã-rays produced from nuclear reactions induced by the incident proton beam (2-4 MeV). The determination of F merits special mention as like hydrogen its determination in solid matrices by conventional analytical techniques is extremely difficult. $^{19}F(p,p\tilde{a})^{19}F$ or $^{19}F(p,\acute{a}\tilde{a})^{16}O$ nuclear reactions that emit 110 and 197 keV and, 6-7 MeV ã-rays respectively are reactions of choice for F determination. PIGE has the capability of isotopic composition of elements like B and N : $^{10}B/^{11}B$ and $^{14}N/^{15}N$ atom ratios in materials non-destructively. IBA (PIXE and PIGE) can also be practiced in air, called external IBA, where in beam is extracted into air or a cover of suitable gas using an exit window. Large and non-standard geometry objects which are not compatible with vacuum can be analyzed by external PIXE and or PIGE. This technique has been very useful in the analysis of alloys and archaeological and forensic (glass and ceramics) samples.

Conventional IBA measurements utilize beams of <2 mm size which are obtained through proper collimation. Nuclear microcopy is relatively new branch of IBA wherein beams of about 1 micron are used as probes. These probes are formed by electrostatic or magnetic focusing. The technique facilitates the examination of a sample with any IBA technique such as PIXE, RBS or RBS with high spatial resolution. In fact, µ-NRRA or µ -RBS can, by virtue of their inherent depth profiling capability, can provide three-dimensional imaging of elemental distribution in the near-surface regions of materials. Nuclear microscopy has found applications in biological, environmental and geological sciences.

We thank IANCAS and Editor, IANCAS Bulletin for giving us opportunity to bring out this important Bulletin on Ion Beam Analysis (IBA) and all contributors/authors (as listed in the Contents) for their valuable scientific contributions. It contains seven articles out of which five are IBA techniques namely PIXE, PIGE, NRA, RBS and Channeling and two articles are included (i) Literature Survey on IBA and (ii) five IBA facilities in India utilizing both low and medium energy ion beams for basic and applied studies using tandem particle accelerators and a new upcoming PIGE facility using Cyclotron.

R. Acharya, **Sanjiv Kumar**

Ion Beam Analysis for Materials Characterization

Guest Editors

R. Acharya
Radiochemistry Division, BARC, Mumbai
Email: racharya@barc.gov.in

AND

Sanjiv Kumar
NCCCM, BARC, Hyderabad
Email: sanjukumar@barc.gov.in

Particle Induced X-ray Emission: Principle and Applications

K.M. Varier[1], Daisy Joseph[2], G.J. Naga Raju[3], P. Sarita[4]& K.B. Dasari[5]

[1]Department of Physics, Kerala University, Thiruvananthapuram
[2]Nuclear Physics Division, Bhabha Atomic Energy Research Centre, Mumbai, djoseph@barc.gov.in
[3]JNTUK- University College of Engineering, Vizianagaram, gjnraju@yahoo.com
[4]Department of Physics, GIS, GITAM University, Visakhapatnam, spadala3@gitam.edu
[5]Korea Atomic Energy Research Institute, Daejeon, South Korea, dasari@kaeri.re.kr

Abstract : Particle induced X-ray emission (PIXE) is an accelerator-based ion beam technique for simultaneous analysis of chemical elements. The technique of usinglight ion beams from accelerators to induce X-rays that are characteristic of thesurface being bombarded has been adequately reviewed over the years. The basic principle, sample preparation, and methodology of the PIXE technique using Folded Tandem Ion Accelerator, BARC, Mumbai and 3 MV Tandem Pelletron Accelerator at Ion Beam Laboratory, IOP, Bhubaneswar facilities are presented in this article. The broad range of PIXE applicationsin environmental, biological, archaeological, and forensic sciences for elemental identification and quantification have immense societalbenefits.The aim of this article is to bring together key references and applications using national PIXE facilities.

Introduction

Over the last half century, analytical techniques that exploit instrumentation typical of nuclear physics have assumed a relevant role in analysis of samples from every conceivable field of scientific or technical interest. Particle induced X-ray emission (PIXE) is one such nuclear physics-based ion beam analysis technique that is respected for its practical accuracy and detection range of parts per million. The basic idea of PIXE that is based on identification of characteristic X-rays emitted by excited elements, dates back to the pioneering work of Mosley in 1913. Mosley established a relationship between the energy of the X-rays and the atomic number of the atom emitting the X-rays. In 1912, Chadwick had observed and identified X-rays from elements exposed to alpha particles from radioactive sources. Later, when energetic protons became available from particle accelerators, these were used for X-ray production and the capability of the proton induced X-rays was realized. The pioneering work of Johansson and his group in 1970 at Lund Institute in Sweden put the PIXE technique on a solid foundation in the field of trace elemental analysis [1,2]. Since then the popularity of PIXE increased and it became a full potential technique for elemental quantification. The unique features of the PIXE technique which distinguishes it from the other methods are the following:

i. Multi-elemental nature: All elements present in the sample can be qualitatively estimated simultaneously in one shot.

ii. High sensitivity: The sensitivity of PIXE is less than parts per million (ppm). This is primarily due to the fact that X-ray production cross sections are much larger (barns) as compared to the cross sections for other processes. Also, cross sections are smoothly varying functions of the atomic number of the elements and proton energy.

iii. Non-destructive nature: PIXE further offers the possibility of preserving the sample intact for later use. Very small quantities of the sample are required for analysis. Absolute amounts as small as pico grams can be analyzed under favorable conditions.

Basic principle

The basic principle of PIXE technique involves the excitation of the orbital electrons of the target atom with energetic charge particles(generally protons) and subsequent detection of characteristic X-rays emitted from the target. The high-energyprotons strike the target atoms and eject electrons from the innermost orbit leaving theatoms in the excited state. As a result, a vacancy is created in the innermost orbit,subsequently it is filled with higher orbit electrons and characteristic X-rays are emitted inthis de-excitation process. Measurement of X-ray intensities leads to the quantification ofanalyte concentrations in the sample as both are directly related to each other. Generally inPIXE, 1-3 MeV proton beam is used for determination of low to high Z elements. Theinteraction probability of 1-3 MeV of protons with orbital electrons by Columbic interactionis high with respect to that of nucleus. A schematicdiagram of X-ray production due to charged particle interaction with atom has beenshown in Fig 1(a). These transitions between orbitalscan be radiative or non-radiative. In the radiative transitions, the excess energy between the orbital energies is emitted in the form of characteristic X-rays with energy given by

$$h\nu = E_1 - E_2 \quad \text{.....(1)}$$

In non-radiative transitions, the excess energy is given to another electron of the atom, which consequently gets dislodged from its shell and emerges out from the atom. This process is called Auger effect [1]. In radiative transitions, depending on the sub shell from which the electron has been removed from the atom as a result of the ionization, K-, L-, M-X-rays are emitted. The various types of X-rays emitted from the various sub shells are indicated in Fig. 1(b). Transitions to the K-shell result in K X-rays (K_α, K_β etc). Similarly, transitions to the L-shell lead to the emission of L X-rays (L_α, L_β etc) and so on. The energies of the emitted X-rays, detected by a suitable X-ray detector, give information on the various elements present in the material (Qualitative Analysis). The intensity of the X-rays gives information on the concentration of the elements (Quantitative Analysis) [1,2].

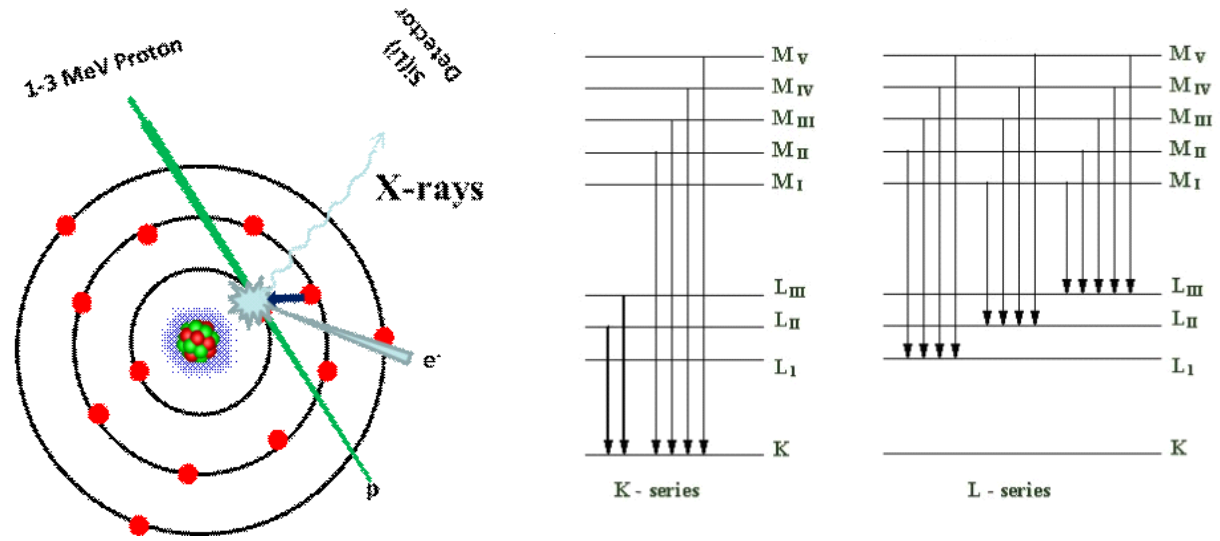

Fig. 1(a) Schematic diagram of proton interaction with orbital electron and; (b) X-rays from various sub shells

Experimental Details

PIXE experimentation consists of three parts: preparation of targets, experimental setup including data acquisition and concentration calculation.

Sample preparation and experimental set-up: Non-conducting thick samples requires conducting material to be mixed with sample for current measurement from the target. Generally, non-conductive samples are mixed with high purity graphite in 3:1 ratio. The resultant mixture is compressed with KBr pressing machine into pellets with dimensions of 12 mm diameter and ~1 mm thickness. These pellets are mounted on an aluminium or stainless-steel ladder and kept inside a high vacuum (~10^{-6} torr) scattering chamber to perform the analysis. The target ladder arrangement facilitates the irradiation of several targets during a single loading into the scattering chamber. Through a viewing window the ladder position can be observed and adjusted to exactly focus the beam onto the target. This ensures the pellet position in the IBA chamber at 45° to the beam direction. The PIXE experiments were carried out at Folded Tandem Ion Accelerator (FOTIA), BARC, Mumbai and Ion Beam Analysis Laboratory (IBL), IOP, Bhubaneswar. The tandem accelerator has two types of negative ion sources; one is Alphatross (for He ions) and other one is Multi-Cathode Source of Negative Ions by Cesium Sputtering (MC-SNICS). A stream of singly charged negative ions generated by the ion source is accelerated to about 55 keV through a pre-accelerating column before being sent into the injector. The negative ions convert to positive ions during the collisions with argon gas atoms or nitrogen gas molecules (used as a stripper) at the high voltage terminal (0.5-2 MV). After emerging from the accelerator, the ion beam is analyzed and focused by a 90^0 analyzing magnet. Then the beam is focused into the exit slits of the switching magnet which directs the beam to the experimental port at 45^0 to carry PIXE experiments. Proton beam of 1-3 MeV energies (current ~10 nA) are usually used for PIXE experiments [3,4]. Characteristic X-rays emitted from the samples are detected using liquid nitrogen fill Si(Li) semiconductor detector at FOTIA and Peltier cooled Si-drift detector coupled to PC based MCA at IBL. The PIXE experimental set up at FOTIA is depicted in Fig. 2.

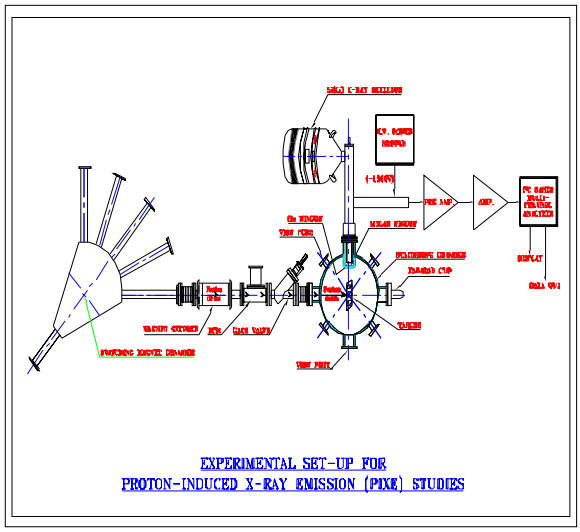

Fig. 2 Experimental set up for PIXE at FOTIA, BARC

X-ray production cross sections are directly proportional to energy of the proton beam and inversely proportional to atomic number [5]. PIXE is a reasonably sensitive technique and all elements with Z > 11 can be determined with detection limit up to trace levels about 1 ppm for Z ~ 39 by K X-rays, Z ~ 40-78 by L X-rays Z~79-92 by M X-rays. A typical detection limits through filter paper and ideally measured elements from potassium to uranium on periodic table by PIXE are shown in Fig. 3. Different X-rays energies of element are presented in Annuxure-1.

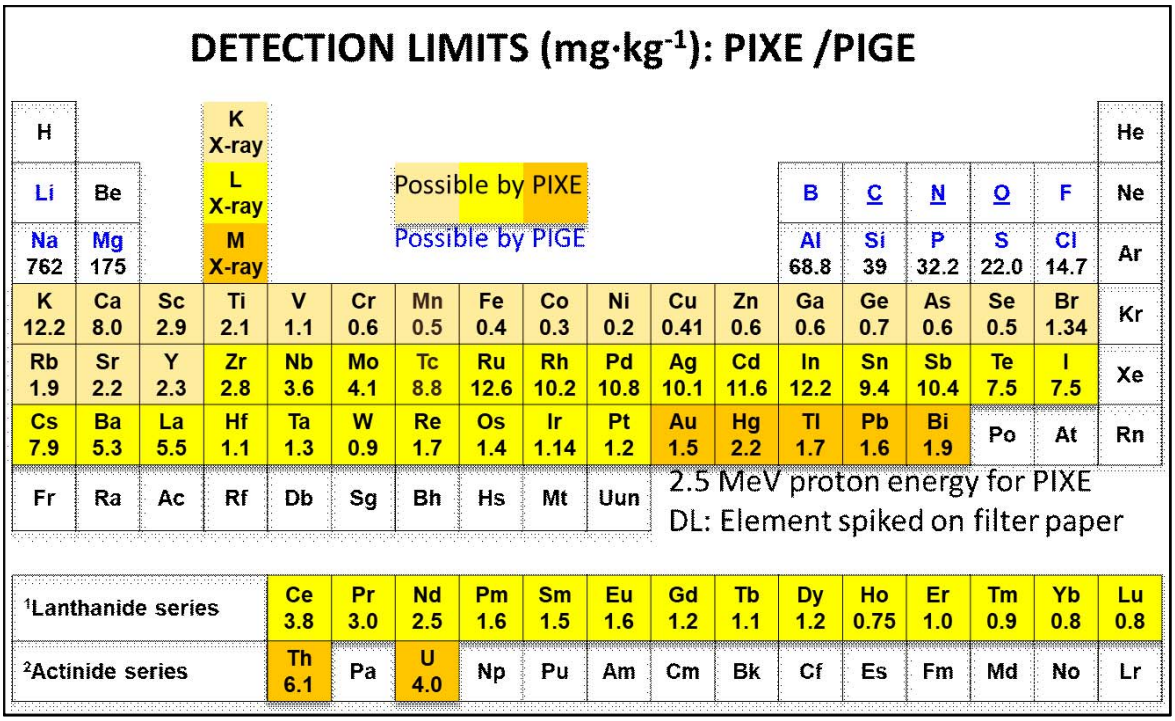

Fig. 3 Periodic table of elements analyzed by PIXE/PIGE and detection limits

Concentration calculations: The PIXE spectrum is usually a complex one, consisting of a number of characteristic peaks of the various elements present in the sample superposed on a continuous background. Typical PIXE spectra of various samples are shown in Fig.4. The background mainly arises from the bremsstrahlung generated by the electrons ejected from these elements as a result of the Coulomb interaction of the incident projectiles. Very minor contributions to the background result from the bremsstrahlung produced by the incident protons and the low energy continuum of nuclear reaction gamma ray photons. These latter contributions can be neglected for protons of energies in the range 2 – 3 MeV. The net area under each peak is proportional to the number of characteristic X-rays emitted by the particular element in the sample. The X-ray emission is assumed to be isotropic. The number of characteristic X-rays is in turn, proportional to the amount of the element in the sample [1]:

$$N_X = N_P (mN_0 / A)\sigma_X T \eta \quad \text{.....(2)}$$

η is the detector efficiency, T is a correction factor for the attenuation of the X-rays in the sample itself as well as in any other material in the path of the X-rays like detector cover etc. N_0 is the Avogadro number and A is the atomic mass number of the element and Np is the number of protons incident on the sample. From the experimentally measured N_x and N_p, m can be determined. This is little complex for manual calculations. There are several software programs available for X-ray spectra analysis and concentration calculations. The inter-comparison of PIXE software packages can be found in the IAEA techdoc-1342 [6,7].

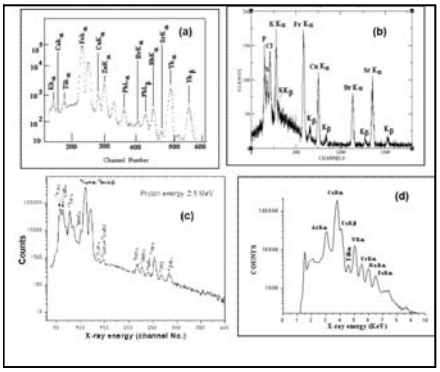

Fig.4 PIXE spectra of different samples (a) lead poisoned blood sample; (b) drinking water sample; (c) archaeological pottery sample; (d) External PIXE Spectrum of GTL4 (Tsavorite Garnet)

Applications

Biological Samples: PIXE is a promising analytical tool for biological samples because of its non-destructive nature and ability to analyse the sample even if it is available in small quantity. A lot of studies were carried out successfully to analyse biological samples such as body fluids (like blood and urine), biological tissues, blood samples (serum and whole blood), hair, nail, bone, skin etc [8]. With the rise of several types of cancers more attention has been paid towards the human cancer afflicted organs. Among all the elements observed in the analyzed organs, the elements copper, iron, zinc, selenium, chromium, nickel, and arsenic are generally accepted as the vital elements that influence cancer. Therefore, the variations in these elemental concentrations observed in the cancer tissues relative to the normal tissues are to be attributed to pathological factors in that cancer afflicted tissues [9]. The variations of trace elements reported in cancerous and normal tissues are presented in Table 1.

Table1. Comparison of trace elemental concentrations in normal and cancerous human tissues

Tissue	Tissue type	Cr	Ni	Fe	Cu	Zn	Se	As	Ref.
Breast	Normal	31.9	7.4	299	42	56	0.66	2.57	[10]
	Cancerous	52.7	8.56	376	60.7	126	1.32	4.12	
Thyroid	Normal	6.2	8.4	569	54.9	149	ND	125	[11]
	Cancerous	29.8	7.7	1397	12.9	71.8	ND	2.8	
Kidney	Normal	9.3	9.7	325	9.1	66	1.8	ND	[12]
	Cancerous	8.2	7.6	305	8.2	78	ND	1.11	
Rectum	Normal	28.0	28.6	340	6.3	83.8	ND	0.6	[13]
	Cancerous	11.4	11.4	980	21.9	145.4	ND	5.5	
Stomach	Normal	7.3	10.5	2408	63.5	818	ND	ND	[12]
	Cancerous	12.6	60	684	21.2	229	ND	1.71	
Penis	Normal	4.6	ND	650	7.5	58.2	ND	2.1	[9]
	Cancerous	2.6	ND	464	79.6	148	ND	5.6	
Testis	Normal	102	ND	426.4	3.9	91.7	ND	ND	[9]
	Cancerous	125	ND	391.9	14.9	34	ND	ND	

Elevated levels of copper observed in most of the cancer tissues might be responsible for the onset and progression of cancer through oxidative DNA damage and angiogenesis, respectively. The observed higher levels of iron in cancer tissues might also be a consequence of cancer. As tumour grows beyond a certain size, it requires an increased supply of oxygen and nutrients to the cells. This results in the formation of new blood vessels (angiogenesis). This in turn increases hemoglobin, which is an iron containing protein that carries oxygen to tissues. Balanced levels of zinc are very important for the proper functioning of the immune system since both deficiency and excess of zinc cause defects in immune function. Zinc deficiency results in depressed immune functions. Both tissue-mediated and humoral responses are affected. Excess levels of zinc enhance tumour cell growth and promote neoplastic transformation.

Hair is the most easily available biological sample. It contains trace elements which reflect biological processes over long periods of time. Also, continuous exposure to environment, leaves an imprint of atmospheric pollutants. In one study, hair samples from the different parts of the head of the same person and from different persons were subjected to PIXE analysis. The samples were irradiated as such or after wet acid digestion. The standard deviations in the estimated trace levels were about 17 - 28 % in samples from same person and about 30% to 69% in samples from different individuals. Lead content was more in samples from persons in urban area, which could be undoubtedly attributed to automobile exhaust. No definite trend in the copper content of black hair (blackness is basically due to a copper containing pigment called melanin) versus grey hair had been noted. The reason may be that other sources of copper content may mask the copper in melanin. It was observed that married women have more lead in their hair, obviously due to the kumkum which they traditionally apply on their foreheads [14].

Forensic science : Elemental analysis has been found to be quite helpful in the identification of crime related samples, with possibility of identifying the criminal [15] and offset printing ink tagged with rare-earth taggants [16]. For example, in cases of gunshot firing, the type of bullet and distance of firing are important parameters. The bullet carries along with it a part of the primer, gun powder and also a part of the material of the gun itself. Some of these get deposited around the bullet hole on the body of the victim. An analysis of the radial distribution of these elements (antimony, barium, copper, lead and iron) can be helpful in this aspect. Laboratory simulated Whatman filter paper samples were analysed for the gunshot residues by the PIXE technique. Fig.5(a) shows the radial distribution of some elements. Radial distribution of the various elements was found to depend considerably on the distance of firing. Representative variations are given in Fig.5(b). Copper jacketed bullets contain more copper. This shows up remarkably well in the PIXE spectrum leading to the possibility of identifying the bullet used. The non-destructive nature of the PIXE technique becomes handy in such analyses. Other crime related samples which can be subjected to the PIXE analysis include typewritten papers, nails, hair, blood stains etc.

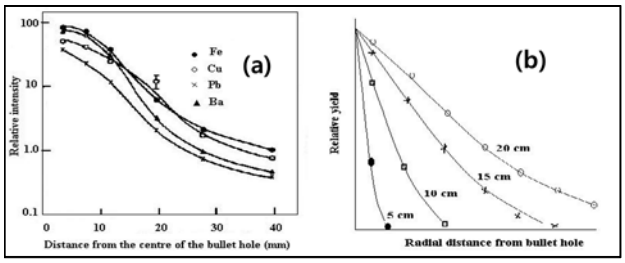

Fig. 5 (a) Radial distribution of elements in gunshot residue sample; (b) Gunshot residue elemental distribution – dependence on firing distance

Archaeological Samples: Provenance studies are carried out in two ways: either by classifying samples according to their physical characteristics, decoration, and style or by chemical composition analysis. Chemical composition analysis of artifacts is the most important tool for providing useful information like geographical origin and manufacturing techniques [17,18]. In the provenance studies, archaeological artifacts like pottery, bricks, stones, coins and paints are analysed by variety of analytical methods. Among the artifacts, potteries are most studied because the chemical composition of a clay pottery is strongly related to the source of clay and recipe of the making. Few archaeological pottery samples are shown in Fig. 6(a). The analytical method of examination and analysis should be non-destructive or minimal sample extraction from the whole sample. The novel external proton beam PIXE technique is highly suitable for elemental constituents in archaeological samples directly [19]. Alkali and alkaline elements, transition elements and Rare Earth Elements can be used for grouping / provenance studies [3]. Elements which are non-volatile and immobile, exhibit high stability in clay minerals and therefore are good candidates for provenance study. Chemical analyses together with statistical data treatment are accepted methods for provenance study and have been extensively used in the archaeological investigations. Multivariate statistical methods like cluster analyses (CA) and principal component analysis (PCA) are mainly used for this purpose [3,17,19]. In the present study 22 different ancient pottery samples were

analyzed using 2.5 MeV proton energy from tandem accelerator at IBL, IOP facility. PIXE spectra were analyzed for absolute elemental concentrations by using GUPIX software package [7]. Elemental concentrations, namely those of Si, K, Ca, Ti, V, Cr, Mn, Fe, Ni, Cu, Zn, Rb, Sr, and Zr, are determined in ancient potteries. Preliminary grouping using two or three key elements correlation to predict the source or distinguish the samples. Si, Ca and K concentrations varied from sample to sample, and Ca showed a strong leaching effect, which led to its exclusion from the grouping study. The transition elemental concentrations of Ti, V, Cr, Mn, Fe, Ni, Cu, and Zn were used for grouping the artifacts under study. The concentrations of these elements are expected to remain unchanged in the samples with time. The multivariate statistical cluster analysis (CA) method by STATISTICA 5.1 package was used to identify the similarities and dissimilarities between the artifacts using their chemical profile. The essential components of this analysis are based on linkage methods or clustering algorithms and distance measurement (cluster separator). In this study, CA using Ward's method complete linkage approach and Euclidean distance measurement between the samples were used for grouping study.

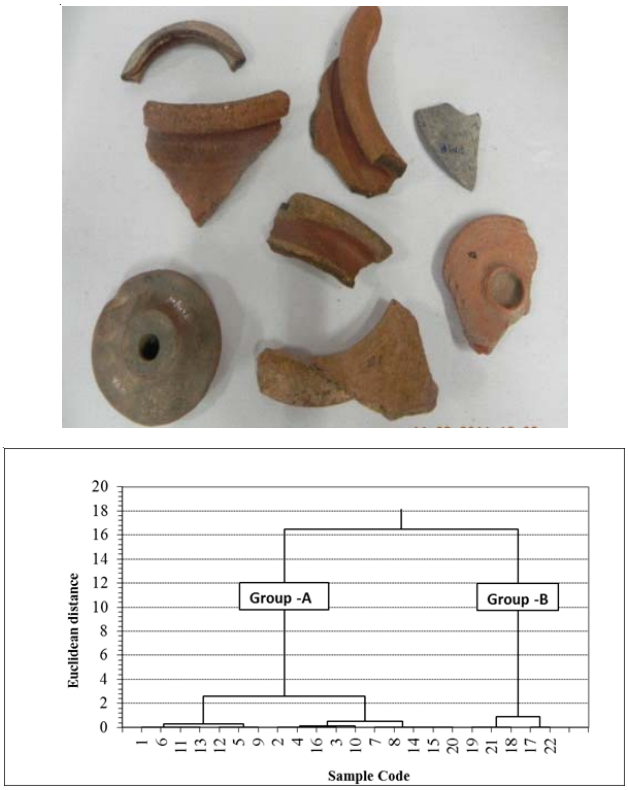

Fig.6 (a) Archaeological pottery samples; (b) Dendrogram of pottery samples obtained by cluster analysis using transition elemental concentrations (V, Cr, Ti, Mn, Fe, Ni, Cu, and Zn).

The Cluster Analysis (CA) dendrogram of the pottery samples using transition elements is given in Fig. 6(b). As per the CA dendrogram and preliminary grouping using limited elements and sample history, all samples fell into two major groups: (A) 1–16 and (B) 17–22 (except 20) with maximum 10% variance within the groups. Though samples 1–6 and 7–16, were collected two different but nearby locations, CA showed that they are similar indicating that the source clays were almost similar, and they might have been prepared with clay materials from same or nearer location. Sample 20 did not fall in Group B (but in Group A), which indicated this might have been brought from Group A locations. Based on the preliminary studies by Archaeologists on physical characteristics (design on artifacts, thickness and color) of artifacts, it was indicated that group B artifacts are different from group A artifacts [3,17]. Thus the findings by CA using concentrations of transition elements are in good agreement with the collection history and physical characteristics of the artifacts.

Sediment Samples : Pollutants and toxic elements in the environment are generally determined through the detection of trace elemental concentrations in aerosol, water, soil and sediment samples. Trace pollutants present a major threat to human, animals, plant life, and oceans. Elemental concentrations of contaminated Kakinada Bay sediment samples were determined by PIXE. Other analytical techniques INAA, PIGE are also performed for determination of toxic and hazardous elements present in the sediment samples. Various hazardous elements followed the order of concentrations As< Co < Zn < Cr < Ba <Mn< Fe are determined in sediment samples. According to previous studies and present study the hazardous elemental quantity showed an increase in levels and this may be ascribed to industrial effluents from textiles industries and anthropogenic activities around the Godavari peninsula and Kakinada Bay. Contamination of the environment by heavy metals can be confirmed by studying the chemical forms of different metals present in the sediment. Future pollution studies can assess the level of pollution and provenance in sediments of the Godavari estuary and Kakinada Bay [18].

Gemological Samples : For the analysis of gemstones, External PIXE is used. This particular technique has many advantages:1. It is non-destructive and the data points can be taken across any angle of the object. 2. Sample handling is easy, samples of large sizes and shape can be handled and analyzed without the need of sampling, especially suited for art objects and precious stones [20]. 3.There is no radiation damage to the samples 4.Proton charge does not build up on the sample. Its principle lies in extracting the ion beam out in air through a window sufficiently resistant to stand atmospheric pressure and beam induced damage but thin enough to minimize the energy loss and energy straggling the incident beam.A proton beam of 4 MeV energy and current of 8 nA intensity was extracted from FOTIA in air through a Kapton foil of 8 mm thick mounted on a Teflon cone. For the measurements, the samples were kept in air over a sample stand (of 5 kg capacity) making an angle of 45??to the beam direction. The samples were irradiated with maximum beam current of 8 nA passing through the 8 mm thick Kapton TM window. A Si (Li) detector having energy resolution of full-width at half maximum 170 eV at 5.9 keV placed at 90??with respect to the beam direction was used to detect characteristic X-rays emitted from the target. The detector has an active area of 30 mm^2 and an entrance beryllium window of 1 mil thickness. Spectra were recorded

using a PC based multichannel analyzer [20]. Besides the above applications we also carried out PIXE on gold standards, and studied intensity ratios on thin and thick targets [21].

Aerosol Samples : One of the most important applications of PIXE is in atmosphere research to analyze aerosol samples for their trace elemental content and composition of the particulate matter (PM) as a function of particle size Establishing the elemental composition of aerosols would help to identify the sources (natural or anthropogenic) and consequently monitor their health impacts. Studies of this kind can be used for scientifically defensible air quality management. Air particulate matter is collected by pumping air through a suitable filter or a cascade impactor. Particles with aerodynamic range 0.1-10mm are deposited on a Mylar foil or a Nuclepore filter (<1mg/cm^2) to minimize the matrix effects. Such samples are ideal for PIXE. Ravi Kumar et al (2010) observed that the high levels Pb, Mn and Ni in the aerosol samples collected from NAD Kotha Road, Visakhapatnam compared to the environmental pollution free area. The observed high levels were attributed to effluent gases released from nearby industries and smelters. The high levels of Zn observed in Gajuwaka area was due to the presence Hindustan Zinc Limited and other industries located near the sampling station [22,23].

Semiconducting Materials : Semiconducting materials are an integral part of electronic devices having innumerable applications. Hence, it is very important to study their actual properties and the alteration in their properties when subjected to extreme conditions so as to know their effectiveness in a particular application. Moreover, studies on material modification can be carried out by measuring trace contamination in semiconducting materials. PIXE has been extensively used to determine the presence and concentrations of elements acting as impurities in some semiconducting materials, analyze thin films for photovoltaic applications and high Tc superconductors [2].

References

1. Johansson SAE, Campbell JL, Malmqvist KG,1996. Particle-Induced X-Ray Emission Spectrometry (PIXE) Edited by. Wiley & Sons: New York. J. Am. Chem. Soc. 1996, 118, 27, 6528–6529.
2. Nastasi M, Mayer JW, Wang Y,2014. Ion Beam Analysis: Fundamentals and Applications, CRC Press, Boca Raton
3. Dasari KB. 2013.Provenance studies of arcaehological artifacts using nuclear analytical techniques, Ph.D. Thesis, GITAM University, India.
4. Joseph D, Saxena A, Kailas S, 2005. PIXE studies at Van-de-Graaff accelerator, International Journal of PIXE, 15,1 and 2.
5. PaulH, Sacher J, 1989. Fitted empirical refrence cross sections for K-shell ionization by protons.Atomic Data Nucl. Data 42, 105–156.
6. IAEA TECDOC-1342, 2003. Intercomparison of PIXE spectrometry software packages. IAEATECDOC-1342, Vienna.
7. Campbell J L, Boyda N I, GrassiN, Bonnick P, Maxwell JA, 2010. The Guelph PIXE software package IV, Nucl. Instrum. Methods B 268, 3356-3363.
8. Joseph D, 2005. Proton Induced X-ray Emission (PIXE) technique-some applications in bio-sciences, Indian Journal of Radiation Research,Vol 2,No. 2.
9. Naga Raju G J, John Charles M, Bhuloka Reddy S, Sarita P, Seetharmi Reddy B, Rama Lakshmi PVB, Vijayan V, 2005. Trace elemental analysis in cancer-afflicted tissues of penis and testis by PIXE technique. Nucl Instrum Methods Phys Res B 229:457–464.
10. Raju G J Naga, 2006. Trace elemental correlation study in malignant and normal breast tissue by PIXE technique." Nuclear Instruments and Methods in Physics Research Section B 247.2, 361-367.
11. Reddy S Bhuloka, 2003. Trace elemental analysis of carcinoma kidney and stomach by PIXE method." Nuclear Instruments and Methods in Physics Research Section B 207.3, 345-355.
12. Reddy S Bhuloka, 2005. Trace elemental analysis of adenoma and carcinoma thyroid by PIXE method." Nuclear Instruments and Methods in Physics Research Section B 196.3-4, 333-33.
13. Raju, G J Naga, Sarita P, Murthy K S R, 2017. Comparative trace elemental analysis of cancerous and non-cancerous tissues of rectal cancer patients using PIXE. Nuclear Instruments and Methods in Physics Research Section B 404, 146-149.
14. Pradeep A S, Naga Raju G J, Abdul Sattar S, Sarita P, Durga Prasad Rao A, Dinesh Kumar Ray, Seetharami Reddy, B Bhuloka Reddy, S, 2014. Trace elemental distribution in the scalp hair of bipolars using PIXE technique, Medical Hypotheses 82, 470-477.
15. Bailey M J, Kirkby K J, JeynesC, 2009. Trace element profiling of gunshot residues by PIXE and SEMEDS: a feasibility study, X-Ray Spectrom, 38, 190–194
16. Joseph D, Maind S D, Saxena A, ChoudhuryRK, 2007.Characterisation of Offset Printing ink tagged with rare-earth taggants by X-ray Emission techniques**,** International Journal of PIXE, Vol. 17, Nos. 3 & 4, 183"191.
17. DasariKB, AcharyaR, RayDK, Lakshmana DasN, 2017. Application of PIXE for the determination of transition elements in the grouping study of archaeological clay potteries, X-ray Spectrometry, 46, 180.
18. Dasari K B, Ratna Raju M, Lakshminarayana S, 2016. Compositional characterization of Kakinada Bay sediment by INAA and IBA methods: preliminary study, J Radioanal Nucl Chem, 307, 875.

19. Calligaro T, Dran J-C, Salomon J, Walter Ph, 2004. Review of accelerator gadgets for art and archaeology, Nucl. Instru. Meth. B, 226, 29.

20. Joseph D, 2010. Characterization a few Gemstones by X-ray Emission Techniques (EDXRF and External PIXE), International Journal ofPIXE, 21, 22.

21. Joseph D, Saxena A, Gupta S K, Kailas S, 2004. PIXE studies in gold standards by protons of energy 3.3 MeV, International Journal of PIXE 14, 141.

22. Oswal M, Kaur R, Kumar A, Singh K P, Kumar S, Mohanty B P, Kumar S, 2012. Trace element analysis of aerosol samples using PIXE technique. International Journal of PIXE, 22, 271-285.

23. Ravi Kumar M, Naga Raju G J, Sarita P, Seetharami Reddy B, Bhuloka Reddy S, 2010. Trace elemental analysis of aerosols samples using the particle induced x-ray emission technique. International Journal of Environmental Protection 30(7), 593-603.

Dr. K.M. Varier is former Professor of Department of Physics, University of Kerala. He is expert in various fields included nuclear physics, nuclear safety nuclear reactions and radiation detection. He has published more than 70 peer reviewed international articles and contributed several book chapters. He has guided several students for M.Phil and Ph.D. degrees and has handled several projects included UGC, FRP.

G J Naga Raju, presently working as Assistant Professor at Jawaharlal Nehru Technological University College of Engineering, Vizianagaram. He completed his graduation in 1998 and post graduation in 2000 from Andhra University, Visakhapatnam. He obtained Doctoral Degree from Andhra University. After his Ph.D, he served as an Assistant Professor in GITAM University for 6 years. His area of research is ion and atom collision processes and applications of nuclear analytical techniques. He is having 18 years teaching and 15 years research experience, contributed 50 research papers in various refereed journals. He has presented 40 research articles at various national and international conferences.

With a doctorate in Nuclear Physics from Andhra University, P Sarita is an Associate Professor in the Department of Physics at GITAM University, Visakhapatnam. She has 14 years of work experience in teaching and research. Her specific research interests are applications of accelerator based analytical techniques. She has 28 journal publications and has presented 37 papers at various national and international conferences. She has guided 3 students towards their Ph.D. degree and has served as a resource person in a few conferences.

Kishore B. Dasari completed his M.Sc. and M.Phil (Nuclear Physics) degrees at Department of Nuclear Physics, Andhra University, Visakhapatnam. He obtained Ph.D. (Physics) degree from GITAM University, Visakhapatnam in 2013. After that he joined as post-doctoral fellow at Korea Research Institute of Standards and Science, Daejeon. Presently, he is working as research scientist at Korea Atomic Energy Research Institute (KAERI), Daejeon, South Korea. His major research area is Applications and development of nuclear analytical techniques (INAA, IBA, WD-XRF and XANES) for institutional and societal benefits. He published 16 articles in peer-reviewed journals and 50 symposia.

Dr. Daisy Joseph is a Scientist from BARC, Mumbai. She obtained her PhD in Physics fromMumbai University in 2007. She is an expert in EDXRF and PIXE and has around 100publications in peer reviewed journals. She is the Associate Editor for World Research Journal of Bio-Science, Editorial Member of Journal of Advance Research in Applied Science, International Journal of Current Science and Multidisciplinary Research, Madridge Journal of Analytical Science and Instrumentation. She is the Academic Editor of the book on Synchrotron Radiation,Trace elements and its effects in Human health and Diseases published by Intech Open Publishers, London, UK.

Annexure 1 : Reference major intensity X-ray energies (keV) of elements

	Z	Element	Kα1	Kβ1	Lα1	Lβ1		Z	Element	Kα1	Kβ1	Lα1	Lβ1
3	Li	Lithium					34	Se	Selenium	11.224	12.497	1.379	1.419
4	Be	Beryllium	0.108				35	Br	Bromine	11.924	13.292	1.481	1.526
5	B	Boron	0.183				36	Kr	Krypton	12.648	14.112	1.585	1.636
6	C	Carbon	0.277				37	Rb	Rubidium	13.396	14.961	1.692	1.751
7	N	Nitrogen	0.392				38	Sr	Strontium	14.165	15.835	1.806	1.871
8	O	Oxygen	0.525				39	Y	Yttrium	14.958	16.739	1.924	1.998
9	F	Fluorine	0.677				40	Zr	Zirconium	15.775	17.668	2.044	2.126
10	Ne	Neon	0.849				41	Nb	Niobium	16.615	18.625	2.169	2.26
11	Na	Sodium	1.04				42	Mo	Molybdenum	17.48	19.606	2.292	2.394
12	Mg	Magnesium	1.254	1.302			43	Tc	Technetium	18.367	20.626	2.423	2.535
13	Al	Aluminium	1.486	1.557			44	Ru	Ruthenium	19.279	21.656	2.558	2.683
14	Si	Silicon	1.74	1.837			45	Rh	Rhodium	20.216	22.724	2.697	2.834
15	P	Phosphorus	2.01	2.139			46	Pd	Palladium	21.177	23.818	2.838	2.99
16	S	Sulfur	2.309	2.465			47	Ag	Silver	22.163	24.941	2.983	3.15
17	Cl	Chlorine	2.622	2.812			48	Cd	Cadmium	23.173	26.093	3.133	3.315
18	Ar	Argon	2.958	3.19			49	In	Indium	24.21	27.275	3.286	3.487
19	K	Potassium	3.314	3.59			50	Sn	Tin	25.271	28.485	3.444	3.663
20	Ca	Calcium	3.692	4.013	0.341	0.345	51	Sb	Antimony	26.359	29.725	3.604	3.842
21	Sc	Scandium	4.093	4.464	0.395	0.4	52	Te	Tellurium	27.473	30.993	3.768	4.029
22	Ti	Titanium	4.512	4.933	0.452	0.458	53	I	Iodine	28.612	32.294	3.938	4.221
23	V	Vanadium	4.953	5.428	0.51	0.518	54	Xe	Xenon	29.775	33.62	4.11	4.418
24	Cr	Chromium	5.415	5.947	0.572	0.582	55	Cs	Cesium	30.973	34.982	4.285	4.619
25	Mn	Manganese	5.9	6.492	0.637	0.648	56	Ba	Barium	32.194	36.378	4.466	4.828
26	Fe	Iron	6.405	7.059	0.705	0.718	57	La	Lanthanum	33.442	37.797	4.647	5.038
27	Co	Cobalt	6.931	7.649	0.775	0.79	58	Ce	Cerium	34.72	39.256	4.839	5.262
28	Ni	Nickel	7.48	8.267	0.849	0.866	59	Pr	Praseodymium	36.027	40.749	5.035	5.492
29	Cu	Copper	8.046	8.904	0.928	0.947	60	Nd	Neodymium	37.361	42.272	5.228	5.719
30	Zn	Zinc	8.637	9.57	1.012	1.035	61	Pm	Promethium	38.725	43.827	5.432	5.961
31	Ga	Gallium	9.251	10.267	1.098	1.125	62	Sm	Samarium	40.118	45.414	5.633	6.201
32	Ge	Germanium	9.886	10.982	1.188	1.218	63	Eu	Europium	41.542	47.038	5.849	6.458
33	As	Arsenic	10.543	11.726	1.282	1.317	64	Gd	Gadolinium	42.996	48.695	6.053	6.708

	Z	Element	Kα1	Kβ1	Lα1	Lβ1	Mα1
65	Tb	Terbium	44.482	50.385	6.273	6.975	1.24
66	Dy	Dysprosium	45.999	52.113	6.498	7.248	1.293
67	Ho	Holmium	47.547	53.877	6.72	7.526	1.348
68	Er	Erbium	49.128	55.674	6.949	7.811	1.404
69	Tm	Thulium	50.742	57.505	7.18	8.102	1.462
70	Yb	Ytterbium	52.388	59.382	7.416	8.402	1.526
71	Lu	Lutetium	54.07	61.29	7.655	8.71	1.58
72	Hf	Hafnium	55.79	63.244	7.899	9.023	1.646
73	Ta	Tantalum	57.535	65.222	8.146	9.343	1.712
74	W	Tungsten	59.318	67.244	8.398	9.672	1.775
75	Re	Rhenium	61.141	69.309	8.652	10.01	1.843
76	Os	Osmium	63	71.414	8.911	10.354	1.907
77	Ir	Iridium	64.896	73.56	9.175	10.708	1.98
78	Pt	Platinum	66.831	75.75	9.442	11.071	2.05
79	Au	Gold	68.806	77.982	9.713	11.443	2.123
80	Hg	Mercury	70.818	80.255	9.989	11.824	2.195
81	Tl	Thallium	72.872	82.573	10.269	12.213	2.271
82	Pb	Lead	74.97	84.939	10.551	12.614	2.342
83	Bi	Bismuth	77.107	87.349	10.839	13.023	2.423
84	Po	Polonium	79.291	89.803	11.131	13.446	2.499
85	At	Astatine	81.516	92.304	11.427	13.876	2.577
86	Rn	Radon	83.785	94.866	11.727	14.315	2.654
87	Fr	Francium	86.106	97.474	12.031	14.771	2.732
88	Ra	Radium	88.478	100.13	12.339	15.236	2.806
89	Ac	Actinium	90.884	102.846	12.652	15.713	2.9
90	Th	Thorium	93.351	105.605	12.968	16.202	2.996
91	Pa	Protactinium	95.868	108.427	13.291	16.703	3.082
92	U	Uranium	98.44	111.303	13.614	17.22	3.171
93	Np	Neptunium	101.059	114.234	13.946	17.751	3.25
94	Pu	Plutonium	103.734	117.228	14.282	18.296	3.339
95	Am	Americium	106.472	120.284	14.62	18.856	3.438

Particle Induced Gamma-ray Emission (PIGE) : Principle, Developments and Applications

R. Acharya and P.K. Pujari

Radiochemistry Division, Bhabha Atomic Research Centre,
Trombay, Mumbai 400085, India
[email: racharya@barc.gov.in/pujari@barc.gov.in]

Abstract : Particle Induced Gamma-ray Emission (PIGE) is an Ion Beam Analysis (IBA) technique capable of determining low Z elements (Li to Ti) using charge particles (mainly proton beam) from particle accelerators. It is an isotope specific technique which involves measurement of prompt gamma-rays obtained from proton induced nuclear reactions. This article describes briefly fundamentals of PIGE, experimental (both vacuum chamber and external beam), methodologies like conventional and in situ current normalized methods, brief literature survey and some recent applications. The article briefly presents application of PIGE for non-destructive quantification of low Z elements in glass with forensic importance, ceramics like lithium titanate, Li-ion batteries and archaeological artifacts, environmental and food samples, and simultaneous quantification of total B and its isotopic composition in boron-based neutron absorbers.

Introduction

Chemical characterization of materials is the most important step under chemical quality control (CQC) to ensure the material suitability as per the specified composition. Among various techniques conventional and nuclear analytical techniques, Ion Beam Analysis (IBA) techniques are very useful for materials characterization. IBA techniques utilize energetic charge particles (p, d and á) for quantitative information of elements in surface and near surface regions. IBA techniques like Particle Induced X-Ray / Gamma-ray Emission (PIXE/PIGE) are used for chemical analysis of various materials to obtain concentrations of low to high Z elements [1-8]. PIGE is mainly used obtain quantitative information on low Z elements (Z<17), whereas PIXE is used for medium and high Z elements.

In samples like ceramics, glass, soil, sediment and geological origin, low Z elements like Si, Al, Na, K, Mg, and Ca are the major matrix elements whereas in samples like lithium-based ceramics and boron carbides, again low Z elements are the main constituents. Low Z elements are also minor and trace constituents in various samples like F in environmental samples. Thus, quantification of low Z elements in these solid samples without sample destruction is a challenge to the analyst. Instrumental NAA, XRF and PIXE techniques are mainly used for determination of medium and high Z elements in solid samples, and thus these techniques are not suitable for low Z elements up to F. Activation techniques namely photon activation analysis (PAA) (using Bremsstrahlung radiation from electron beam accelerators) and charge particle activation analysis (CPAA)(using energetic charge particles like p and á form particle accelerators) can determine low Z elements, however many of the products of low Z elements are neutron deficient decaying by 511 keV annihilation gamma-ray (non-characteristic), which makes it difficult to determine simultaneously as well as non-destructively. PGNAA is a suitable technique for a few low Z elements including H, neutron poisons like B, Cd and Gd and rare earth elements (REEs). On the other hand, PIGE is the most suitable nuclear analytical method for simultaneous determination of low Z elements from Li to S using low energy proton beam (2-5 MeV) [9-14] and for C,N,O as well as medium to higher Z elements using medium energy proton beam (7-9 MeV) [15].

Principle of PIGE

PIGE involves measurement of prompt gamma-rays when energetic charged particles (p, d and α) are bombarded on the target. The proton induced reactions involve measurement of prompt gamma rays from inelastic-scattering (p, p'γ) or from nuclear reactions like (p, $\alpha\gamma$), (p, nγ) and (p, γ). Fig. 1 gives various IBA techniques; Fig. 2 gives schematic diagram of (p, p'γ) reaction and Fig. 3 gives gamma-rays from excited state of ^{19}F produced from ^{19}F(p, p'γ)^{19}F.

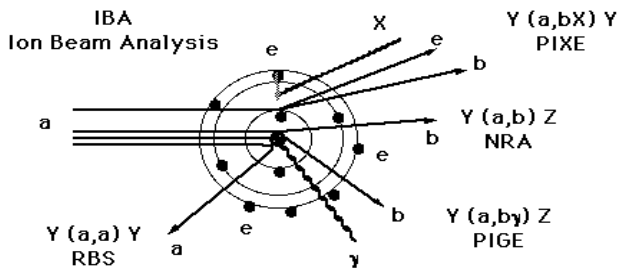

Fig. 1 Interaction of energetic charged particle with target in IBA

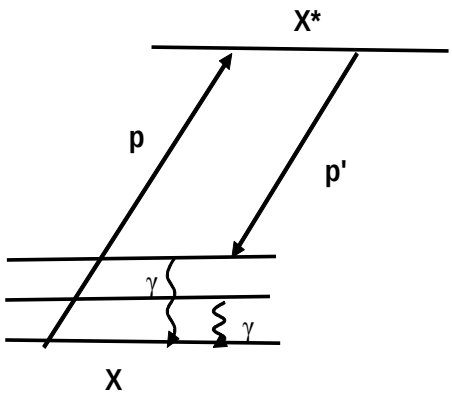

Fig. 2 Schematic diagram in (p, p'γ) reaction

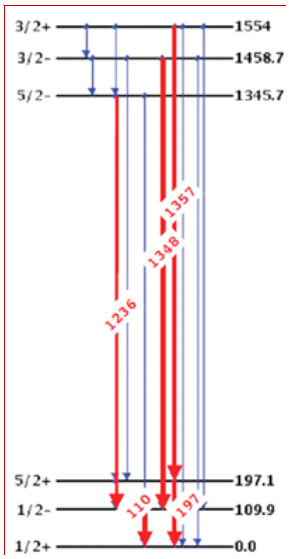

Fig. 3 ^{19}F energy levels

For quantitative information on elemental concentrations using peak areas under characteristic gamma-ray spectra, it is important to have the knowledge of parameters like cross-sections, stopping power of material and beam current as given below in the activity equation in PIGE using energetic particle beam.

$$A = NI_a \int_0^x \sigma(E)dx \qquad (1)$$

$$A = N \times I \int_{E_0}^{E_f} \sigma(E)dE \Big/ S(E)$$

where, N is the number of analyte atoms in the target per cm^3, I is the beam current on the target, s(E) is the nuclear reaction cross section, *S(E)* stopping power or cross-section of the sample in units of energy loss per unit length (dE / dx) or energy per mass density (1/ r . dE/dx) (energy per µg/cm^2) and E_0 and E_f are initial and final beam energies. Thus, the count rate (cps) is given by,

$$\text{Count Rate (cps)} = \varepsilon_{abs}(E_\gamma) \,.\, N.\, I.\, \int_0^{E0} \sigma(E) \,/\, S(E)\, dE \qquad (2)$$

where, $å_{abs}(E_ã)$ is the absolute efficiency of the $E_ã$ as the emitted energy, which is equal to W/4p, For practical use and to get higher sensitivity instead of thin sample thick sample in pellet forms are used. Thus, instead of cross section (for thin samples), thick target gamma-ray yield (Y) in terms of Counts (Nγ) / µC / Sr i.e., counts (number of photons)/ micro coulomb/ Sr (solid angle) is used [7]. Table 1 gives some relevant reactions of low Z elements and corresponding thick target gamma-ray yields at two selected proton energies (4 and 7 MeV) [7,8]. The thick target gamma-ray yields are facility independent and efficiency normalized values and, thus, they give idea about relative sensitivities of low Z elements for same as well as for different proton energies (Table 1). The most prominent reaction is (p,p'γ) compared to (p,γ), (p, ng) and (p,αγ) reactions. Though many elements like Li, F, B and Al have good sensitivity at 4 MeV proton beams, elements like C, N, O, Al, P, S, Cl, Mg, K and Ti have better sensitivities (except (p,γ) reaction) in higher energy (7 MeV) proton beam due to higher effective cross sections or higher thick target gamma-ray yields.

Since 1960, various samples of geological, archaeological, ceramic, steel, dust, aerosol and biomedical origin have been analyzed by conventional method of PIGE. Sippel and Glover [9] for the first time showed that gamma-rays emitted by using energetic protons of the order of MeV could be used for determining low Z elements like Li, Be, C, N, O, F, Na, Mg Al and P in geological samples. PIGE using deuteron beam was used for carbon and 4 MeV proton beam was used for Si in different kind of steel samples [10]. Fluorine was quantified by PIGE in SiF_x etch residues on silicon using 197 keV of ^{19}F [11]. The PIGE technique was utilized for determination of C,N, O, Si and S in coal samples using 9.5 MeV proton beam [4]. GE. Coote, in 1992 reviewed specifically the nuclear reactions for PIGE analysis of F and other low Z elements in different materials including biological (like teeth, bone and fish scales), archaeological and atmospheric samples [19]. PIGE was employed to determine Li, Be, B and F in the individual grains of micas using alpha particle beam of energy 1-3 MeV [5]. Clay samples were analyzed by Savidou et al using 4 MeV proton beam for low Z elements namely Li, B, F, Na, Mg, Al, Si and P [7]. Nsouli et al. analyzed F concentration in a drug as a part of CQC exercise [13]. A number of glass samples of archaeological importance have been studied using PIGE-PIXE combination, wherein PIGE was used to determine Na, Mg, Al and Si [14]. Different samples of geological importance and environmental reference materials have been analyzed by Valkovic et al. using PIGE methods [2]. In addition to in-beam PIGE, external PIGE (beam in air) keeps promise for analysis of many solid and non-standard geometry samples of importance including archaeological samples/ceramics. Using external PIGE, Saarela et.al determined low Z elements like Na, Mg, Al, P and Mn in plant samples using 3 MeV proton beam [15]. Sunitha and Kumar et al., have determined oxygen in materials and ^{10}B/ ^{11}B atom ratio in B_4C by conventional PIGE methods [16,17].

Thus PIGE, a complementary technique to PIXE, XRF and INAA, has several advantages like simultaneous determination of low and medium Z elements, often solid sample for analysis, thus non-destructive in nature, less matrix effect for thick and diluted pellet samples and no or very less spectral interference. Most of the applications have been carried out mainly by conventional PIGE methods using RBS or charge (µC) normalized approaches to the best of our knowledge. Present article gives a summary of our work on development and application of *in situ* current normalized as well as conventional PIGE methods for quantification of low Z elements using proton beams (4 and 8 MeV) from accelerators and their applications to various samples including glass, ceramics, carbides and alloys [18-32].

Experimental

Conventional (vacuum chamber) PIGE

Both conventional and in situ current normalized PIGE methods were standardized using 4 and 5 MeV proton beams from tandem particle accelerators in India namely FOlded Tandem Ion Accelerator (FOTIA), BARC, Mumbai and 3 MV

Tandetron of Ion Beam Laboratory (IBL), Institute of Physics (IOP), Bhubaneswar and 8 MeV proton beam from BARC-Tata Institute for Fundamental Research (TIFR) Pelletron, Mumbai. A typical IBA set up for PIGE and PIXE with RBS facility is given in Fig. 4a and A PIGE set up at FOTIA is given in Fig. 4b. Samples analyzed were glass, lithium-based ceramics, clay ceramics, and boron-based neutron absorbers as well as geological, environmental and biological samples. Samples were in pellet forms either in cellulose or graphite matrix, keeping in mind of similar or negligible stopping power. Samples were irradiated in vacuum (~10^{-6} torr) with proton beam current in the range of 10-50 nA. In situ current normalization method was used in which either F or Li (not present in the sample) was mixed in the sample and standard. Otherwise conventional RBS approach using thin gold foil and conducting target using graphite matrix were employed for beam current monitoring/normalization. The prompt gamma-rays of low Z elements were measured by HPGe detector based conventional high-resolution gamma-ray spectrometry. The typical gamma-ray spectra of samples in PIGE using proton beams are given in the Figs. 6-8, for borosilicate glass using 4 MeV proton beam, lithium titanate sample using 8 MeV proton beam and boron carbide sample using 4 MeV proton beam, respectively. Gamma-ray spectra were analyzed using peak-fit software called Pulse Height Analysis SofTware (PHAST) for the peak area determination. A conventional IBA set up for PIGE and PIXE is given below in **Fig 4a**:

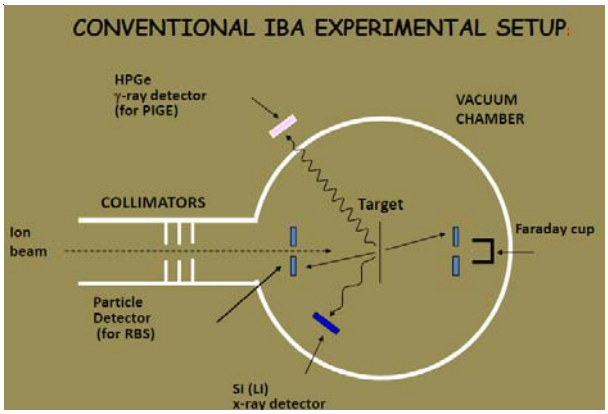

Fig. 4a A conventional IBA Set-up for PIGE and PIXE along with RBS for Current monitoring

Fig. 4b PIGE facility at FOTIA with scattering chamber and HPGe detector

External PIGE (beam in air) at FOTIA, BARC

Conventional PIGE setup requires sample in pellet form, sample ladder which fixes the no of samples and high vacuum inside sample chamber (> 10^{-6} torr). Thus the method of analysis becomes slow, in the process of satisfying all these conditions. If beam is extracted in air like in external PIGE, this method becomes rapid thus reducing the turnaround time of analysis as well as overcome the sample pellet preparation and irradiation limitations of conventional PIGE method. Necessary for direct analysis of "as received" samples in non-standard geometry motivated us for the setup of external PIGE at FOTIA using Tantalum window (25 μm thickness) and collimator (~ 2 mm diameter) where the beam is extracted in air thus making the method simpler for irradiating samples with any geometrical size and shape. Several windows like aluminium, Si_3N_4 (100-200 mm thick), Upilex have been reported for extracting the proton beam in air, here we have used Ta as window material. The proton beam energy on the target was 3.5 MeV and the experimental setup with sample holder, detector with shielding and the beam exit window has been shown in Figs 5 (a) and (b) and external PIGE facility for the analysis of non-standard geometry sample was shown in **Fig 5 (c)**.

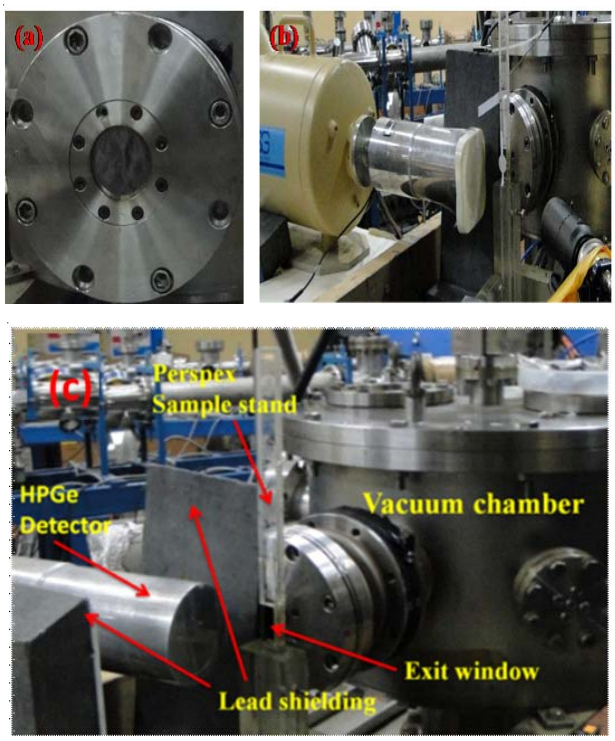

Fig. 5 (a) Tantalum window (25 μm thick) used for the extraction of proton beam **(b)** External (in air) PIGE setup with a sample holder (for hanging pellets) and HPGe detector (for detecting prompt γ-rays from samples during proton irradiation) and (c) External PIGE for "as received" non-standard geometry samples

The *in situ* current normalized and conventional PIGE methods:

Concentration calculation

The count rate *R* (counts per second, cps) of gamma-

rays of interest emitted in bombardment of a thick target by a proton beam of energy (E_{max}) is given by [35],

$$R(cps) = \left[\frac{\rho . N_A . \theta . C}{M}\right] . I_o . \varepsilon_r . \int_{E_{max}}^{0} \frac{\sigma(E) dE}{\left(dE/dx\right)_E} \qquad (3)$$

where N_A is the Avogadro number, M is the atomic mass, r is elemental density (in g cm^{-3}), e_r is the absolute detection efficiency, q is isotopic abundance of analyte, I_o is the beam current, ó$(E)$is the energy dependent gamma-ray production cross-section for a particular nuclear process, $(dE/dx)_E$ is the stopping power of target (S) at the beam energy E and C is the concentration (wt% or mg kg^{-1}) of analyte in the pellet. The count rate ratio of a gamma-ray corresponding to an element/isotope in the sample (Sam) and the standard (Std) is given by,

$$\frac{R_{Sam}}{R_{Std}} = \frac{C_{x,Sam}}{C_{x,Std}} \times \frac{(I_o)_{Sam}}{(I_o)_{Std}} \times \frac{S_{Std}}{S_{Sam}} \qquad (4)$$

When exact sample composition is unknown the stopping power correction is difficult. In the case of powder samples, they are mixed with cellulose or graphite as the major matrix and care is taken to achieve same stopping powers of sample and standard pellets for the proton beam and thus the ratio becomes unity. Then the above equation becomes simple as given below.

$$\frac{R_{Sam}}{R_{Std}} = \frac{C_{x,Sam}}{C_{x,Std}} \times \frac{(I_o)_{Sam}}{(I_o)_{Std}} \qquad (5)$$

Now it is necessary to know the value of beam current ratio $[(I_o)_{Sam}/(I_o)_{Std}]$, which is an important aspect in accelerator-based experiments. The beam current variation in thick sample is monitored or normalized by measuring the current directly from the conducting sample or by RBS method using thin foils like Au and Ag in which backscattered particles are measured using a Si based surface barrier detector kept at a fixed backward angle with respect to the ion beam. In our work, we have optimized an *in situ* current normalization approach wherein an element namely F or Li not present in the sample and having higher sensitivity in PIGE, is mixed homogenously in the sample and standard in constant amount. If it is difficult to mix with the samples like paraffin wax or any metal and alloy, the in situ current normalizer (like Al) can be kept or wrapped over the sample and standard. The variation of beam current, if any, is obtained by measuring simultaneously the count rate of element of interest and the *in situ* current normalizer.

$$\frac{R_{Sam}}{R_{Std}} = \frac{C_{x,Sam}}{C_{x,Std}} \times \frac{(S)_{CN,Sam}}{(S)_{CN,Std}} \qquad (6)$$

This method does not demand sample to be conducting and also does not require a separate arrangement (like RBS set-up) for current measurement. The count rate (R in counts per second, CPS) of the gamma-ray of interest is normalized with the sensitivity (S = CPS per unit mass or concentration) of the added element to account for the current variations, if any, during the experiment. This normalization procedure makes the analysis independent of any fluctuation in beam current during irradiation as the count rate of the current normalizing standard as well as the element of interest changes proportionally with the beam current. For thick and non-conducting samples, if RBS method is used taking thin gold foil, then above concentration ratio can be written as,

$$\frac{R_{Sam}}{R_{Std}} = \frac{C_{x,Sam}}{C_{x,Std}} \times \frac{R_{RBS,Sam}}{R_{RBS,Std}} \qquad (7)$$

where R_{RBS} is the count rate of gold peak in RBS spectrum.

Similarly for conducting sample, where current is measured from the target, the equation can be written as,

$$\frac{R_{Sam}}{R_{Std}} = \frac{C_{x,Sam}}{C_{x,Std}} \times \frac{Q_{Sam}}{Q_{Std}} \qquad (7)$$

Where Q is the total charge in µC. Further details of calculations are found in our publications [18, 28]. Some of the results are briefly discussed below. Relevant nuclear data of some of the common elements were tabulated in **Table 1**.

Table 1. Thick target gamma-ray yields (Counts/µC/Sr) of some relevant proton induced reactions of low Z elements [7,8]

Element	Reaction	Eg (keV)	Yield at 4 MeV proton	Yield at 7 MeV proton
Li	^{6}Li (p, γ) ^{7}Be	429	1.1x10^{7}	NA
	^{7}Li (p, p'γ) ^{7}Li	478	8.1x10^{7}	3.6x10^{8}
	^{7}Li (p, n γ) ^{7}Be	429	2.6x10^{7}	4.3x10^{7}
Be	^{9}Be (p, αγ) ^{6}Li	3526	2.5x10^{6}	1.95x10^{8}
B	^{10}B (p, αγ) ^{7}Be	429	1.1x10^{7}	NA
	^{10}B (p, p'γ) ^{10}B	718	3.0´10^{6}	1.2´10^{8}
	^{11}B (p, p'γ) ^{11}B	2125	1.1´10^{6}	2.8´10^{8}
C	^{12}C (p, p'γ) ^{12}C	4439	NA	7.5x10^{8}
	^{13}C (p, p'γ) ^{13}C	3089	4.1´10^{4}	NA
N	^{14}N (p, p'γ) ^{14}N	2313	5.4x10^{4}	1.8x10^{7}
O	^{16}O (p,γ) ^{17}O	495	2.2´10^{3}	NA
	^{16}O (p, p'γ) ^{16}O	6129	NA	1.2x10^{7}
F	^{19}F (p, p'γ) ^{19}F	110	1.1x10^{7}	NA
	^{19}F (p, p'γ) ^{19}F	197	4.3´10^{7}	NA
	^{19}F (p, p'γ) ^{19}F	1236	6.8x10^{6}	NA
	^{19}F (p, α'γ) ^{16}O	6129	5.0x10^{7}	1.94x10^{8}
Na	^{23}Na (p, p'γ)^{23}Na	440	3.9´10^{7}	7.3´10^{8}
	^{23}Na (p, p'γ)^{23}Na	1636	NA	4.8´10^{8}
	^{23}Na (p, p'γ)^{23}Na	1951	2.6´10^{7}	NA

Mg	^{24}Mg (p, p'γ)^{24}Mg	417	4.5x10^5	NA
	^{24}Mg (p, p'γ)^{24}Mg	585	1.2x10^6	NA
	^{24}Mg (p, p'γ)^{24}Mg	1369	NA	7.3x10^8
Al	^{27}Al (p, p'γ) ^{27}Al	844	7.5´10^6	3.8´10^8
	^{27}Al (p, p'γ) ^{27}Al	1014	1.6´10^7	5.0´10^8
Si	^{28}Si (p, p'γ) ^{28}Si	1779	1.0´10^7	2.1´10^8
	^{29}Si (p, p'γ) ^{29}Si	1273	8.7´10^5	NA
	^{30}Si (p, γ) ^{31}P	1266	3.6´10^5	NA
P	^{31}P (p, p'γ) ^{31}P	1266	8.9´10^6	9.7´10^7
	^{28}Si (p, αγ) ^{28}Si	1779	1.1´10^6	5.2´10^7
S	^{32}S (p, p'γ) ^{32}S	2230	8.9x10^5	6.2x10^7
Cl	^{35}Cl (p, p'γ) ^{35}Cl	1763	6.8x10^5	9.5x10^7
K	^{39}K (p, p'γ) ^{39}K	3019	NA	1.8x10^7
	^{41}K (p, p'γ) ^{41}K	1214	1.4x10^5	NA
Ca	^{40}Ca (p, p'γ) ^{40}Ca	3736	NA	7.4x10^7
	^{40}Ca (p, p'γ) ^{40}Ca	3904	NA	8.6x10^7
Ti	^{48}Ti(p, p'γ)^{48}Ti	983	NA	6.15x10^7
	^{48}Ti(p, p'γ)^{48}Ti	1312	NA	4.34x10^6
Ta	^{181}Ti(p, p'γ)^{181}Ti	135	NA	
	^{181}Ti(p, p'γ)^{181}Ti	165	NA	

Results and discussion

Barium borosilicate glass (BaBSG) is a promising matrix for nuclear waste vitrification and such glass samples with varying composition of Si, B, Al and Na with F were prepared to examine the retention or loss of F during vitrification at a higher temperature. Typical Gamma ray spectrum of barium borosilicate by PIGE method using 4 MeV proton beam was shown in **Fig 6**. Both conventional and *in situ* current normalized PIGE method were utilized for determination of total F as well as other low Z elements (Si, Al, Na, B and/or Li) as a part of chemical quality control (CQC) exercise [18,19]. The concentrations of low Z elements were obtained with total propagated uncertainties within ±3.0%, which are due to uncertainties on peak areas of analyte of interest of sample, standard and *in situ* current normalizer and their corresponding masses. The %loss of F is in the range of 5-12%, for borosilicate glass with added F concentration in the range of 0.2-3 wt% [19].

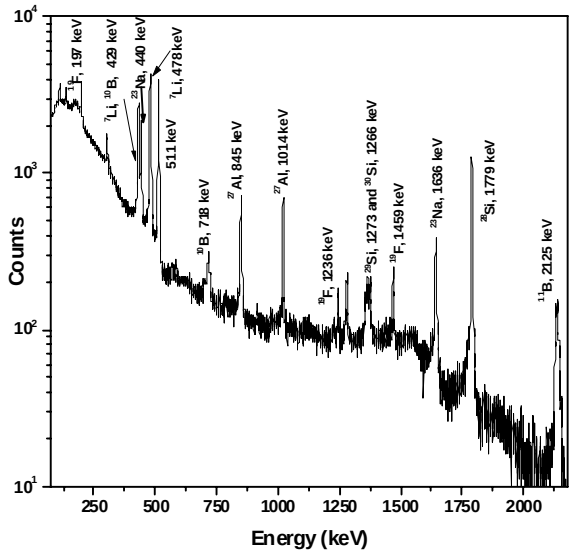

Fig. 6 Gamma-ray spectrum of a barium borosilicate glass sample in PIGE irradiated using 4 MeV proton beam

The PIGE method was extended for analysis of archaeological artifacts for quantification of major elements like Si, Al and Na [20, 21]. The chemical composition of clay potteries is strongly related to the sources of clay, from which they have been prepared. Compared to major elements, trace elements like transition elements as well as REEs are more suitable for provenance study as they have similar geo-chemical and/or non-volatile properties. In our studies on archaeological artifacts, we have indicated that both major elements (Si and Al) by PIGE [20] and trace elements like transition elements by PIXE [21] are useful for provenance/ grouping study. Bothe ceramics and glass samples frequently used in forensic studies [22].

The *in situ* current normalized PIGE method (using F as current normalizer) was extended for the determination of lithium and other low Z elements in sol-gel synthesized (i) Li doped neodymium dititanate [23] and (ii) lithium titanate (Li_2TiO_3) [24] and lithium aluminate ($LiAlO_2$) [25], which are difficult to be analyzed using wet chemical methods. PIGE method using 4 MeV proton beam was further used for the determination of Li and Ti in Li_2TiO_3 and Li and Al in $LiAlO_2$, which are important proposed tritium breeder blanket materials in proposed D-T based fusion reactor under ITER programme [24,25]. Li concentrations in the range of 11.0-12.7 wt% and Ti concentration in the range 42.7-44.7 wt% (by PIGE and INAA) were determined. As O could not be determined using 4 MeV proton beam, PIGE method using 8 MeV proton beam was developed for simultaneous determination of Li, Ti and O **(Fig. 7)** [26]. Experiments were carried out using samples in graphite matrix and RBS method using thin Au foil for the current measurement. The *in situ* current normalized PIGE method applied to lithium iron phosphate ($LiFePO_4$) based Li-ion rechargeable batteries. While synthesizing these samples lithium has a tendency to sublime, hence a more amount of lithium is used. In order to know exact amount of Li in synthesized Li-ion batteries with respect to added Li, PIGE method using F as in situ current normalizer was applied 27]. The results helped to take slightly

higher Li during preparation, so that intended stoichiometric compound can be prepared for its desired application.

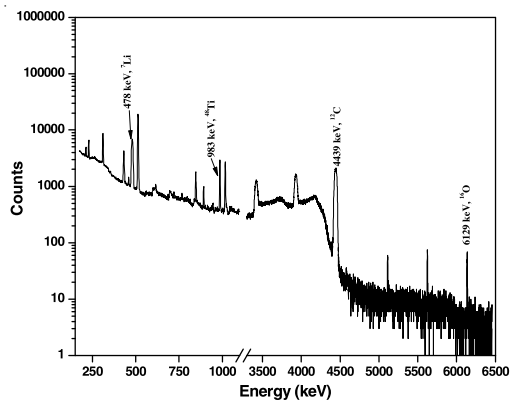

Fig. 7 Gamma-ray spectrum of a lithium titanate sample (showing peaks of Li, Ti and O) irradiated using 8 MeV proton beam

Isotope specific nature of PIGE was advantageously utilized for simultaneous quantification of total boron as well as its isotopic composition (IC) i.e. $^{10}B/^{11}B$ atom ratio in natural and enriched boron-based samples. Boron based materials find extensive applications in various fields including nuclear technology due to its high thermal neutron absorption cross section. Various solid boron-based materials (like boric acid, boron carbide, rare-earth and Ti and Ti-Cr based refractory borides) are extensively used in nuclear industry as control/ shutoff rods and shielding against neutrons. In situ current normalization was carried out using F for total boron concentration determination. In addition to the knowledge of total boron, PIGE was helpful for its isotopic composition ($^{10}B/^{11}B$ atom ratio) and ^{10}B atom% (which gives ^{10}B enrichments) with respect to their natural abundances of 19.8 atom% (^{10}B) and 80.2 atom% (^{11}B). The total boron concentrations obtained in various boron-based compounds and materials were in the range of 5-78 wt% and ^{10}B atom % was in the range of 19.8-67% [28-30]. Fig 8 describes the typical PIGE spectrum of a B_4C sample with F as *in situ* current normalizer irradiated with 4 MeV proton beam. The PIGE method was simple for determining the IC values as current normalization is not a requirement. It has been observed that for complex matrix samples including carbide and refractory matrices, PIGE is a simple and fast method for determination of IC as well as total B as compared to TIMS and ICP-MS.

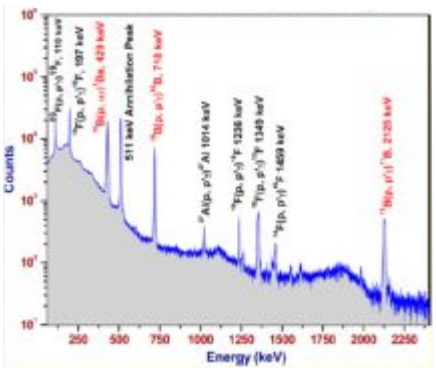

Fig. 8 Typical PIGE spectrum of a B_4C sample with F as *in situ* current normalizer irradiated with 4 MeV proton beam

Additionally, PIGE method has been used for determination of F in environmental and food samples like soil (**Fig. 9**), sediment, coal, coal fly ash, and food (rice, wheat and tea) samples. Soil and food samples from Fluoride affected and unaffected areas were collected and analyzed by in situ current normalized (taking Li as current normalizer) PIGE method using 4 MeV proton beam [31-32]. PIGE method is being applied for quantification of F and other low Z elements in various reference materials, environmental samples and ores and minerals like Rock Phosphate.

The *in situ* current normalized PIGE methods were validated (as a part of QC) by analyzing stoichiometric chemical compounds and/or reference materials from NIST and IAEA. As it was difficult to obtain suitable reference materials, the methods were validated by analyzing synthetic samples in cellulose or graphite matrix. As a part of QA/QC, in addition to validation of methods, total propagated uncertainty in the measurements and detection limits all elements of interest were evaluated. The total propagated uncertainties were arrived at from the (i) counting statistics of samples, standard, *in situ* current normalizer, (ii) uncertainties on their corresponding masses, and (iii) uncertainty on the concentration of current normalizer. The propagated uncertainties for elements of interest like F, Li, B, Si, Na, Al and Ti were in the range of ±1-5 % except for O in which propagated uncertainty was about ±8%.

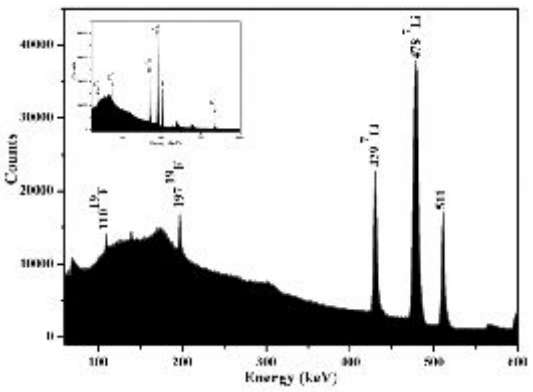

Fig. 9 PIGE spectrum of a soil sample indicating 197 keV peak of ^{19}F

Recently, we have utilized the external PIGE facility at FOTIA, BARC using low energy proton beam for the analysis of various geological, environmental and reactor materials important for the nuclear energy program having non standard geometry. In-situ current normalization in external PIGE was used with pelletized samples for quantification of low Z elements in lithium and boron based ceramics, soda lime and borosilicate glass samples [33]. Prompt gamma-rays from Tantalum window ($^{181}Ta(p,p'g)^{181}Ta$) can be utilized for current normalization and the method has been standardized for quantification of major elements in "as received" glass samples [34].Overall experimental arrangement of external PIGE was found to be simple and prompt ã-ray measurement of low Z elements could be performed with less turnaround time compared to conventional vacuum chamber PIGE method. The external PIGE has the capability for Chemical

Quality Control (CQC) of non-standard geometry samples of lithium and boron-based ceramics. The external PIGE method has capability to analyze "as received" as well as large and non-standard geometry samples as there is no restriction in sample shape and sizes since the experiment is carried out in air. In addition to non-destructive analysis of nonstandard geometry samples by external PIGE, the samples can be returned back to the user after analysis as no radioactivity is generated in the sample using this low energy proton beam. External PIGE keeps promise for its application to environmental, biological, geological, forensic and archaeological samples along with energy/nuclear based materials like alloys, oxides and carbides containing low Z elements.

Application of External (in-air) PIGE for compositional characterization in glass and ceramics and Forensic Studies

Conventional (in vacuum) PIGE requires samples to be in powder form. To make the method simple and suitable for applications in forensic, cultural heritages samples etc., it is required to restore the samples after analysis, hence direct or "as-received" analysis of samples is preferred. In this case, there is a need to find a new approach for the current measurement or current normalization for the analysis of "as received" samples. In the literature, the samples are either wrapped with thin aluminum foil or the exit window is coated with Ag/Au and variation in the beam current is monitored from the variation in the count rate of Al or the Ag/Au layer on the exit window[6,7]. J.-O. Lill [37] carried out indirect measurement of beam current using N_2 molecules or Ar gas present in the air [38]. Vilaigues et al. [39] have utilized the external micro beam PIGE/PIXE for the characterization of 15th and 16th century stained glasses. The study resulted into the important conclusion that corrosion has been taken place due the reaction of moisture and atmospheric CO_2 with the oxalic acid secreted by micro-organisms not because of acid rain . Bugoi et al.[40] have carried out the ion beam analysis of glass bracelets from 18th -19th century and found that the all the fragements had different recipes indicating their manufactures were different and can utilize for the provenance studies of the archeometric objects. Further, in 2013, they have also characterized the twenty more glass bracelet fragments from Byzyntine site from 10th -13th century AD by utilizing external PIGE/PIXE methods and identified these fragments as "mixed natron plant ash" based soda-lime glasses which are found to contain Co, Mn, Cu and Fe as chromophores [41]. The work has been extended to analyse more glass bracelets (78 in nos) fragments and glass making recipe and raw materials were also identified and pigment used for the decoration of the external surfaces was identified as lead stannate and gold alloy. Results were also confirmed that bracelets were prepared by recycling the different coloured glasses in local market [42]. Mader and Neelmeijer [43] have utilized the combination of three IBA methods namely PIGE, PIXE and RBS for evaluating the chemical stability of glass objects those are valuable for artistic and cultural heritage purposes using external proton beam at Rossendorf . We have utilized our external PIGE facility for the chemical characterization of sodalime/automobile windshield glasses and borosilicates and analytical results have showed that the class of glasses can easily be confirmed. Al was found as the one of the discriminating elements for distinguishing the glass samples among the similar type for the possible forensic applications [34]. An external (in air) PIGE method using tantalum (window material) as the external current normalizer was standardized for the first time for rapid compositional characterization of "as-received" sodalime (automobile) and borosilicate glass samples. It involves irradiation of glass fragments in air using 3.5 MeV proton beam from FOTIA and simultaneous measurement of prompt gamma-rays from proton induced reactions of isotopes of low Z elements (Si, Na, Al and/or Mg and B) and 135 or 165 keV from tantalum window (^{181}Ta). The results of external PIGE were compared with those obtained by conventional (vacuum chamber) in situ current normalized PIGE by analyzing sample pellets in a cellulose matrix. External and conventional PIGE methods were validated by analyzing both sodalime and borosilicate glass certified reference materials. The external PIGE method is found to be a rapid non-destructive method for discriminating sodalime and borosilicate glasses both qualitatively and quantitatively through their composition, which is important for forensic applications. Among the major elements determined by external PIGE, aluminum was found to be the only marker element for distinguishing sodalime (automobile) glasses. Gamma ray spectra of a borosilicate glass and automobile (sodalime) fragment irradiated with 3.5 MeV proton beam using our external PIGE facility are shown in **Figs.10 and11**,respectively. Utilization of nuclear analytical techniques (NATs) namely external (in air) PIGE and INAAare helpful for automobile glass forensics [34], as shown is Fig. 12.

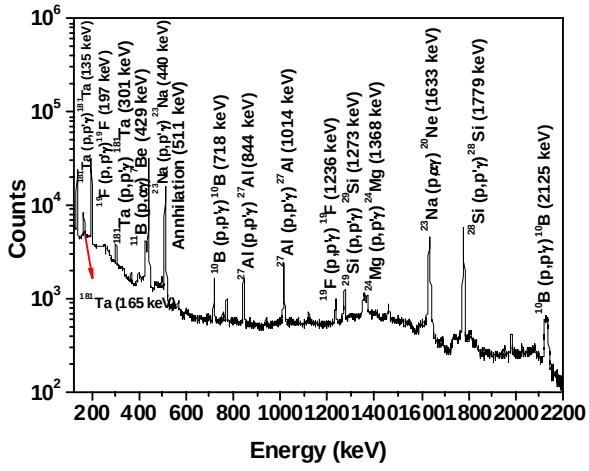

Fig. 10 Gamma ray spectrum of a borosilicate glass fragment using external PIGE with 3.5 MeV proton beam.

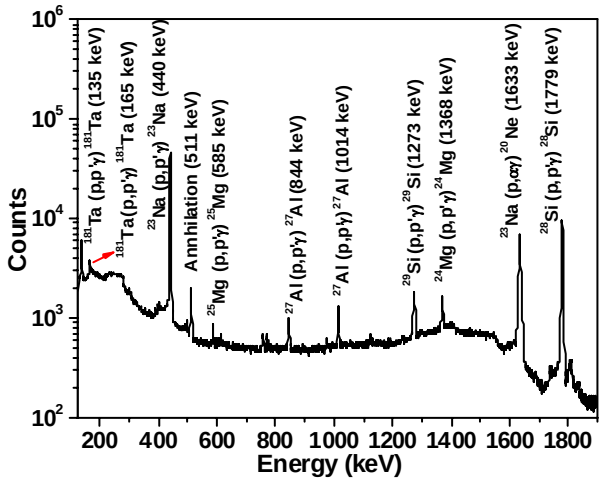

Fig. 11 Gamma ray spectrum of an automobile (sodalime) glass fragment in the external PIGE method using a 3.5 MeV proton beam.

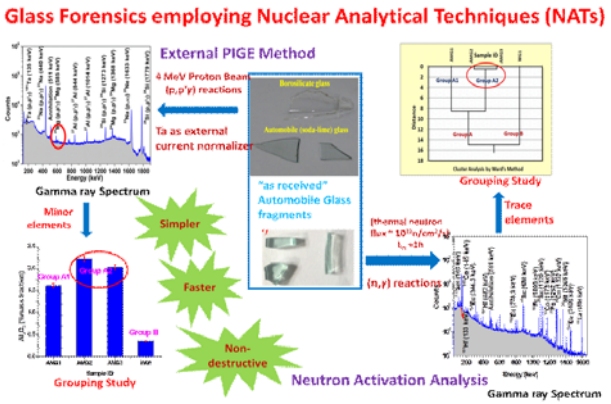

Fig. 12. Utilization of NATs (external PIGE and INAA) for automobile glass forensics

Conclusions

PIGE using proton beam is a simple, sensitive and on-line measurement technique for non-destructive quantification of most of the low Z elements in various like glass, ceramics, carbides, alloys and refractory materials. In addition to conventional PIGE method, efficacy of the *in situ*current normalized PIGE method has been successfully demonstrated utilizing 4 and 8 MeV proton beams for quantification of low Z elements in nuclear technology materials as well as in Li ion batteries and other samples. Most important is that PIGE method is capable of giving quantitative information on isotopic composition of B (^{10}B/^{11}B) and total B simultaneously in boron-based materials. Quantification of Li in Lithium based ceramics and simultaneous determination of Li, Ti and O are important contributions, which helped in preparation method optimization. Compositional characterization of glass and ceramic samples is helpful for provenance study as well as for forensic applications. PIGE keeps promise for its application to various samples of environmental, biological, biomedical and pharmaceutical importance as well as energy/ nuclear energy related materials.External PIGE with external (in situ) current normalizer (135 or 165 keV of ^{181}Ta window) is important for rapidand non-destructive characterization of non-standard geometry samples and thus keeps promise for analysis of alloys, forensic and archaeological samples.

Acknowledgments

Authors are thankful to all contributors / co-workers and operation crew members of accelerator facilities namely FOTIA, BARC, IBL, IOP and BARC-TIFR, Mumbai. Authors thank Dr. S. Krishnagopal, Head, IADD, BARC and Mr. A. Agarwal, OIC, FOTIA, IADD, BARC for their help and support.

References

1. Willy M, Nucl Instrum Methods Phys Res B35 (1988) 388–403.
2. Valkoviæ O, Jakšiæ M, Faziniæ S, Valkoviæ V, Moschini G, Menapace E, Nucl Instrum Methods Phys Res B99 (1995) 372-375.
3. Smita Z, Milavecc T, Fajfarb H, Rehrend Th, Lanktone JW, Gratuze B, Nucl Instrum Methods Phys Res B311 (2013) 53–59.
4. Macias ES, Radcliffe CD, Lewis CW, Sawicki CR, Anal Chem 50 (1978) 1120-1124.
5. Volfinger M, Robert JL, J Radioanal Nucl Chem 185 (1994) 273-291.
6. Kiss AZ, Koltay E, Nyako B, Somorjal E, Anttila A, Raisanen J, J Radioanal Nucl Chem 89 (1985)123-141.
7. Savidou A, Aslanoglou X, Paradellis T, Pilakouta M, Nucl Instrum Methods Phys Res B152 (1999) 12-18.
8. Raisanen J, Witting T, Keinonen J, Nucl Instrum Methods Phys Res B28 (1987) 199-204.
9. Sippel RF, Glover ED, Nucl. Instrum.Methods 9 (1960) 37–48.
10. Pierce TB, Peck PF, Henry WM, Analyst 90 (1965) 339–345.
11. Van Ijzendoorn LJ, Haverlag M, Verbeek A, Politiek J, de Voigt, Nucl. Instrum. Methods B113 (1996) 411–414.
12. Coote GE, Nucl Instrum Methods B66 (1992) 191-204.
13. Bejjani Nsouli A, Negra SD, Gardon A, Thomas JP, Anal Chem 82 (2010)7309–7318.
14. Mosbah M, Metrich N, Massiot P, Nucl Instrum Meth B58 (1991).227–231.
15. Saarela KE, Harju L, Lill JO, Rajander J, Lindroos A, Heselius SJ, Talanta 51 (2000) 717–725.
16. Sunitha, Y, Kumar, Sanjiv, J. Radioanal. Nucl. Chem., 314 (2017) 1803-1812.
17. Sunitha, Y, Kumar, Sanjiv, Appl Radiat Isot 128 92017) 28-35.
18. Chhillar S, Acharya R, Sodaye S, Sudarshan K, Santra

S, Mishra RK, Kaushik CP, Choudhury RK, Pujari PK, J Radioanal Nucl Chem 294 (2012) 115-119.

19. Chhillar S, Acharya R, Mishra RK, Kaushik CP, Pujari, PK, J Radioanal Nucl Chem. 312 (2017) 567-576.

20. Dasari KB, Chhillar S, Acharya R, Ray DK, Behera A, Das NL, Pujari PK, Nucl Instrum. Methods Phys Res B39 (2014)37–41.

21. Tamilarasu S, Velraj G, Ray DK, Acharya R, J Radioanal Nucl Chem., 310 (2016) 363–370.

22. Acharya R, Pujari PK, Forensic Chemistry 2018 DOI: https://doi.org/10.1016/j.forc.2018.01.002.

23. Chhillar S, Acharya R, Pai RV, Sodaye S, Mukerjee SK, Pujari PK, J Radioanal Nucl Chem 293 (2012) 437-441

24. Chhillar S, Acharya R, Vittal Rao TV, Bamankar YR, Mukerjee SK, Pujari PK, Aggarwal SK, J Radioanal Nucl Chem 298 (2013) 1597-1603.

25. Modi KB, Acharya R, Munot Samyak, Parida SC, Pujari, PK, J Radioanal Nucl Chem 314 (2017)1113-1120.

26. Chhillar S, Acharya R, Triptahi R, Sodaye S, Sudarshan K, Rout PC, Mukerjee SK, Pujari PK, J Radioanal Nucl Chem 305 (2015)463-467.

27. Halankar Kruti K, Mandal BP, Jangid Manoj K, Mukhopadhyay A, Meena Sher Singh, Acharya R, Tyagi, AK, RSC Advances 8 (2018) 1140-1147.

28. Chhillar S, Acharya R, Sodaye S, Pujari PK, Anal Chem 8 (2014) 11167-11173

29. Venkatesh K, Chhillar Sumit, Kamble Granthali S, Pande Shailaja P, Venkatesh Manisha, Kumar Sanjukta A, Kumar Sanjiv, Acharya R, Pujari PK, Reddy, AVR, J Radioanal Nucl Chem 302 (2014) 1425-1428.

30. Acharya R, Wasim Raja Sk, Chhillar Sumit, Gupta J, Sonber JK, Murthy TSR Ch, Sasi Bhushan K, Rao Radhika M, Majumdar S, Pujari PK, J Anal At Spectrom. 33 (2018) 784-791.

31. Srivastava A, Chhillar S, Kaur N, Singh D, Acharya R, Pujari PK, J Radioanal Nucl Chem 302 (2014) 1461-1464.

32. Dhorge Pooja S, Acharya R, Rajurkar N S, Chahar Vikas, Tuli Vishal, Srivastava A, Pujari PK, J Radioanal Nucl Chem. 311 (2014)1803 –1809.

33. Samanta SK, Raja SW, Sharma V, Girkar PS, Acharya R, Pujari PK Journal of Radioanalytical and Nuclear Chemistry 325 (3) (2020)923-931.

34. Sharma V, Acharya R, Bagla H K, Pujari P K ,J Anal At. Spectrom 36 (2021) 630-643.

35. J. Raisanen, Int. J. PIXE, 1992, 02, 339–350.

36. L. Beck, L. Pichon, B. Moignard, T. Guillou and P. Walter, Nucl Instrum Methods Phys Res B 2011, 269, 2999–3005.

37. J.-O. Lill, Nucl Instrum Methods Phys Res B 1999, 150, 114–117.

38. L. Giuntini, Anal. Bioanal. Chem., 2011, 401(3), 785–793.

39. M. Vilarigues, P. Redol, A. Machado, P.A. Rodrigues, L.C. Alves, R.C. da Silva, Materials Characterization 62 (2011) 211217.

40. R. Bugoi, I Poll, GH Manucu-Adamesteanu, T Calligaro, L Pichon, C Neelmeijer, F Eder Romaninan reports in physics. 63 (4) (2011) 912-922.

41. R. Bugoi, I Poll, GH Manucu-Adamesteanu, T Calligaro, L Pichon, C Neelmeijer, F Eder Journal of archeological science, 40(7) (2013) 2881-2891.

42. R. Bugoi, I Poll, GH Manucu-Adamesteanu, T Calligaro, L Pichon, C Pacheco J. Radioanal Nucl Chem, 307 (2016) 1021-1036.

43. M Mader and C Neelmeijer Nucl Instrum Methods Phys Res B 226 (1-2) (2004) 110-118.

Dr. Raghunath Acharya after joining Radiochemistry Division, BARC in 1994 is engaged in R&D work on Nuclear Analytical Chemistry utilizing research reactors and particle accelerators. He is instrumental in developing k_0-based (Single Comparator) conventional and internal monostandard neutron activation analysis (NAA) and prompt gamma NAA (PGNAA) as well as in situ current normalized Particle Induced Gamma-ray Emission (PIGE) methods for non-destructive chemical characterization of materials relevant to nuclear technology. He has developed in situ current normalized IBA and in particular conventional and external (in air) PIGE methods using proton beam from FOTIA for non-destructive determination of low Z elements in lithium-based ceramics, boron-based neutron absorbers and borosilicate glass as well as Forensic samples/automobile glasses. He obtained his PhD degree in 2000 from University of Mumbai and pursued his Postdoctoral studies in Dalhousie University, Canada during 2000-2002. His R&D work has resulted in 145peer reviewed journal publications and more than 250 conference presentations. He is a recipient of IANCAS Dr. Tarun Datta Memorial Award 2003, Young Scientist Award 2008 (YSA 2008) of the International Committee of Activation Analysis (ICAA) and "Scientific and Technical Excellence Award" of the DAE for the year 2009. Currently, he is heading the Nuclear Analytical and Accelerator Chemistry Section of Radiochemistry Division, BARC.

Dr P.K. Pujari joined the 28th batch of BARC Training School after completion of MSc (Chemistry) from IIT, Delhi. He received Homi Bhabha medal as topper of the chemistry Discipline in 1985. Subsequently he joined the Radiochemistry Division and has been specializing in positron annihilation spectroscopy and its applications. He has developed a state of the art positron laboratory at Bhabha Atomic Research Centre (BARC). He has received T.D. Memorial young scientist Award (1997), Japan Society for the promotion of Sciences (JSPS) Fellowship (1998-2000), DAE-SRC Outstanding Research Investigator Award (2008) and Homi Bhabha Science and Technology Award (2008). He has been a visiting professor to Osaka University. Dr. Pujari is a Distinguished Scientist and he is a Senior Professor at the Homi Bhabha National Institute as well as Director of Radiochemistry and Isotope Group and Head, Radiochemistry Division, BARC. Presently, he is the Vice President, IANCAS and President Elect (2021-2024) of IANCAS and President of ASSET.

Rutherford Backscattering Spectrometry (RBS) for Characterization of Materials

Sumit Kumar[1], G. L. N. Reddy[2], B. S. Tomar[3]

[1]Radioanalytical Chemistry Division, Bhabha Atomic Research Centre, Mumbai-400085
[2]National Centre for Compositional Characterization of Materials, BARC, Hyderabad
[3]Institute Chair Professor, Homi Bhabha National Institute, Mumbai-400094
[Email: sumitk@barc.gov.in, glnreddy@barc.gov.in, bstomar@barc.gov.in]

Abstract : Material analysis, in terms of composition and diffusion depth analysis, is of central importance for functional materials. In the present article, two important ion beam analysis techniques, namely, Rutherford backscattering spectrometry (RBS) and Elastic recoil detection analysis (ERDA), have been covered starting from the description of the underlying principles behind these two techniques followed by some of their applications in composition characterization and depth profiling in materials ranging from thin films, amorphous materials (glass) and bulk samples.

1. Introduction

Ion Beam Analysis (IBA) refers to a multitude of techniques which probe surface and near surface regions of the materials. In IBA an energetic beam of ions, called projectiles, produced from an accelerator, is impinged on the target material. Upon bombarding the target material, various interactions take place, emitting different kinds of particles or radiations which carry intricate information about the target material. Based on the kind of interaction and particle being detected different IBA techniques have emerged. These are (1) Rutherford Backscattering spectrometry (RBS), (2) Elastic Recoil Detection Analysis (ERDA), (3) Particle Induced X-ray emission spectroscopy (PIXE),(4) Particle Induced ?-ray emission (PIGE) and (5) Nuclear reaction analysis (NRA). These well-established surface analytical techniques are widely used in materials science, semiconductor industry, environmental sciences, biological sciences etc. In the present articlebasic aspects of RBS and ERDA techniques and their applications to material science has been discussed.As in some cases, particularly while using protons as projectile, the projectile energy might be above the Coulomb barrier for its interaction with target nuclei, the scattering is no more pure Coulombic and hence the term Backscattering spectrometry is used in such cases. However, for the sake of general description, the term RBS has been used in this article.

2. Rutherford Backscattering Spectrometry:

This IBA techniquefacilitates rapid and non-destructive multi-elemental characterization of the materials in surface and near surface regions (Chu et al [1]).Along with the elemental identification, it enables quantification and depth distribution studies. In combination with ion channeling investigations, it as well provides crystal structure and defect information. As RBSis based on first principles, itdoes not require any material standard for characterization. It is known as RBS in the honor of Lord Rutherford who first successfully explained the famous gold foil experimental results leading to the discovery of the atomic nucleus.

RBS experiments are carried out, under ultra-high vacuum, by impinging a mono energetic (E_0; typically 0.5 – 4 MeV) beam of ions of mass M_1, known as projectiles, on target atoms of mass M_2 and detecting the energy of scattered projectiles at backward angle (an angle (è) more than 90º) with respect to the incident beam direction. Incident and scattered beam direction arenear-normal to sample surface and co-planner. The energy, E_1, of the scattered projectiles depends on E_0, M_1, M_2 and è and is defined by K ($=E_1/E_0$)followingthe principles of elastic collision. K is referred as kinematic factor. From principles of elastic collision, it follows that for a backscattering event to take place $M_1<M_2$. The fraction of particles backscattered, which is a measure of scattering cross section (ó), depends on E_0, è , Z_1, Z_2 and to a lesser extent on M_1, M_2 , where, Z_1 and Z_2 are the atomic number of projectile and target atoms respectively. Another important aspect of RBS is its depth perception which arises from the stopping power/ stopping cross section, which is the energy lost by projectile while traversing the target material. RBS has a typical depth resolution of 20nm. Concepts like Kinematic factor, scattering cross section, stopping cross section, detector resolution and straggling, play crucial role in RBS. A short introduction of these important concepts has been given below for the convenience of the reader.

2.1. Kinematic factor, K:

It is the relation between scattered energy, E_1, and incident energy, E_0, of the projectile, in laboratory frame of reference, $K=E_1/E_0$. The kinematic factor, K is a function of M_1, M_2 and ???and is given by equation (1.1)derived from conservation of kinetic energy and linear momentum of the projectile and target before and after the collision. A schematic representation of elastic collision between a projectile of mass M_1, velocity v_0, energy E_0 and a target of mass M_2 at rest is given in Fig.1.1.

$$K_{M_2} = \left\{ \frac{\left[1 - \left(M_1/M_2\right)^2 \sin^2\theta\right]^{1/2} + \left(M_1/M_2\right)\cos\theta}{1 + \left(M_1/M_2\right)} \right\}^2 \quad \text{—} \quad (1.1)$$

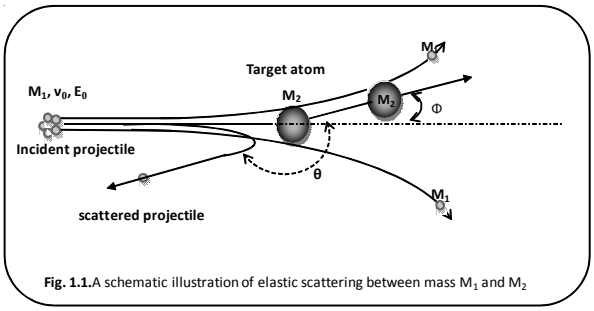

Fig. 1.1.A schematic illustration of elastic scattering between mass M_1 and M_2

In a backscattering experiment, for a projectile of known mass M_1 and energy E_0, by measuring the energy, E_1, of the backscattered particle at a specified angle ?, M_2 can be determined by using $K=E_1/E_0$ and equation 1.1. The difference in projectile energies scattered from different M_2 is maximum at most backward angles. As a result, the mass resolution in RBS is maximum at the most backward angles. This is the reason why RBS measurements are done by keeping the charged particle detector at an angle close to 160° or 170° with respect to the incident beam direction.Further, RBS has better mass resolution for low Z elements as compared to high Z elements.

The above interpretations result from the equation (1.2)

$$\Delta K = \frac{\Delta E_1}{E_0} = (4-\delta^2)(M_1/M_2{}^2)\Delta M_2 \quad \text{——————} \quad (1.2)$$

Where, $\delta = \pi - \theta$ (in the vicinity of 180°)

This is best illustrated in figure 1.2, where the backscattering energy and backscattered yield for some of the elements are shown. Maximum energy separation in the backscattered projectile can be obtained for nearby masses by (a) increasing the incident energy, E_0 (b) increasing the mass M_1 of the projectile and (c) detecting the scattered particle near 180°.

1.2. Scattering cross section, σ:

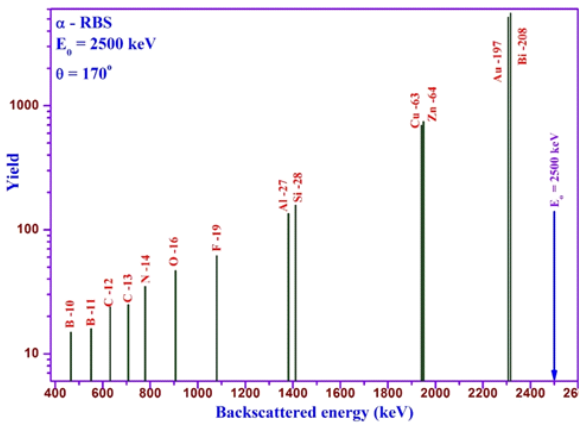

Fig 1.2 Backscattered energy and yield for different elements for α particles.

It is the probability of a projectile beingscattered by a target atom for a given energy in a particular direction. In laboratory coordinate system, it is given by Rutherford's formula for differential scattering cross section, $d\sigma/d\Omega$ and has dimensions of area, and unit as barn (1barn = 10^{-24} cm^2)

$$\frac{d\sigma}{d\Omega} = \left(\frac{Z_1 Z_2 2e^2}{4E}\right)^2 \frac{4}{\sin^4\theta} \frac{\left\{\left[1-\left(\left(M_1/M_2\right)\sin\theta\right)^2\right]^{1/2} + \cos\theta\right\}^2}{\left[1-\left(\left(M_1/M_2\right)\sin\theta\right)^2\right]^{1/2}} \quad \text{——————} \quad (1.3)$$

where, M_1, Z_1 are mass and atomic number of projectile atom and M_2, Z_2 are that of target atom, *e* and W are electronic charge and solid angle, respectively. $d\sigma/d\Omega \infty 1/E^2$ means RBS yield is higher at lower energy of the projectile resulting in higher sensitivity. This is the reason why RBS is carried out with low energy ion beams. Typically 2 MeV alpha particles are used for RBS measurements. $d\sigma/d\Omega \infty Z_2{}^2$ means higher the Z, higher the sensitivity (**Fig 1.2**). Thus the detection limits for higher Z elements are lower than that for lower Z elements.

The scattering cross section enables elemental quantification by determining scattering yield and using following expression.

$$A = .Nt\frac{d\sigma}{d\Omega}d\Omega.Q \quad \text{——————} \quad (1.4)$$

Here, A is the number of scattered projectile atoms detected, *N* is the number of targets atoms per unit volume and t is the thickness of the target, dΩ is the solid angle subtended by the detector at the targetand Q is the total number of incident particles impinged on the target.

2.3. Non-Rutherford cross section, σ_{NR} :

At sufficiently high energies the cross-sections deviate from Rutherford's formula due to the influenceof the nuclear force. At high energies the distance of closest approach between the projectile and target nuclei reduces to nuclear dimensions and nuclear forces begin to influence the scattering process. The value of scattering cross section is strongly dependent on energy, scattering angle and on the combination of projectile and target nuclei. For certain combination of projectile and target nuclei, non- Rutherford cross section, σ_{NR}, exhibit resonance. Utilization of these, σ_{NR} and its resonances for materials characterization is known as elastic (non-Rutherford) backscattering spectrometry (EBS). The prominent ones are $^{16}O(???)^{16}O$ and $^{12}C(???)^{12}C$ resonant scattering at 3.05 and 4.265 MeV which have cross sections 22 and 123 times σ_{RBS} respectively (Feng et al.[2], Leavitt et al.[3]). These scatterings are widely used for determination of oxygen and carbon. **Fig 1.3** shows the 3.05MeV a-backscattering spectrum of SiO_2(675nm) film on Silicon substrate. The signal of oxygen and Si from film and substrate are marked. It can be seen that due to EBS cross-section oxygen signal is prominently seen. The figure also shows the simulated spectra using EBS and RBS cross-sections. The EBS technique enables sensitive depth profiling of oxygen in different materials (Reddy et.al [4]).

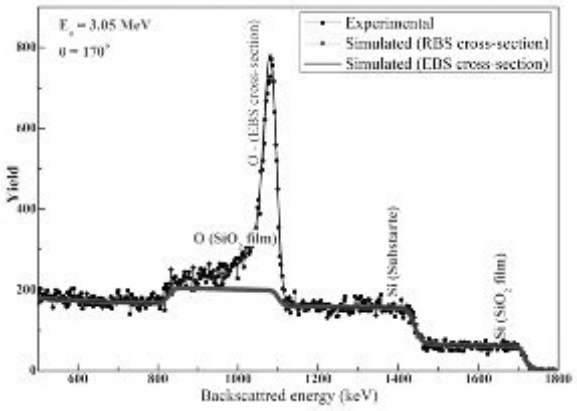

Fig 1.3 EBS investigation of SiO_2 film on silicon substrate

Figure 1.3 a-EBS spectrum of SiO_2(675nm)/Si

2.4. Stopping cross section, ε :

It isone of the most important parameters in ion beam analysis which lends depth perception capability to the technique. The energy dissipated, *dE*, by a projectile, at energy E, while traversing in a target material is known as the stopping power S(E), and is given by

$$S(E) = \frac{dE}{dx} \text{ ———————— (1.5a)}$$

The stopping cross section, ε, is given by

$$\varepsilon = \frac{1}{\rho} S(E) \text{ or } \varepsilon = \frac{1}{N} S(E) \text{ —— (1.5b)}$$

where, ρ and N are the target densities in terms of gm/cm^3 and atoms/cm^3 respectively. ε is expressed in terms of keV/(mg/cm^2) or keV/(atoms/cm^2) where mg/cm^2 and atoms/cm^2 are known as areal densities. A projectile while traversing in a target material loses its energy by two processes: (a) excitation and ionization by inelastic collision with the electrons, known as electronic energy loss, ε_e and (b) by small angle scattering with the target atom nuclei, known as nuclear energy loss, ε_n. For the energy regions of ion beam analysis (0.5 – 4 MeV), predominant contribution is from electronic energy loss. The electronic stopping power is given by

$$(dE/dx)|_e = NZ_2[4\pi(Z_1e^2)^2/m_e v_1^2]\ln(2m_e v_1^2/I) \text{ ——— (1.6)}$$

where, m_e is mass of electron, 'I' is the average overall excitation and ionization energies of the target atom

Fig 1.4 shows the energy loss of α–particle in magnesium target. It can be seen that electronic energy loss is the predominant process and is almost linear in the energy region of interest (0.8 – 4 MeV) for RBS studies. Further, electronic energy loss increases with decrease of energy. This feature is sometimes utilized in the analysis of very thin films, where beam energy is decreased to obtain perceptible energy width, ΔE_1, in backscattering spectrum.

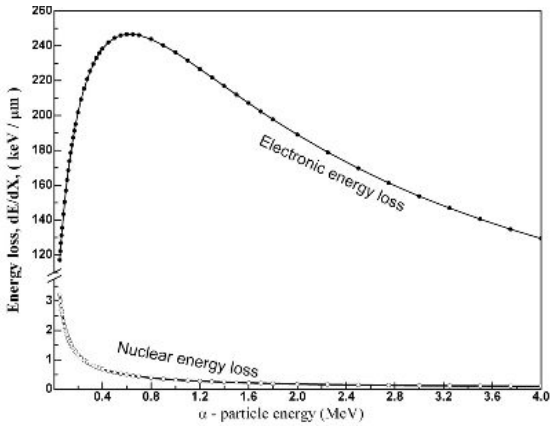

Fig 1.4. Energy loss spectrum of α–particle in magnesium target

It is in contrast to the earlier proposition, in section 2.4., that energy of incident particles need to be increased for good mass resolution. In view of such intricacies, a judicious choice of experimental parameters is desirable for an effective and more meaningful RBS analysis.

The stopping cross section for a multi-elemental target is given by the weighted average of individual elemental stopping cross sections and is known as Bragg's rule. For a compound of A_mB_n the stopping cross section is given by

$$\varepsilon^{A_mB_n} = m\varepsilon^A + n\varepsilon^B \text{ ———————— (1.7)}$$

The stopping cross sections for different projectiles in varying target materials can be calculated using a popular software program, Stopping and Range of Ions in Matter (SRIM) [5].

2.5. Straggling Σ:

Due to the statistical nature of the energy loss process of projectiles while travelling in the target, energy of the projectiles will have a spread and is described by straggling. The expression for energy straggling is given by,

$$\Sigma^2 = 4\pi.(Z_1e^2)^2.Z_2.Nx \text{ ———————— (1.8)}$$

where, Z_1 and Z_2 are atomic numbers of projectile and target atom, and N is the atomic density and *x* is the depth in the target material.

For a target material of more than one element, the Bragg's rule applies. Since straggling contributes to beam energy spread, it affects the mass and depth resolution.

2.6.Detector energy resolution:

Silicon solid state detectors (or silicon surface barrier detectors, SSBD) are used in RBS measurements for the energy analysis of backscattered particles. For good mass and depth resolution the energy resolution of the SSBD has to be very good.The depth resolution R which is given by the relation,R = FWHM/(dE/dX). where FWHM is the full width at half maximum of the monoenergetic charged particles in the spectrum using SSBD (i.e detector energy resolution), and dE/dX is the stopping power of the target for the

backscattering ions. Depth resolution of a few nanometers is commonly achieved in typical RBS experiments. As is clear from the equation, heavier ions as projectile give higher depth resolution owing to high dE/dX. However, the energy resolution of silicon detectors is different for different projectiles. It is poorer for heavier projectiles. Further, multiple scattering of the back scattered ions complicates the spectra and should be taken into consideration while analyzing the data.

For proton the energy resolution is typically 12 keV. It puts limit on the ultimate depth and mass resolution in RBS. However, by utilizing electrostatic and magnetic analyzers, energy resolution can be improved to better than 2 keV, which in turn gives better mass and depth resolution.

Fig 1.5 shows scattering of projectile of mass M_1, energy E_0, from the surface and from the depths of the target material of mass M_2 and the resulting backscattering spectrum. The projectile, on its inward journey in the target material losses energy continuously and reaches energy E (< E_0) before getting backscattered at depth *x*. After backscattering and on its outward journey (with energy *K*×E) it again loses energy continuously. Since ε is function of energy, various approximations exist for calculating å during its inward and outward journeys. Surface energy approximation is widely used for smaller depths, where å is calculated at E_0 and KE_0 energies for inward and outward journeys respectively. These energy losses are represented by stopping cross section factor, [ε] and is used for calculating the thickness of the films.

$$[\varepsilon]_0 = \frac{K}{\cos\theta_1}\varepsilon_{E_0} + \frac{1}{\cos\theta_2}\varepsilon_{KE_0} \qquad (1.9)$$

$$x = \frac{\Delta E}{[\varepsilon]_0} \qquad (1.10)$$

Here depth '*x*' is measured in atoms/cm^2 or gm/cm^2. To obtain thickness or depth in linear scale *x* needs to be divided by the density of the target. Composition and thickness are calculated using equations 1.4 and 1.10 respectively. It is widely used for characterization of thin films. Various simulation programs exist such as SIMNRA, RUMP, DATA Furnace to fit the RBS experimental data and to extract the thickness and depth distribution of different elements. RBS is ideally suited for the analysis of high Z elements. The detection sensitivity is poor for low Z elements in high Z matrix. However, caution must be exercised while analyzing RBS data with regard to accidental channeling (Feldman [6]), roughness of the films (Prity Rao et al [7] and the references therein), charging effects etc.

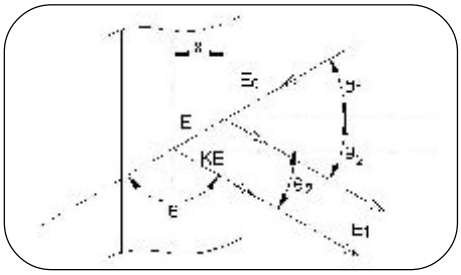

Fig 1.5 Backscattering from the sample surface and from the depths

With the above concepts forming the basis for the RBS technique, it is a powerful multi-elemental analytical tool for unraveling compositionand thickness of thin films and for diffusion studies. **Fig 1.6** shows the schematic of a typical experimental setup for carrying out RBS experiments. After mounting the samples, the scattering chamber is pumped down to 1×10^{-6} mbar vacuum using turbo-molecular pump (TMP). A well collimated beam of ions (protons, α particles) is impinged on the specimen. The total number of particles being impinged on the specimen is measured using a current integrator (CI). An electron suppressor is used to measure true current. The backscattered particles are detected using SSB detector. The signal from the detector is fed to the pre-amplifier and spectroscopy/shaping amplifier and recorded using well calibrated multichannel analyzer.

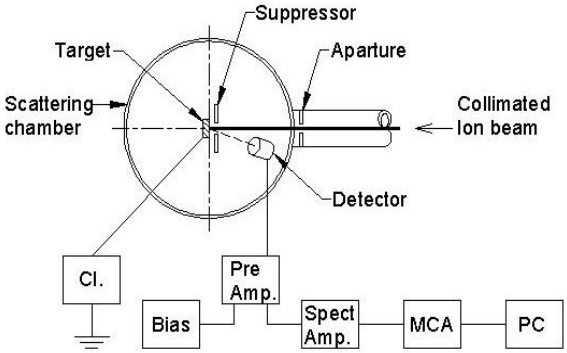

Fig 1.6 Schematic of RBS experimental setup

The multi-elemental nature of RBS technique is clearly evident from Fig 1.7 where the experiments were carried out using 3.6 MeV á particles at normal incidence (beam parallel to surface normal) and at a tilt angle incidence (beam at an angle with surface normal) on an unknown multilayer coating sample, to unravel its layer structure.At tilt angle the trajectory of the incident beam across any of the films in the sample is lengthened by the 'secant' of the tilting angle. In effect, the top layer now appears correspondingly thicker, and the signal from the underlying elemental films is shifted toward lower energies. The signal of the top layer widens correspondingly, but the high-energy edge of that signal remains fixed on the energy scale. The signal whose high-energy edge does not change position upon tilting the sample thus identifies the top layer. By these measurements at two incident angles, it is possible to unravel the total number of layers and the ordering of layers based on the energy shift of the elemental signals. This experiment, combined with the other IBA techniques, was used to determine the number of layers and their positioningand compositionof unknown multilayer coatings on ZnS substrate.

3. Elastic Recoil Detection Analysis (ERDA) :

It is the technique of choice for quantifying and depth profiling light elements in materials, specifically for hydrogen and can be considered as complimentary to RBS. It is based on the detection of recoiling light atoms in the forward direction (??< 90°) when the target is impinged with heavier projectiles (i.e. $M_1 > M_2$) in glancing angle geometry. The physical concepts of ERDA, similar to RBS, follow the

kinematics of elastic collision of two body system and the kinematic factor (of recoil atom), scattering cross section and stopping powers enable elemental identification, quantification and depth profiling respectively. Much like RBS, ERDA enables fast and simultaneous multi elemental (light elements) depth profiling with reasonable sensitivity. Since the principles of elastic collision do not allow recoiling of projectiles more than 90°, ERDA is carried out at ??less than 90°.

The expressions for kinematic factor and scattering cross section are given below

$$K = \frac{4M_1M_2\cos^2\Phi}{(M_1+M_2)^2} \qquad (1.11)$$

$$\sigma(E) = \frac{[Z_1Z_2e^2(M_{1+}M_2)]^2}{[2M_2E]^2\cos^3\Phi} \qquad (1.12)$$

and the yield equation is given by

$$Y(E) = \frac{Q.N.\sigma.\Omega.\delta E}{\cos\theta_1.dE/dx} \qquad (1.13)$$

where M_1, Z_1 and M_2, Z_2 are mass and atomic number of projectile and recoil atoms respectively, ??is scattering angle, ?? is angle between surface normal and incident beam direction, N is the target atom density, Ω is the solid angle, Q is the number of particles impinging on the target.

However, to construct depth profiles, unlike RBS, the stopping cross section of heavy projectile for inward journey and the stopping cross section of recoiling light atom in outward journey need to be considered. Fig 1.7 shows the schematic of ERDA experimental geometry. It can be seen that, in a marked difference to RBS geometry, a stopper foil is placed in front of the silicon detector to prevent entering of the scattered projectiles into the detector and thereby to reduce the background. Most often mylar foil is used as stopper foil and whose thickness depends on the mass and energy of the projectiles and also on the mass of the recoiling light atoms that need to be analyzed. It is to be noted that even recoiling light atoms also lose energy, ΔE, in mylar foil before entering the silicon detector. Hence the energy of recoiling atom will be KE - ΔE.The energy loss of recoiling light atoms again depends on their masses.

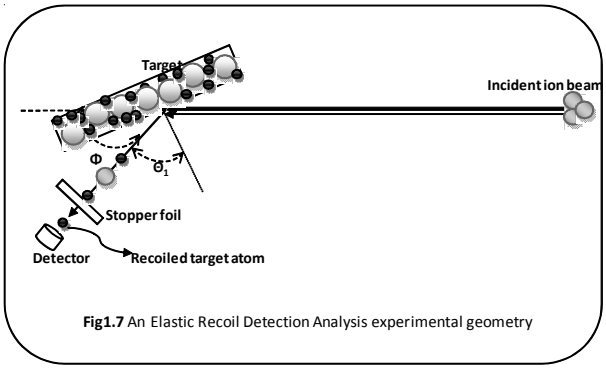

Fig1.7 An Elastic Recoil Detection Analysis experimental geometry

Fig1.8 shows how the energies of recoiled light atoms vary, upon bombardment with 24 MeV Cl^{5+} beam, after passing through 6?m mylar foil (Tesmer J.R. et al.[8]). Because of the presence of stopper foil the ERDA data analysis becomes a bit cumbersome. However, the use of stopper foil can be avoided by using heavy projectile and placing the detector above a critical angle $?_c = \sin^{-1}(M_2/M_1)$ at which the projectile cannot be scattered kinematically.

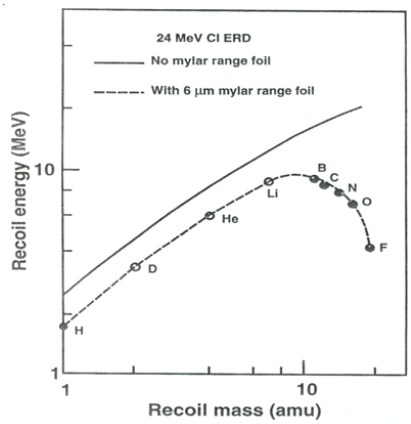

Fig 1.8 Energies of recoiling light atoms,after bombardment with 24 MeV Cl^{5+} beam, before and after passing through 6ìm mylar foil

4.Applications of RBS and ERDA

4.1 Application of RBS to thin layers

The RBS technique has beenextensively employed in the inter-diffusion and hydrogen and de-hydrogenation studies of Pd/Mg bi-layer films (Kumar et al [9-12]). **Fig 1.9** shows the 1.5 MeV a-RBS spectra of an as-deposited as well as annealed Pd (50 nm)/Mg (300 nm)/Si films. The experiment has clearly brought out the diffusion of Pd into the Mg layer. Based on these measurements the diffusion coefficients were determined. **Fig 1.10** shows 3.6 MeV α-RBS of 21-layered SiO_2/TiO_2multilayer Fabry–Perot interference narrow band-pass filter developed by using a reactive electron beam deposition process. The detailed geometries of the TiO_2 and SiO_2 layers, and their thickness, elemental composition were determined. The thickness of the individual layers ranged from 200 to 400 $x10^{15}$atoms/$cm^2$with an intermediate TiO_2 space layer of 700 $x10^{15}$ atoms/cm^2 thick (Sahoo et al [13]). The experimental spectrum is well fitted with the simulated spectrum using SIMNRA. **Fig 1.11** the 6.0 MeV Li-RBS of 43-layered SiO_2/HfO_2coatings.

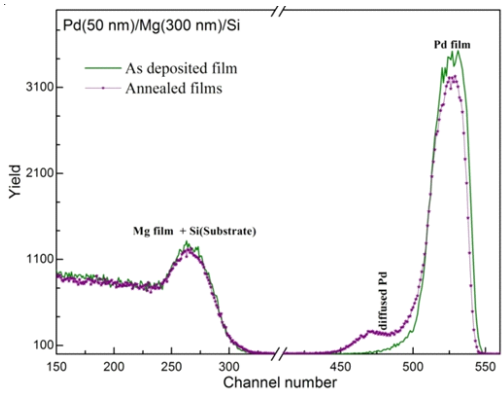

Fig 1.9 1.5 MeV α-RBS spectra Pd/Mg/Si films

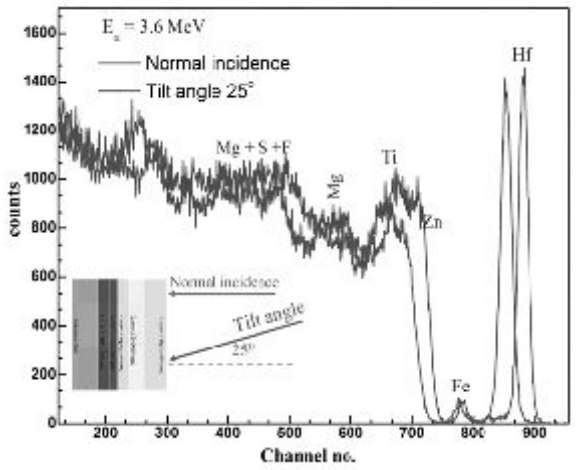

Fig 1.10 3.6 MeV α-RBS of 21-layered SiO_2/TiO_2multilayer

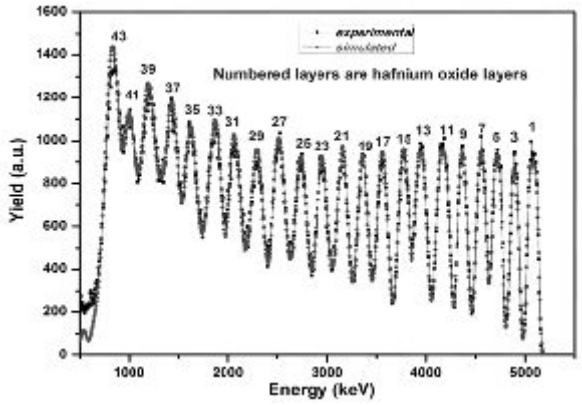

Fig 1.11 6.0 MeV Li-RBS of 43-layered SiO_2/HfO_2 multilayer coatings

4.2. Heavy-ion RBS (HIRBS) Study of radionuclides diffusion in glas **s matrix**

High level liquid waste (HLW) generated from reprocessing of spent nuclear waste is vitrified in borosilicate matrix which, after an interim storage period, is to be buried in deep underground geological repository [14]. Depending upon the constituents of the HLW, additives are added to the glass matrix to facilitate the homogenous glass formation ensuring solubility of entire HLW constituent elements in a single phase final waste form, e.g., Barium is added to inhibit phase separation due to sulphate presence in HLW. Conventionally the long term chemical durability of waste forms is studied using leaching experiments, which take long time and usually are performed with Na^+ as a marker.

RBS can be used to study the diffusion of immobilized fission products in the glass matrix at nanometre scale, which in turn can help understand the long term chemical durability of glass waste form. Long term chemical durability of such waste form has been studied using RBS. Heavy ion ($^{19}F^{5+}$) beam was used as projectile in the study of the diffusion of fission products ^{137}Cs and ^{90}Sr in the glass matrix. Heavy ion Rutherford Backscattering Spectrometry (HIRBS) provides better depth resolution than normal RBS with low energy light charged particles (e.g., 2 MeV alpha) owing to higher linear energy transfer (LET) of the heavier ion.

Diffusion profiles of the fission products in the glass samples were produced by annealing a thin layer of fission products sandwiched between two polished-surface cylindrical glass pieces at different temperatures. **Fig 1.12** represents the experimental diffusion profile of Cesium in borosilicate glass. The nominal composition of the studied glass (mol%) is SiO_2 : 69; Na_2O: 5; K_2O: 2.9; Al_2O_3: 1.1 and B_2O_3: 22.A methodology was developed to generate concentration vs. depth profile from the RBS spectra; details of the methodology have been discussed in ref. [15]. Subsequently the depth profile was fitted with the thin film solution of first law of Fick's second law of diffusion to obtain diffusion coefficient. Increasing temperature was found enhancing diffusion of Cesium (**Table 1**) in the glass matrix with the activation energy barrier for diffusion is 22.2 ± 3.6 kJ/mol.

Temperature (K)	Annealing time (s)	Diffusion coefficient ($m^2 s^{-1}$)
473	43200	$(2.70 \pm 0.16) \times 10^{-19}$
573	43200	$(5.79 \pm 0.35) \times 10^{-19}$
673	43200	$(1.47 \pm 0.15) \times 10^{-18}$

Table 1.Diffusion coefficients of Cesium in borosilicate glass below glass transition temperature (Tg = 723 K).

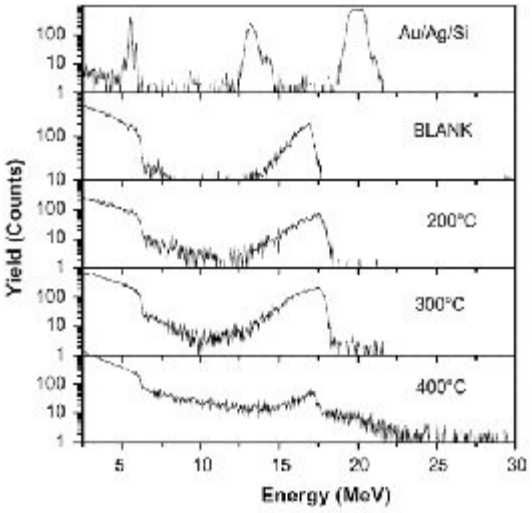

Fig 1.12 Heavy-ion RBS (HIRBS) spectra of Cesium diffusion in borosilicate glass samples created at different temperatures. Top figures shows the HIRBS spectrum of the silicon wafer having thin layers of gold (~100 nm) and silver (~10 nm) on one surface, used for energy calibration.

Table 2 Composition of glass and activation energy for cesium diffusion in borosilicate glasses having varying boron content [17].

Sample	SiO_2	B_2O_3	Na_2O	K_2O	Al_2O_3	E_a (kJ/mol)
A	69.0	22.0	5.0	2.9	1.1	22.2 ± 3.3
B	69.0	15.0	12.0	2.9	1.1	15.0 ± 2.3
C	69.0	5.0	22.0	2.9	1.1	9.0 ± 1.4

Diffusion rates have been reported to be dependent upon several factors, such as glass transition temperature, glass composition and concentration of the exchanging cations.

Increasing boron composition in the borosilicate glass has been found increasing activation energy barrier for Cesium diffusion (**Table 2**).The obtained activation energies have been found to be close to those expected for ion exchange mechanism responsible for diffusion in glasses [16].

Sample	SiO_2	B_2O_3	Na_2O	K_2O	Al_2O_3	E_a(kJ/mol)
A	69.0	22.0	5.0	2.9	1.1	22.2±3.3
B	69.0	15.0	12.0	2.9	1.1	15.0±2.3
C	69.0	5.0	22.0	2.9	1.1	9.0±1.4

Table 2 Composition of glass and activation energy for cesium diffusion in borosilicate glasses having varying boron content [17].

Na (glass)↔Cs (surface) exchange has been proposed in this study for Cesium diffusion in borosilicate glasses having varying amount of boron and sodium.

In another study, diffusion of strontium in the glass was studied using barium as the analogue for strontium keeping the content of alkali (Na) and alkaline elements (Ca) constant (~25 wt %) in the borosilicate glass. Diffusion coefficient (~10^{-17} m^2s^{-1}) for barium diffusion was found increasing with calcium content. Presence of calcium increased the rigidity of the glass network rigid thereby hindering inter-diffusion between Ba(II) and Na(I) ions. The activation energy for Ba(II) diffusion in borosilicate glass with and without Ca are 23.6 (± 0.28) and 18.6 (± 0.22) kJ/ mole, respectively [18].

Though HIRBS method may be quite helpful in delineating diffusion profile of higher valence metal ions in glass and other substrates owing to high linear energy transfer and hence high depth resolution, multiple scattering will be progressively contaminating single scattering data. Proper methodology need to be employed to isolate the single scattering data to get correct diffusion coefficient value.

4.3 Depth profile of metal ions in a polymer inclusion membrane (PIM):

Measurement of the distribution of organic carrier and metal ions across the thickness of the membrane provide valuable information about the quality of the membrane.

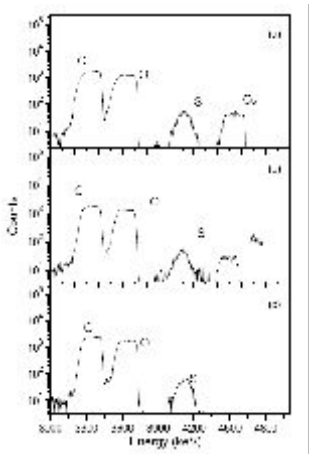

Fig 1.13 BS spectra of PIMs (a) Blank PIM, (b) Ag^+ loaded PIM and (c) Cs^+ loaded PIM.

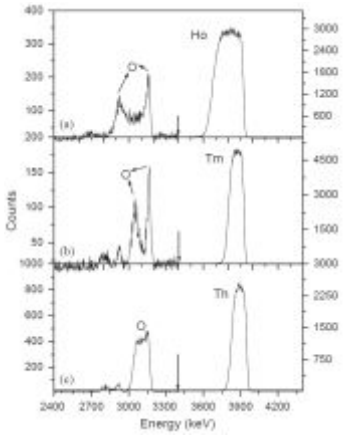

Fig 1.14 BS spectra of Oxygen in Ho, Tm and Th metal foils using 4 MeV proton beam. Left- and right- hand sides of the vertical scale are different. Spectra with different scale are separated by arrow.

Tripathi et al. usedbackscattering spectrometry (BS) employing 4.8 MeV proton beam from Folded Tandem Ion Accelerator (FOTIA) at Trombay for the depth profiling and quantification of Cs^+ and Ag^+ ions having different hydration radii, in PIMs. As the proton energy is above the Coulomb barrier for light elements, backscattering is not purely Columbic. The metal ions were used as a probe to investigate the distribution of the organic carrier molecule, assuming the distribution of the metal ion and the carrier to be same. The metal ion was found to be uniformly distributed across thethickness of the PIM (**Fig 1.13**) indicating the uniform distribution of the carrier molecule throughout the membrane [19].

In one of the unique application of BS, thickness of oxide layer on the front and back surface of rare earth metal foils (due to oxidation) was determined as shown in **Fig 1.14.**

Summary

In the cluster of IBA techniques, RBS can be used as a primary reference technique for the best traceable accuracy available in non-destructive model-free methods for a large array of samples, especially for thin films. Choice in case of lighter elements targets shifts to ERDA. As it is well known that no technique is universal, IBA techniques (RBS & ERDA) as well carry their unique advantages and limitations. These limitations are largely overcome with proper choice of experimental setup and synergistic use of IBA methods.

References

1. Chu W.K., Mayer J.W., Nicolet M.A.; Backscattering spectrometry, Academic press Inc, 1978.
2. Feng et al. Nucl. Instrum. Methods B 86 (1994) 225.
3. Leavitt et al.Nucl. Instrum. Methods B 44 (1990) 260.
4. Reddy et al.Appl. Surf. Sci.253 (2007) 7230.
5. James F Ziegler, http://www.srim.org/
6. Feldman L.C.; Materials Analysis by Ion Channeling Academic press Inc, 1982

7. Rao,P., Kumar, S. Nucl.Instr. Meth. B (2010)
8. Tesmer J.R., Natasi M., et al; Hand book of modern ion beam analysis, Materials Research Society (1995).
9. Kumar et al.J Alloys Compd, 476 (2009), 500.
10. Reddy et al. J. Alloys Compd 481 (2009) 714.
11. Reddy et al. J. Hydrog. Energy 43 (2018)2840.
12. Sunitha et al. Appl Surf. Sci., 256 (2009) 1553.
13. Sahoo et al.Appl. Opt. 52 (2013) 2102.
14. Audero et al.J. Nucl. Mater. 223 (1995) 151.
15. Tomar, et al. Nucl. Instr. and Meth. B 227 (2005) 391.
16. Ojovan, M. I.: 6th International Conference on Nuclear and Radiochemistry, Aug. 29 – Sep. 3, 2004, aachem, Germany, Extended abstracts (Qain, S. M., Coenen, H. H., eds.) ForschungszentrumJulich (2004) p. 631.
17. Kumar. et al. Radiochim. Acta 94 (2006) 343.
18. Kumar, et al. Nucl. Instr. and Meth. B 266 (2008) 649.
19. Tripathi, et al. Nucl. Inst. Meth. B. 211, (2003) 138.

Dr. Sumit Kumar, Scientific officer (G), RACD received his Ph. D. from HBNI, Mumbai and carried out Postdoc work on Synchrotron based X-ray absorption and emission spectroscopy for geometrical and electronic structure determination of radionuclides. His current research interest is in delineating sorption mechanism of radionuclides on iron oxide surfaces under various chemical conditions.

Dr. G. L. N. Reddy did his M.Sc.(1996), Physics, from Osmania university and M.Phil.(1997), Physics, from University of Hyderabad and joined BARC after successful completion of one year orientation course from 41st batch of BARC training school. His areas of expertise are Ion Beam Analysis (IBA) of materials, development of thin film and bulk materials for energy and semiconductor technology applications, materials characterization by X-ray diffraction, Atomic Force Microscopy and Scanning Electron Microscope (SEM).

Dr. B.S. Tomar is a Raja Ramanna Fellow at Bhabha Atomic Research Centre and Institute Chair Professor, Homi Bhabha National Institute, Mumbai.Dr. Tomar did his M.Sc. in Chemistry from Garhwal University in 1979 and joined Radiochemistry in 1982 after graduating from 25th batch of BARC Training School. He has worked in the area of nuclear fission, heavy ion reactions, ion beam analysis, perturbed angular correlation and actinide speciation and has published more than 200 papers in international journals. Dr. Tomar is a faculty of Mumbai University and Homi Bhabha National Institute (HBNI). He served as Dean of chemical sciences (BARC) as well as Convener, Board of Studies, Chemical Sciences, HBNI. So far 16 Ph.D. and 3 M.Sc. students have obtained their degrees under his supervision from Mumbai University and HBNI.

Dr. Tomar was a visiting Professor to Technical University, Delft, Netherlands during 2007-2008. He was invited by IAEA to serve as an expert on Radiation Detection and Measurement and as a member of the Standing Advisory Group on Safeguards Implementation. He has received the DAE special contribution and group achievement awards for his contribution towards the strategic programmes of the Department. Dr. Tomar superannuated recently as Director, Radiochemistry & Isotope Group, BARC.

Nuclear Reaction Analysis: Principles and Applications

Sanjiv Kumar

National Centre for Compositional Characterization of Materials
Bhabha Atomic Research Centre, ECIL Post, Hyderabad-500062
Email: sanjukumar@barc.gov.in

Abstract: Nuclear reaction analysis is a prominent ion beam analysis technique. It utilizes particle-particle and particle-gamma nuclear reactions for probing the surface and near-surface regions of materials. Sensitivity to low Z-elements, depth profiling using resonance or non-resonance nuclear reactions and isotope tracing are some of the important features of this technique. It can be performed with low /medium energy particle accelerators using protons, deuterons, a-particles or beams of nitrogen, fluorine etc. as probes. The measurements are performed in vacuum, and g-ray and charged particle detectors are some of the basic gadgetries. A concept of stopping power is required for designing the experiments and also for qualitative and quantitative spectral analysis. In this article an effort has been made to present the basic aspects of nuclear reaction analysis. In addition, a few examples are also described to highlight these aspects and to demonstrate the prowess of nuclear reaction analysis in materials development.

1. Introduction:

Nuclear reaction analysis (NRA) is a prominent ion beam analysis (IBA) technique for probing elemental composition and depth distribution in surface and near surface regions of materials [1]. As the name suggests, the technique utilises a nuclear reaction, preferably with a high Q-value and involves *prompt* measurement of one of the reaction products. The projectiles often used in the nuclear reactions are protons, deuterons, a-particles or such heavy ions as ^{15}N, ^{19}F etc. The energy of a projectile, depending on the nature of the reaction, may vary from ~100 keV to several MeV. The reaction products can be a charged particle, g-rays or both as in [$^{11}B(p,a)2a$], [$^{27}Al(p,g)^{28}Si$] and [$^{1}H(^{19}F,ag)^{16}O$] respectively. NRA is isotope specific and usually enables its interference free determination. The detection sensitivity of NRA varies from percentage to trace levels. Sensitivity to light elements and non-destructive depth profiling capability are the two most attractive features of NRA which make it a powerful surface technique, particularly in the area of thin film technology. It is worthwhile mentioning that such surface analytical techniques as X-ray photoelectron spectroscopy (XPS), Auger electron spectroscopy (AES) or secondary ionization mass spectrometry (SIMS) also provide the detection of light elements but depth profiling by these techniques is destructive as it is accomplished by sputtering.

2.Concepts essential to NRA

2.1 Energetics

The utilization of NRA requires a comprehensive understanding of kinematics and energetics of a nuclear reaction. A nuclear reaction, depicted pictorially in **Fig.1**, is characterized by Q value. If the Q value is +ve , the reaction is exoergic and if it is –ve the reaction is endoergic. For all endoergic reactions there is a threshold energy for the incident particles below which reaction cannot occur. This threshold is always greater than the absolute value of Q and is given by equation 2.

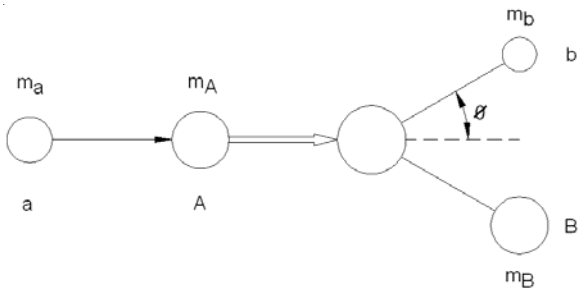

Fig.1 A schematic of a nuclear reaction ('m' represents the mass of ions)

$$Q = (m_B + m_b - m_A - m_a)\cdot c^2 \quad \text{MeV} \quad \text{---(1)}$$

$$E_{th} = -Q \cdot \frac{m_B + m_b}{m_B + m_b - m_a} \quad \text{MeV} \quad \text{---(2)}$$

The energy of ejectile depends on Q value and the angle of emission. As mentioned earlier, reactions with high +Q values are preferred for analysis as the ejectlies would have higher energies which would facilitate better discrimination against other charged particles, e.g. backscattered ions. An extensive description of kinematics of a nuclear reaction is presented in ref.[1]. It is important to note that the energy of the ejectiles usually increases with incident beam energy. However, certain reactions exhibit 'inverse kinematics' wherein beyond certain backward angles, the energy of the ejectiles decreases with beam energy. It is illustrated in **Fig.2**. The reaction shows normal kinematics at all emission angles, however, $^{7}Li(p,a)a$ reaction exhibits inverse kinematics beyond ~120° laboratory angle. The nuclear reaction $D(^{3}He,p)^{4}He$ also follows inverse kinematics for both protons and a-particles at the backward laboratory angles of emission [2]. A list of nuclear reactions along with their Q values is given in **Table. 1.**

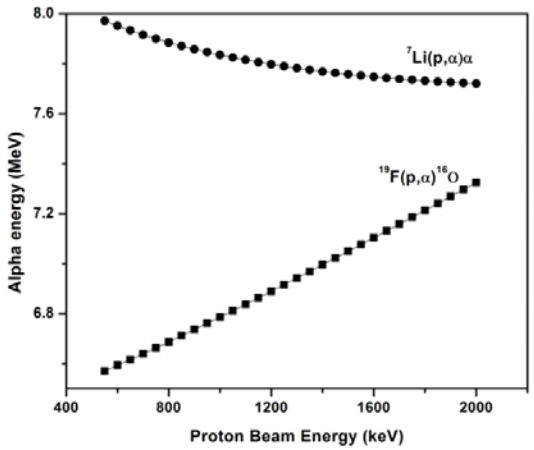

Fig.2 Energy of a particles from ^{7}Li(p,a)a and ^{19}F(p,a)^{16}O nuclear reactions emitted at 150° laboratory emission angle at different proton beam energies. Note that the ^{7}Li(p,a)a reaction shows inverse kinematics.

2.2 Stopping power and straggling:

In addition to kinematics, a concept of stopping power or stopping cross-section is essential for NRA. In fact, it is the quantity which lends non-destructive depth profiling capability to NRA or other IBA techniques. A useful treatment of stopping power is given in ref.[1]. Briefly, it provides the energy loss suffered by an energetic ion beam in traversing unit distance in a medium and is expressed in the units of keV/micron or eV/10^{15} atoms/cm^2. The stopping power has contributions from nuclear stopping and electronic stopping. The former is predominant at lower beam energies while the later, at higher beam energies. **Fig. 3** provides a general information on the relative contributions of nuclear and electronic stopping in different beam energy regions. Straggling is yet another concept central to NRA. It refers to the statistical fluctuations in the energy loss suffered by a particle and has the units of energy. It is minimal at the surface of a material and increases with depth or thickness. The occurrence of straggling deteriorates the depth resolution of the measurements.

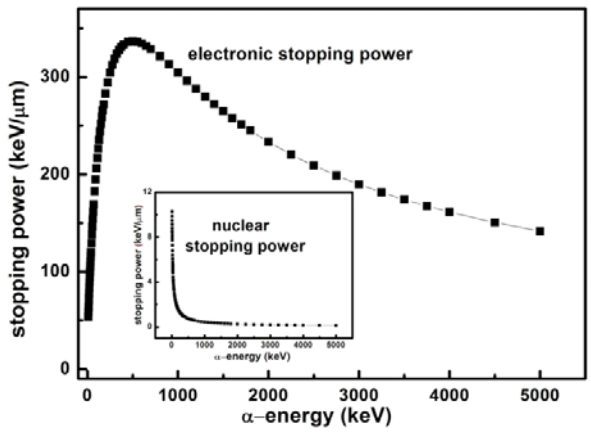

Fig. 3 The electronic and nuclear stopping powers of Si for a-particles.

2.3. Nuclear Reaction Cross Section and Quantification:

The nuclear reactions have a finite probability of occurrence which is denoted by reaction cross section and is expressed in terms of barns (1 barn = 10^{-24} cm^2). A plot of the incident particle energy vs the yield of the reaction is termed as the excitation function of the reaction. The excitation function can have elevations and or dips. It can also exhibit resonance, sharp or broad, at specific projectile energies. Such reactions are very useful for depth profiling applications. The related NRA is often referred to as nuclear resonance reaction analysis (NRRA). The resonances should be strong, narrow and isolated for sensitive and high depth resolved measurements. The widths of the resonances may range from 50 eV to several keV. Depth profiling using resonances having widths £ 500 eV is known as narrow resonance profiling (NRP). It is instructive to mention that depth profile measurements can be accomplished by non-resonant reactions as well. Incidentally, it is true only for reactions involving particle-particle interactions.

Elemental (isotopic) identification and quantification are the two main or rather the solitary objectives of an analytical endeavour. In NRA, the identification of an isotope is based on the energy of the ejecticles and or g-rays emitted from the nuclear reaction. The identification is usually unambiguous due to the absence of any significant interference; however, care must be excersised while determining the energy of ejecticles as these would lose energy in stopper foils or any overlying layer on the sample. So far as the quantification is concerned, two methods can be employed. The first method is based on fundamental principles wherein the concentration of an isotope is derived by solving a yield equation made up of basic factors that define the propagation of the beam in the sample, the occurrence of the nuclear reaction and the detection process. The yield equation is a complex one , but in the simplest form, the yield or the intensity of the detected radiation (Y) emitted from a layer thickness corresponding to an energy loss DE can be given by

$$Y = \frac{c \times f \times A_V}{M \times S(E)} \times N_o \times \Omega \times \varepsilon_{\text{int}} \times \int_{E}^{E-\Delta E} \sigma(E,\theta) d(E) \quad (3)$$

where c represents the concentration of the isotope and f its natural isotopic abundance; A_v, the Avogadro's number; $N_{o,}$ the total number of incident protons; W, the solid angle, e_{int}, the intrinsic efficient of detector, S(E), the stopping power at incident energy E and and s, the cross-section of the reaction at energy E and emission angle (q). The extraction of the isotopic concentration from the yield formula is apparently non trivial as it requires a knowledge of several parameters and, more importantly, that of the cross-section of the nuclear reaction as function of beam energy.

The second method is the relative method wherein the knowledge of the different parameters as described earlier is not mandatory. The method utilizes reference targets or standards which are examined under identical conditions as those of samples. The following formula can be used to for

the determination of element A in a binary compound of composition A_mB_n:

$$m = \frac{f \times Y_{samp} \times \varepsilon_B}{Y_{std} \times \varepsilon_{std} + f \times Y_{samp} \times (\varepsilon_B - \varepsilon_A)} \quad (4)$$

where f is atomic fraction of the element in the standard, Y_{samp} and Y_{std} are the yields for the sample and standard respectively and e_{std} , e_A and e_B are the stopping cross-sections of standard and elements A and B at the relevant beam energy. The quantification by the relative method is obviously much simpler but the reference targets should meet certain criteria; these should preferably be conducting, these should have lateral as well as depth uniformity, and must be stable in vacuum and under ion bombardment. Even as a reference target is used, accurate charge (current) measurement and reproducible energy calibration are essential for precise quantitative analysis.

So far as the depth scale is concerned, for resonance reactions it can be measured directly using the following relationship

$$x = \frac{E - E_R}{S(E)} \quad (5)$$

where E_R is the resonance energy. Similar approach is employed for the construction of depth scale by non-resonant reactions. However it is slightly complicated as one needs to take the energy loss of the projectile as well as that of ejectile into consideration for calculation. As mentioned earlier, the depth resolution depends on the width of the resonance: lower width implies better depth resolution. Moreover, the depth resolution is higher for resonances occurring at lower beam energy because stopping power is lower at higher beam energies. For nuclear reactions involving the detection of charged particle, the resolution of the detector is also a dominant factor in defining the depth resolution. The stopping powers for beams required for quantification and construction of depth scales can be calculated using a software programme, Stopping and Range of Ions in Matter (SRIM). This programme can be downloaded from web.

3. Experimental

The energetic ion beams i.e. projectiles are obtained from an accelerator; Van de Graaff or tandem. The beam is collimated to about 1-2 mm spot before it impinges on a sample fixed onto a target manipulator, which in turn, is positioned inside a chamber, generally known as scattering chamber. The scattering chamber houses such gadgetries as detectors, electron suppressor etc. A Si-surface barrier detector is employed to detect charged particles whereas a scintillation [NaI(Tl), bismuth germanate (BGO, $Bi_4Ge_3O_{12}$)] or a high purity Ge detector is used for the detection of g-rays. NRA measurements are performed in high or ultrahigh vacuum. Thus, a vacuum better than 10^{-6} torr is maintained in the accelerator, beam line and scattering chamber by a combination of rotary and turbomolecular pumps. The signals of radiations produced in the detector are processed using a combination of preamplifier and amplifier and acquired on a PC based multichannel analyzer (MCA). A typical view of a scattering chamber along with a sample manipulator and a HPGe detector for detecting the g-rays is shown in **Fig.4** for illustration. Related some common nuclear reactions along with their Q-values are compiled in **Table 1** given below.

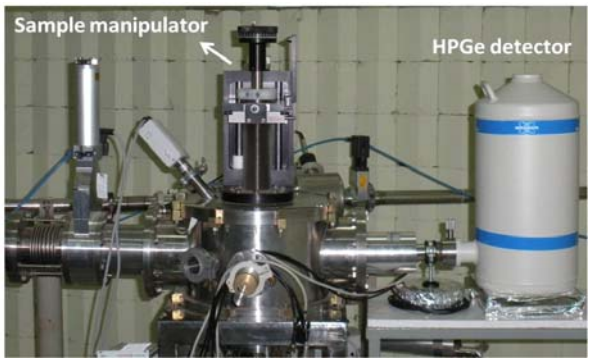

Fig.4 A view of port at the 3 MV Tandtron facility at NCCCM used for nuclear reaction analysis.

Table 1 : List of nuclear reactions and their Q-values

Proton induced reactions	**Q [MeV]**	**Deuteron induced reactions**	**Q [MeV]**	**^{3}He induced reactions**	**Q [MeV]**	**^{4}He induced reactions**	**Q[MeV]**
^{6}Li(p,á)^{3}He	4.02	^{2}H(d,p)^{3}He	4.03	^{2}H(^{3}He,p)^{4}He	18.3	^{10}B(?,p)^{13}C	4.06
^{7}Li(p, á)^{4}He	17.35	^{3}He(d, á)^{1}H	18.3	^{6}Li(^{3}He,p)^{8}Be	6.79	^{11}B(á,p)^{14}C	0.78
^{9}Be(p, g)^{10}B	6.58	^{12}C(d,p)^{13}C	2.72	^{9}Be(^{3}He,p)^{11}B	0.32	^{14}N(á,p)^{17}O	1.19
^{11}B(p, á)2á	8.58	^{13}C(d,p)^{14}C	5.95	^{9}Be(^{3}He,á)^{8}Be	18.9	^{19}F(á,p)^{22}Ne	1.67
^{15}N(p, ág)^{12}C	4.97	^{14}N(d,p)^{15}N	8.61	^{12}C(^{3}He,p)^{14}N	4.78	^{31}P(á,p)^{34}S	0.63
^{18}O(p, ág)^{15}N	3.98	^{14}N(d, á)^{12}C	13.57	^{12}C(^{3}He, á)^{11}C	1.86		
^{19}F(p,ag)^{16}O	8.11	^{16}O(d,p)^{17}O	1.92	^{18}O(^{3}He,p)^{20}F	6.87		
^{23}Na(p, ág)^{24}Mg	11.7	^{16}O(d,?)^{14}N	3.11	^{18}O(^{3}He,d)^{19}F	2.50		
^{27}Al(p, g)^{28}Si	11.6	^{19}F(d, á)^{17}O	10.03	^{18}O(^{3}He,á)^{19}O	12.51		

4. Applications

Hydrogen is probably the most common elemental contaminant in materials, especially in thin films. Its presence can have dramatic effects on the electrical, mechanical and chemical properties of materials. Hydrogen diffuses rapidly, being the smallest and lightest atom. It severely deteriorates the mechanical properties of structural materials such as Zr and Zr-based alloys by way of hydrogen embrittlement or delayed hydrogen cracking (DHC). In electronic materials it displays a range of complex behavior by acting as an amphoteric impurity. It is an indispensable ingredient in the fabrication of integrated circuits as it passivates the defects at Si/SiO2 interface. But in many cases it causes erratic performance of devices by inducing electrically active states. Similarly, the presence of hydrogen is known to decrease the superconducting transition temperature (Tc) of intermetallic (Nb-$_3$Ge) compounds. Due to these reasons the detection of hydrogen and its depth profiling is of immense interest.

NRRA involving ^{1}H(^{15}N,ag)^{12}C or ^{1}H(^{19}F,ag)^{16}O reaction is a very good method for depth profiling hydrogen on materials surfaces [3,4]. ^{1}H(^{15}N,ag)^{12}C reactions exhibits a strong and sharp (fwhm= ~1 keV) resonance at 6.38 MeV and emits 4.4 MeV g-rays. Similarly ^{1}H(^{19}F,ag)^{16}O reaction exhibits a comparatively wide (fwhm = 45 keV) resonance at 6.44 MeV. 6.1, 6.9 and 7.1 MeV g-rays are characteristic of this reaction. It can be easily observed that ^{1}H(^{15}N,g)^{12}C offers highly depth resolved (~1 nm) measurements (the depth resolution of the ^{1}H(^{19}F,ag)^{16}O reaction is ~ 23 nm). The probing depths of the two reactions is about 3 microns. Though a-particle is also a product in both reactions, measurements often involve the detection of 4.4 MeV or 6-7 MeV g-rays primarily because of the absence of any interference.

The detection and depth profiling of hydrogen in materials is a challenging task. The experimental conditions in terms of beam current, position of the detector etc. need to be optimized so as to estimate hydrogen with good sensitivity. A sensitivity of about 0.1 at.% can be obtained with an optimised detection system. Some of the materials undergo loss of hydrogen under the influence of the bombarding beam. Care must be exercised while analyzing such materials. Low beam current and target cooling are useful in alleviating such problems.

Fig.5 shows a typical g-ray spectrum from a hydrogen containing material as a result of ^{1}H(^{19}F,ag)^{16}O resonance reaction. In addition to the main photo peak at 6.1 MeV, the associated first and second escape peaks are also seen in the spectrum. The spectrum is recorded with BGO. The peaks of 7.1 MeV and 6.9 MeV are broad and comparatively much less intense. As a result, these are not clearly discernible in the spectrum. However, the area integrated between 7.1 MeV to 5.0 MeV serves as total hydrogen signal**. Fig. 6** represents the exercise of depth profiling hydrogen in a H-implanted (implantation energy = 19 keV) Si specimen. As mentioned earlier, hydrogen is ubiquitously present on the surface of a material as a contaminant. It is referred to as surface hydrogen and is clearly discriminated against the implanted hydrogen.

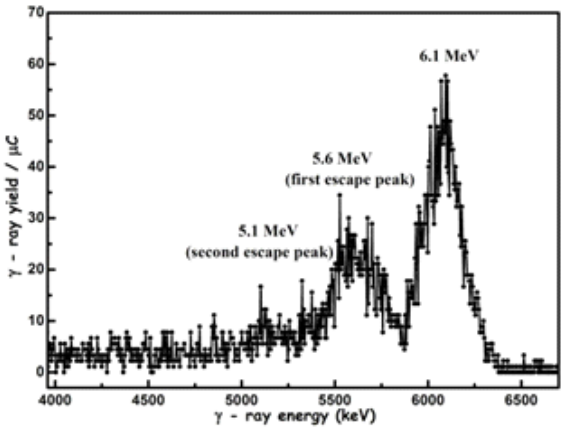

Fig.5 A g-ray spectrum from ^{1}H(^{19}F,ag)^{16}O reaction induced is a MgH_2 film on Si with 6.55 MeV $^{19}F^{+3}$ beam.

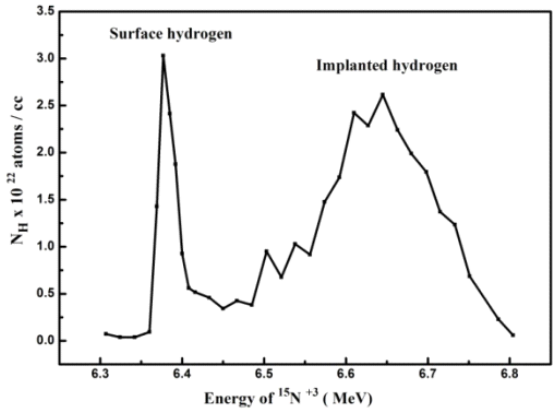

Fig.6 Profiling hydrogen in a H^- implanted Si.

6.55 MeV $^{19}F^{+3}$ beam.

So far as the determination of deuterium (D) is concerned, D(d,p)T (Q= 4.033 MeV) and D(^{3}He, p)^{4}He (Q= 18.352) are the most widely used reactions. The excitation curve of the D(^{3}He, p)^{4}He reaction exhibits a broad resonance at 0.640 keV with a cross-section of about 850 mb and a limit of detection of about 100 ppm. The best depth resolution of a few nm is obtained by recording the a-spectrum while the p-spectrum facilitates measuremts up to 8-40 micron depths, albeit with a rather poorer depth resolution [2]. The reaction, as mentioned above, is characterized by inverse kinematics at backward angles. This aspect must be taken into consideration while designing the experiment.

The determination and depth distribution of Li is required in several technologically important materials. The depth profiling of Li the anode (graphite) as well as the cathode ($LiCoO_2$) of a lithium ion battery is essential for a comprehensive understanding of Li transport, and lithiation and delithiation-the basic processes involved in the working of the device. Neutron depth profiling (NDP) (Q=4.78 MeV) using cold or thermal neutrons is the most widely used nuclear reaction for depth profiling Li in materials [5]:

$$^6Li + ^1n = ^4He(2055\ keV) + ^3H(2727\ keV) \quad (6)$$

The method is non-destructive and has a detection limit of about $9.0´10^{12}$ at./cm^2. The analysis can be performed either by detecting tritium or alpha particles. Tritium is lighter and has comparatively higher energy. Therefore it is used for profiling thicker films. The detection of a-particles provides measurements with better depth resolution.

The depth profile measurements of Li can also be accomplished by ^{7}Li(p,a)^{4}He (Q= 17.3462 MeV) and ^{7}Li(p, g)^{8}Be (Q= 17.2543 MeV) nuclear reactions [6]. The former method apparently involves the detection of a-particles and is endowed with a detection sensitivity of ~ 0.1 at.%, a depth resolution of ~ 100 nm and a probing depth of about 30 µm in the absence and ~ 3 µm in the presence of fluorine in the material. The second recation, on the other hand, exhibits a resonance at E_p = 441 keV and involves the measurement of 14.6 and 17.6 MeV g-rays, characteristic of the reaction. The method has a detection sensitivity of ~0.2 at.% and enables profiling up to a depth ^{3}20 µm with a resolution of ^{3} 150 nm. It is instructive to mention that since the reaction ^{7}Li(p,a)^{4}He has high Q value, the energy of the emitted a-paricles is substantially higher than the scattered proton energy and, therefore, the experiments can be conducted without any stopper foil. The beam current, however, must be low to avoid pulse pileup. The utilization of a stopper foil to stop the scattered proton from entering the detector allows irradiation with higher beam current but the probing depth and depth resolution of the measurements get affected.

Boron in materials, low Z matrices in particular,can be sensitively determined by ^{11}B(p,a)^{8}Be a nuclear reaction. Similar to ^{7}Li(p,a)a recation, reaction is an example of particle-particle reaction. The reaction exhibits a strong and broad resonance [cross section = 600 mb, FWHM = 300 keV] at 660 keV [7].

The detection sensitivity of the method depends strongly on the nature of the matrix. In the case of light elements such as Si the detection sensitivity is about 0.5 ppm. However the pile up of backscattered protons from high Z matrices (SS, zircaloy) limits the sensitivity of this technique to about 10 ppm. The method is interferred by ^{6}Li(p,) a, ^{15}N(^{1}H, a)^{12}C , ^{18}O(p,a)^{15}N and ^{19}F(p,a)^{16}O reactions.

In fact, the reactions ^{15}N(^{1}H, ,ag)^{12}C (E_g = 4.4 MeV) and ^{19}F(p,ag)^{16}O (E_g = 6.1, 6.9 and 7.1 MeV) are extensively utilized for depth profiling nitrogen and fluorine in materials by measuring the respective g-rays where as ^{18}O(p,ag)^{15}N has recently been shown to be very useful for the determination of bulk oxygen in materials [8-10]. The ^{15}N(^{1}H, ,ag)^{12}C reaction has strong resonances at 429 keV and 897 keV. The resonance at 429 keV is very narrow and therefore offers nanometric depth resolution. It is to be noted that these reactions are based on ^{15}N isotope; the natural isotopic abundance of ^{15}N is only 0.39% and therefore the experiments at conducted at relatively higher beam currents. The notable applications of this reaction include the analysis of nitride films and fractured steel components [11]. The later investigation, as a typical example of failure analysis, revealed nitride embrtittlement to be the culprit behind the degradation in the mechanical properties of the components. The ^{19}F(p,ag)^{16}O nuclear reaction, on the other hand, is a popular method for depth profiling fluorine using the resonances at 340.5, 872 or 1375 keV. The resonance at 340.5 keV has a width of about ~2 keV and is therefore preferred in studies requiring high depth resolved measurement analysis. In addition to the ^{19}F(p,ag)^{16}O nuclear reaction, the resonance at 1088 keV in^{19}F(p,p¢g)^{19}F (E_g = 197 keV) nuclear reaction is also useful for depth profiling fluorine. The resonance has a probing depth of about 1.5mm and provides interference free measurement of F down to ~ 10^{20} atoms cm^{-3} with a depth resolution of about 20 nm. An excitation function of the reaction in **Fig. 7** constructed using a thin film of CaF_2 as the target shows the occurrence of the resonance.

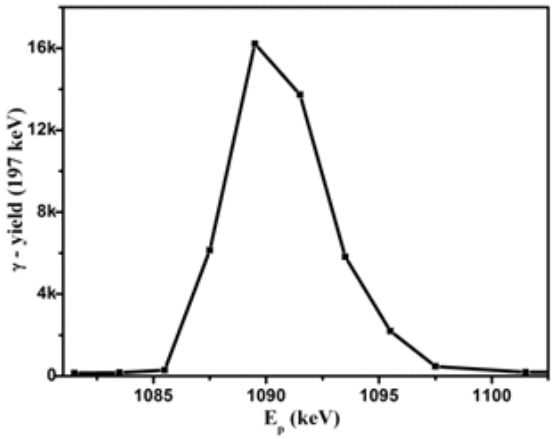

Fig.7 Yield curve of the ^{19}F(p,p'g)^{19}F nuclear reaction

In addition to light elements mentioned above and other such elements as Na, Mg,Al, S etc. NRA has also been applied for depth profiling some mid Z elements such as Ti and Cr as well [12-13]. The depth profiling of Ti can be accomplished using the resonance at 1362 keV in ^{48}Ti(p,g)^{49}V nuclear reaction (sensitivity: ~5.1×10^{20} at.cm^{-3} (~ 1at.%), probing depth :800 nm and depth resolution: of ~24 nm in Si) while that of Cr and be achieved through resonance at 1005 keV in 52Cr(p,g)53Mn nuclear reaction (sensitivity: ~ 3at.%), probing depth : 2.5 mm and depth resolution: of ~25 nm in Si). Incidentally, the determination of Ti is based on the detection of 7.9 MeV g-rays while that of Cr, on the detection of 378 keV g-rays.

NRA is also conducted using deuterons, helium-3 and helium -4 ions. Almost all the light elements undergo deuteron induced reactions. Many of these reactions have high Q values and are suitable for analytical studies. The typical examples of deuteron induced reactions include ^{16}C(d,p)^{13}C and ^{16}O(d,p)^{17}O reactions that are used for the determination of C and O respectively. It is to be noted that deuterons generate high neutron background due to the occurrence of (d,n) reactions. Therefore proper radiation shielding is a major requirement for using deuteron beams. The a-induced reactions are relatively few but ^{31}P(a,p)^{34}S is one amongst the suitable reactions for determining P in materials. Furthermore, 'Li-induced NRA has also been reported to be a useful tool for multi-element analysis of light elements in heavy matrices [14].

Conclusion:

This article provides a preliminary account of the principles and analytical capabilities of nuclear reaction analysis with a view to introduce young researchers to this wonderful technique. Nuclear reaction analysis is an eminently suitable technique ion beam analysis technique for analyzing elemental profiles in the surface regions of the materials. The prowess of the technique lies mainly in its ability to discern the depth profiles of elements, low Z-elements in particular, non-destructively. Its sensitivity to light elements is complementary to other ion beam techniques. Therefore, in combination with Rutherford backscattering spectrometry (RBS) which is more sensitive for mid or high Z elements, NRA can be effectively utilized for complete compositional analysis of materials.

References:

1. G. Deconnick, Introduction to Radioanalytical Physics, Elsevier, 1978.
2. B. Wielunska, M. Mayer, T. Schwarz-Selinger, Nucl. Instr. Meth. B 387 (2016) 103.
3. W.A. Lanford, Nucl. Instr. Meth. in Phy. Res. B66 (1992) 65.
4. Sanjiv Kumar, J.V. Ramana, C.David, V.S. Raju, S. Gangadharan, Nucl. Instr. Meth. B 142 (1998) 549.
5. S. C. Nagpurea, R. G. Downingb, Bharat Bhushana, S.S. Babuc, L. Caod, Electrochim. Acta 56 (2011) 4735.
6. Y. Sunitha, Sanjiv Kumar; Nucl. Instr. Method, B 400 (2017) 22-30
7. E. Ligeon and A. Bontemps, J. Radioanal. Chem. 12(1972) 335.
8. Y. Miyagawa, S. Nakao, L.S. Wielunski, H. Hasegawa, S. Miyagawa, Nucl. Instr. Meth. B 161-163 (2000) 997.
9. S.O.F. Dababneh, K. Toukan and I. Khubeis, Nucl. Instr. Meth. B 83 (1993) 319.
10. Sanjiv Kumar, Y. Sunitha, G.L.N. Reddy, A.A. Sukumar, J.V. Ramana, A. Sarkar, Rakesh Verma, Nucl. Instr. Meth. B 378 (2016) 38.
11. Sanjiv Kumar, S.V. Kumar, G.L.N. Reddy, V. Kain, J.V. Ramana, V.S. Raju, Nucl. Instr. Meth. B 240 (2005) 704.
12. G. L. N. Reddy, S. Vikram Kumar, J. V. Ramana, Sanjiv Kumar, J. Radioanal. Nucl. Chem. 302 (2014) 1461.
13. Pritty Rao, S. Vikram Kumar, Sanjiv Kumar, J. Radioanal. Nucl. Chem. 302 (2014) 1399.
14. J.R. Liu, Z.S. Zheng, N. Yu, W. K. Chu, Nucl. Instr. Meth. B 85 (1994) 780.

Dr. Sanjiv Kumar graduated from 30 th batch of B.A.R.C. Training School. He completed his M.Sc. from Patna University and Ph.D. in Materials Science from I.I.Sc. Bangalore. Dr. Sanjiv Kumar specializes in surface analysis of materials by ion beam analysis (IBA) and X-ray photoelectron spectroscopy (XPS). Development of materials for semiconductor technology and renewable energy are his key research areas. He is a recipient of DAE Science and Technical Excellence Award for 2008. He is currently serving as Head, National Centre of Compositional Characterization of Materials, BARC, Hyderabad.

Studies of Impurity-Defect Interactions with Ion Channeling

Sundaravel Balakrishnan

Materials Science Group, Indira Gandhi Centre for Atomic Research, Kalpakkam 603102, India
Email: bsundar@igcar.gov.in

Abstract : Ion channeling is a versatile technique which can detect lattice site location of impurity atoms and displacements of the order of 0.01 nm. Bcc Fe and FeCr alloy are model systems for ferritic steels which is one of the proposed structural materials for future nuclear reactors. Understanding solute-defect interactions is essential to enhance properties. The O interactions with defects and defect structure are studied using ion channeling and DFT calculations. In presence of excess vacancy defects, O found to be displaced 1.1 Å along <111> direction from substitutional site in Fe. DFT calculations predict similar lattice site of O for O interaction and trapping in vacancy dislocation loops. In presence of excess interstitial defects, O is found at tetrahedral interstitial site and Cr is found to be displaced 0.2 Å from substitutional site in Fe. DFT calculations predict similar lattice sites corresponding to trapping in interstitial dislocation loops. In contrast to Fe, O is found to trap in vacancy dislocation loops in presence of excess interstitial defects in Fe15at%Cr alloy, which is due to Cr segregation in both interstitial and vacancy dislocation loops. The Cr segregation affects O interaction with interstitial dislocation loops and O is trapped in Cr-segregated vacancy dislocation loops.

Introduction

Crystallographic analysis techniques rely on the interference of plane waves in the diffraction grating set up by the crystal lattice. The wavelength of the incident radiation has to be comparable to the grating spacing. For crystal lattices this means using x-rays of keV energies, electrons of ~100 eV and neutrons or atoms of energy less than 1eV. Using MeV He ions, with wavelengths the order of 10^{-12} cm, the lattice is not viewed as a diffraction grating but rather as as a real crystal of rows and sheets of atoms that collimate and steer the beam. When incident ions are aligned parallel to the crystallographic directions, which can be done by orienting the single crystalline or prefered oriented samples on a goniometer, the ions face collective interaction with atomic string potential or planar potential and penetrate deeper into the material compared to incidence angle along a random orientation and is called ion channeling [1,2]. The measurements can be carried out in forward or backscattering geometries. We have used backscattering geometry of Rutherford backscattering spectrometry (RBS).

Ion channeling is a powerful technique which can detect lattice site location of impurity atoms with a precsion of 0.01 nm [1,2]. One can study the crystalline quality [3], mosaic spread [4], tetragonal strain [5,6], tilt [3] and in-plane orientation of epilayers [5,7], type and density of defects [6,8], defect depth profile [8], surface polarity [9], mixed polymorphs [10], rms thermal vibration amplitude [11], surface reconstruction [12], relaxation [2], surface melting [13], and structural phase transitions, etc. An automated ion channeling experimental facility is set up [14] in a general purpose scattering chamber attached to the +10° beam line of 1.7 MV tandetron accelerator at Materials Science Group, Indira Gandhi Centre for Atomic Research, Kalpakkam. This chamber is mounted with a surface barrier detector for detecting backscattered ions, Si(Li) detector for detecting X-rays, NaI detector for detecting X-rays and retractable shutter to block the detector or introduce a foil before the detector. Other than ion implantation, RBS/channeling, ERDA, PIXE and NRA measurements can be carried out. Single crystalline samples can be aligned with the incident ion beam direction using a five axis goniometer. The samples can be heated upto 800°C. Low temperature experiments are possible by coupling a continuous flow cryostat with the sample holder with a flexible copper braid [15]. Lattice site position of impurity atoms (whether substitutional or interstitial) can be studied by taking tilt angular scans along two different directions using triangulation location method. The experimental data can be simulated using FLUX7 software [16]. By studying the lattice site position of impurity atoms in the presence of defects like vacancies or interstitials and comparing with theoretical calculations, impurity defect interactions can be studied.

Ferritic steel is one of the proposed structural materials for future nuclear reactors owing to the better void swelling resistance. The body centered cubic iron (bcc Fe) and iron-chromium alloys (bcc FeCr) are model systems for ferritic steel. To better understand the effect of solute on the radiation induced microstructure of ferritic steels, solute-defect interactions in bcc Fe and FeCr system have been studied by using experiment as well as theoretical calculations [17, 18]. Generally light elements (H, C, N, O and He) occupy interstitial sites and heavy elements (Mn, Cr, Cu etc.) occupy substitutional sites in bcc Fe. The interactions of different solutes present in the structural materials are driving the vacancy and interstitial cluster evolution during irradiation. The C, He, O and N solutes form clusters with vacancies and other substitutional solutes in bcc Fe and bcc Fe-X (X=Cr, Mn, Cu, Ni) alloys [19]. Among the solutes, oxygen (O) plays a crucial role on the radiation induced microstructure in iron based structural materials [17,20]. In this regard, understanding the interaction of O with radiation induced defects is important to improve radiation tolerance of iron based structural materials. In this article, the interaction of oxygen with interstitial and vacancy defects in bcc Fe and FeCr crystals studied by ion channeling experiment is discussed. It is also confirmed with density functional theory (DFT) calculations.

Interaction of oxygen with interstitial defects in bcc Fe

300 keV O^{18} ions are implanted in bcc Fe(110) single crystal ions at a fluence of $5´10^{15}$ ions/cm^2, corresponding to a maximum concentration of 0.2% and annealed at 400 °C. The projected range and straggling of 300 keV O18 ions in Fe is 275 nm and 78 nm respectively, which are obtained from SRIM [21]. The O18 ion implantation produces interstitial and vacancy defects also. The estimated peak damage from SRIM calculation is 3.5 dpa. Formation of dislocation loops is also possible at this damage level. Lattice location of O^{18} is studied by ion channeling technique. Self ions are implanted over the O18 implanted profile and annealed. Lattice location is measured again to study effect of self ion implantation. The range of defects and type of defect formed at O^{18} depth is also verified by ion channeling technique. Positron annihilation spectroscopy technique is used to study vacancy defects. Further, the O interactions with self interstitial defects are studied by using DFT calculations and compared with experiments. With the aim of introducing excess interstitials to overlap with oxygen depth profile, 750 keV Fe^+ ions with a projected range of 266 nm are introduced by subsequent implantation in Fe(110) with the ion fluence of 1×10^{16} ions/cm2 and annealed in-situ at 400 °C for 30 minutes. Total damage produced by 300 keV O^{18} and 750 keV Fe at O^{18} depth is 10.5 dpa after self ion implantation. Here after the sample is denoted as Fe1(O^{18}) and Fe1(O^{18}+Fe@R_p).

The O^{18} and Fe@R_p in the bracket represent O^{18} ion implantation and Fe^+ ion implantation at R_p of O^{18} respectively.

Fig. 1 shows the RBS/channeling spectra from pristne Fe(100) and Fe1(O^{18}) samples taken at aligned and random directions with 2 MeV He^+ ions. The ratio of the backscattering signal from aligned and random spectra taken in the window corresponding to a depth closer to the surface is called minimum yield c_{min} and it is a measure of crystalline quality. It is measured to be 8% for virgin crystal. For an ideal crystal, it has to be 1.3% along [100] and 1.83% along [110] and the measured value is of reasonable quality. The aligned spectrum after O^{18} implantation is having dechanneling step around channel number 640, at the implanted ion range due to the defects produced by O^{18} ion implantation which can be vacancies, self interstitial atom (SIA) defects which are believed to be in dumbbell interstitial configuration or other defect complexes. Oxygen, being a lighter element is not clearly visible at this energy, riding over the large background from Fe signal. For detecting Oxygen, the O^{18} signal is obtained by detecting the out coming á-particle yield from the well-known O^{18}(p,á)N^{15} nuclear reaction which has a broad resonance width at 820 keV (shown in **Fig. 2**) and Q-value of 3.981 MeV [22]. Corresponding RBS/channeling spectra are also taken with the proton beam (not shown).

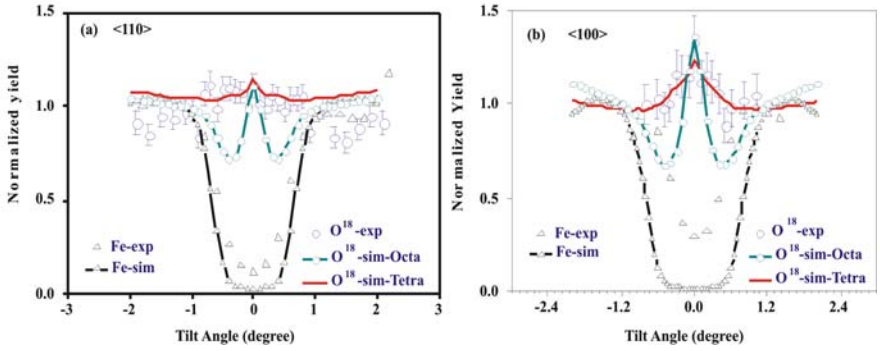

Fig. 1 RBS/channeling spectra from pristine and O^{18} ion implanted Fe(100)

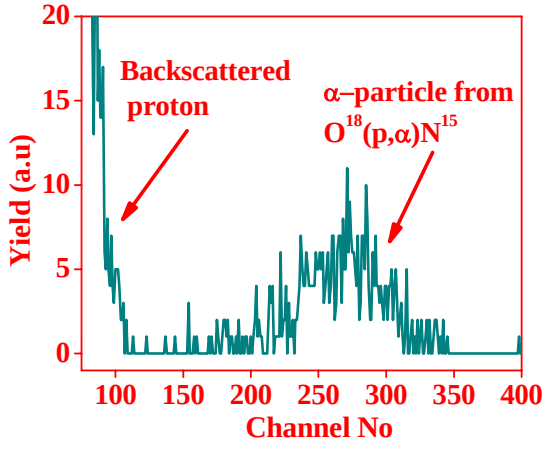

Fig. 2 NRA spectra from O^{18} ion implanted Fe(100)

RBS signal of Fe from the surface and NRA signal of O18 using 840 keV protons are ploted as a function of tilt angle along <100> and <110> directions which are shown in **Fig 3**.

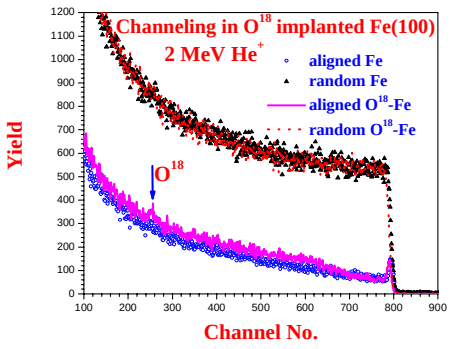

Fig. 3 Experimental and simulated Fe and O^{18} tilt angular scans of Fe1(O^{18}) (a) along <110> axis (b) along <100> axis.

The tilt angular scan is simulated with Oxygen at octahedral interstial position and at tetrahedral interstial position. Good fit for oxygen signal is obtained for tetrahedral interstitial position of oxygen in bcc iron [23]. Oxygen lattice position in octahedral and tetrahedral sites in bcc lattice and the atomic projections along <100> and <110> axes are shown in **Fig. 4**.

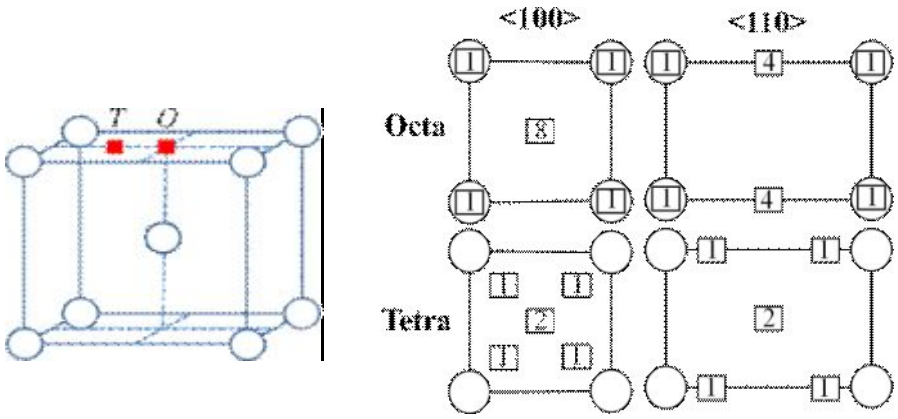

Fig. 4 Octahedral and tetrahedral sites in bcc lattice and the atomic projections along <100> and along <110> axes.

For determining the type of defects in Fe1(O18+Fe@Rp) sample, RBS/channeling spectra are taken at different energies from 1.1 MeV to 3.5 MeV He^{+}/He^{++} ions. along the normal axis (<110>). Random and aligned RBS spectra are simulated using FLUX7 program for all incident energies and are converted to corresponding spectra to yield vs depth, from which variation of c_{min} with depth for pristine (c_V) and ion implanted (c_D) samples are obtained. Dechanneling parameter (DP) is calculated using the expression [1,2] $DP = -\ln\left[\frac{1-c_D}{1-c_V}\right]$ and are the data at various energies are shown in**Fig 5**.

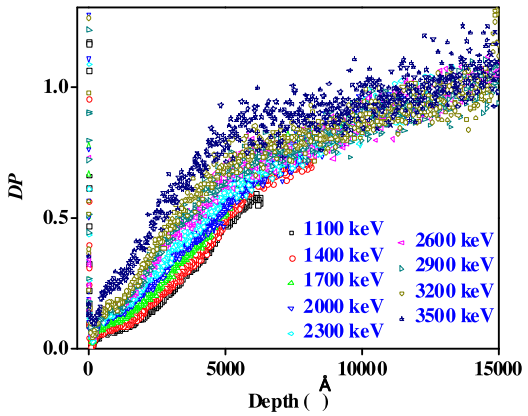

Fig. 5 Experimental and simulated Fe and O^{18} tilt angular scans of Fe1(O18) (a) along <110> axis (b) along <100> axis.

The type of defects at a particular depth can be determined by energy dependence of the dechanneling parameter (DP) [1,2]. The DP of point defects, stacking faults, dislocations show energy dependence of $E^{-0.5}$, E^{0}, $E^{0.5}$ respectively. Theoretically the DP is related to the defect density (n_D) and dechanneling crosssection of defect (s_D) by, $\frac{d}{dz}(DP) = n_D s_D$ **Fig. 5** shows the energy dependence of DP at a depth interval of 200 to 400 nm. The dechanneling parameter per unit length increases linearly up to transition energy of 2.9 MeV (E_s) and becomes constant at higher energies. From transition energy (E_s), mean dislocation loop radius (R) can be determined using Kudo's analysis [24] from the relation $E_s = aR^2$, where a is Thomas-Fermi screening distance (0.142 Å). If one assumes the dislocation loops as ½ <111> loops, the obtained mean radius from Kudo's analysis is 20 nm. If the dislocation loops are <100> loops, the mean radius is 40 nm. The defect density of dislocation loops is calculated from the slope of linear fitting to $d(DP)/dz$ data points (**Fig 6**) and using the relations

$$n_D(z) = \frac{1}{\sigma_D}\frac{d}{dz}(DP) = \frac{slope \times \sqrt{E}}{\sigma_D}, \quad s_D = K\frac{\sqrt{ab}}{y_1}, \quad \text{and}$$

$y_1 = \sqrt{\frac{2Z_1Z_2e^2}{Ed}}$ to be 2.8×10^{10} dislocation loops/cm^2 for the case of <100> loops and 4×10^{10} dislocation loops/cm^2 for the case of ½<111> loops [25].

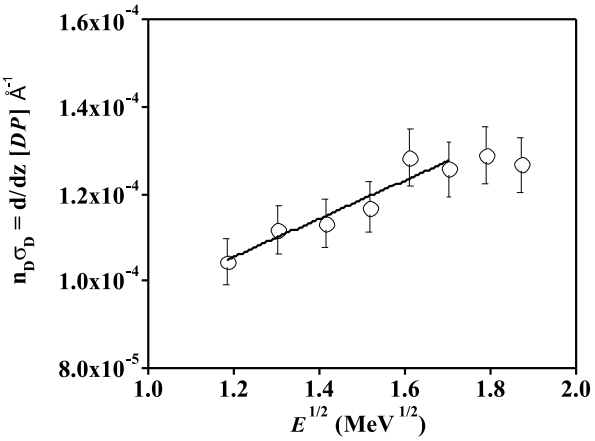

Fig. 6 Energy dependence of dechanneling parameter per unit length measured from 200 nm to 400 nm of Fe1(O^{n+}+Fe@R_p) sample.

O^{18} impurity lattice position is measured in the presence of these dislocation loops in Fe crystal. Figure 7 shows the tilt angular scans of Fe and O^{18} signals along <110> and <100> directions. Experimental scan along <100> is matching with simulated curve corresponding to O^{18} with a displacement of 0.15 Å from tetrahedral towards octahedral interstitial site.

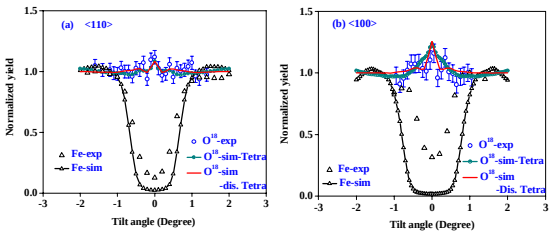

Fig 7: Experimental and simulated Fe and O^{18} tilt angular scans of Fe1(O^{18}+Fe@R_p) sample (a) along <110> axis (b) along <100> axis.

DFT studies are carried out by assuming interaction of oxygen at various locations in bcc Fe with <111> and <100> dislocation loops [25]. One of the considered (I_4-*<100>-O(3)*) defect structures, with a binding energy of 0.24 eV shows that the oxygen is displaced by 0.37 Å from tetrahedral position towards octahedral interstitial site, as shown in **Fig. 8**, which is closer to the experimentally observed 0.15 Å displaced tetrahedral site.This suggests that the oxygen has attractive interactions with interstitial clusters/loops. Hence the observed displaced tetrahedral interstitial site could be due to trapping of oxygen at interstitial dislocation loops [25].

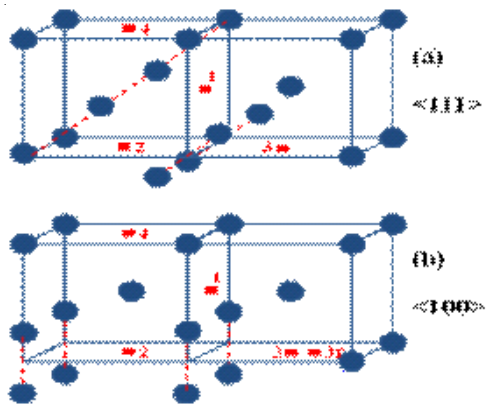

Fig. 8 The schematic of (a) ½ <111> loop structure containing three <111> dumbbells, (b) <100> loop structure containing four <100> dumbbells. The initial lattice location of oxygen is marked as 1, 2, 3, 4. The final oxygen lattice location is marked as 3f for the case of oxygen at position 3.

Interactions of oxygen with vacancy defects in bcc Fe

It is known that higher vacancy concentration will be present at a depth equal to half the projected range ($R_p/2$) of implanted ions due to the forward recoil momentum of displaced atoms and recombination of defects [26]. This $R_p/2$ effect is utilized to introduce additional vacancies overlapping with oxygen concentration depth profile. In this study, bcc Fe(100) crystal is first implanted with 1550 keV Fe^+ ions, which has a range of 540 nm at a fluence of 1×10^{16} ions/cm^2 and sequentially implanted with 300 keV O^{18} ions with ion fluence of $5\acute{}10^{15}$ ions/cm^2 at room temperature and in-situ annealed at 400 °C for 30 mins. The estimated total damage produced by O^{18} and Fe^+ ion implantation is 9.3 dpa at O^{18} depth. Here after, this sample is called as Fe2(O^{18}+1Fe@2Rp). After ion channeling measurements, the Fe(100) crystal is implanted again with 1550 keV Fe^+ ions with the ion fluence of 1×10^{16} ions/cm^2 and annealed at 400 °C with the aim of increasing the vacancy defect concentration further. Now the estimated total damage at O^{18} depth is increased to 15 dpa. Here after, this sample is called as *Fe2(O^{18}+2Fe@2R_p)*. Tilt angular scans from Fe2(O^{18}+1Fe@2Rp) and Fe2(O^{18}+2Fe@2R_p) are shown in **Fig 9**. The shape of the tilt angular scans for oxygen are different from Figures 3 and 7. The experimental data is simulated by placing oxygen at different locations and the best fit shown in Figure 9 (a) and 9(b) is obtained for the site *A* which is displaced 1.2 Å from lattice site along <111> direction, as marked in Figure 9. The best fit in Figure 9(c) and 9(d) is obtained with 70% of O^{18} at site *B* which is displaced 0.85 Å from lattice site to 1st nearest neighbor octahedral interstitial site along <100> or in other words 0.62 Å from octahedral along <100>, as shown in **Fig 10**. This shows that with increase in vacancy concentration, oxygen position is getting displaced to a different location.

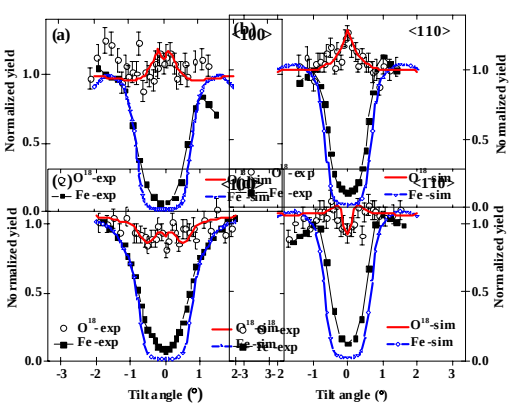

Fig 9: Experimental and simulated Fe and O^{18} tilt angular scans of Fe2(O^{18}+1Fe@2R_p) along (a) <100> (b) <110> axes. Experimental and simulated Fe and O18 tilt angular scans of Fe2(O^{18}+2Fe@2R_p) are given in (c) along <100>, (d) along <110>.

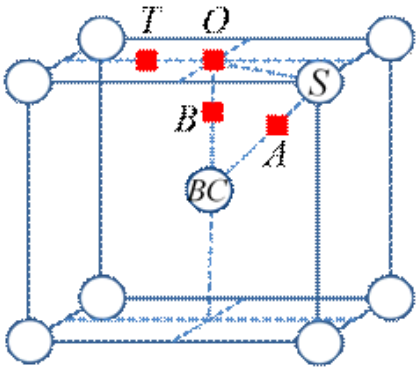

Fig 10: Lattice site locations of substitutional (S), body centre (BC), octahedral (O) interstitial, tetrahedral (T)

interstitial, site A and site B in bcc Fe lattice.

The depth and type of defects are studied in Fe2(O^{18}+2Fe@2R_p) sample by ion channeling and positron annihilation techniques [27]. Positron measurements show the presence of vacancies. Energy dependent dechanneling measurements show $E^{0.5}$ dependence, indicating the presence of vacancy dislocation loops. The defect density of dislocation loops is found to be 6.9 ´10^{10} dislocation loops/ cm^2 for the case of <100> loops and 9.8´10^{10} dislocation loops/ A) in cm^2 for the case of ½ <111> loops.

Oxygen interactions with various vacancy clusters as shown in Figure 11 are studied by using the DFT calculations. Out of the considered configurations in DFT calculations, interaction of oxygen in V4 ½<111>-O(4) configuration (**Fig 11(a))** gives the displacement of 1.16 Å for oxygen from substitutional site along <111> direction comparable to experimental observation of the displacement of 1.2 Å for oxygen from substitutional site along <111> direction (site

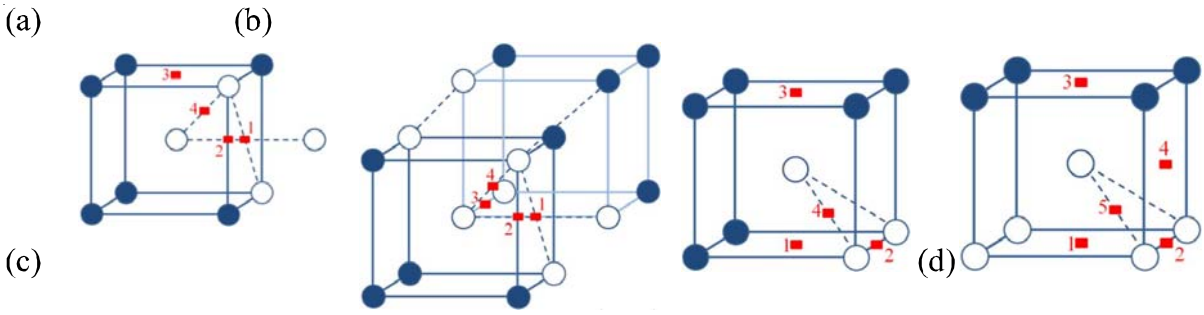

Figure 11: Defect structure of ½ <111> dislocation loop with 4 vacancies (a), 7 vacancies (b), and structure of <100> loops with 3 vacancies (c), 5 vacancies (d). The solid circle represents Fe, open circle represents vacancy and various oxygen positions 1, 2, 3, 4 and 5 are represented as solid rectangle.

Fe2(O^{18}+1Fe@2R_p) sample. The 0.9 Å displacement of oxygen along <111> from substitutional site, observed for the defect configuration V5-<100>-O(5) (Figure 11(d)), is also closer to experimental observation of site A (displacement of 1.2 Å for oxygen from substitutional site along <111> direction) in Fe2(O^{18}+1Fe@2R_p). The experimentally observed site A is found to be stable for interaction of oxygen with both ½ <111> and <100> vacancy loop structures.

Interactions of oxygen and chromium with interstitial and vacancy defects in FeCr alloy

Fe(100) crystal is implanted with 700 keV Cr^+ ions with the ion fluence of 1×10^{16} ions/cm^2. It is followed by implantation of 300 keV O^{18} ions with ion fluence of 1×10^{16} ions/cm^2 and annealed *in-situ* in vacuum at 400 °C for 30 minutes. The energies are chosen so that Cr and O^{18} are at the same implanted depth so that they interact with each other. This sample is called *Fe3(O^{18}+Cr@R_p)*. The lattice location of O^{18} and Cr are measured to study the effect of Cr^+ ion implantation on O^{18} lattice location. at random directions in room temperature. The concentration of Cr at peak position is 0.6% and estimated damage is 5.8 dpa at peak position. The concentration of O^{18} is 0.4% at peak position and the estimated damage level is increased to 15 dpa at O^{18} depth. Energy dependence of dechanneling parameter (*DP*), along <100> axis of *Fe3(O^{18}+Cr@R_p)* around the depth of 200-300 nm is found to be linear with respect to $E^{0.5}$which also confirms the presence of dislocation loops.If one assumes the dislocation loops as ½ <111> loops, the obtained mean radius is greater than 23 nm. If the dislocation loops are <100> loops, the mean dislocation loop radius is 46 nm. The defect density is found to be 4.6 ´ 10^{10} dislocation loops/cm^2 for the case of <100> loops and 6.5 ´ 10^{10} dislocation loops/ cm^2 for the case of ½ <111> loops [28]. As Cr-signal will not be resolvable from Fe-signal in normal RBS, PIXE spectrum is taken with protons to monitor Cr signal along aligned random directions which is shown in Figure 12. Tilt angular scans of O^{18} using NRA and Cr signal using PIXE and Fe signal using RBS from *Fe3(O^{18}+Cr@R_p)* sample are taken along

<100> and <110> directions are shown in **Fig. 12**.

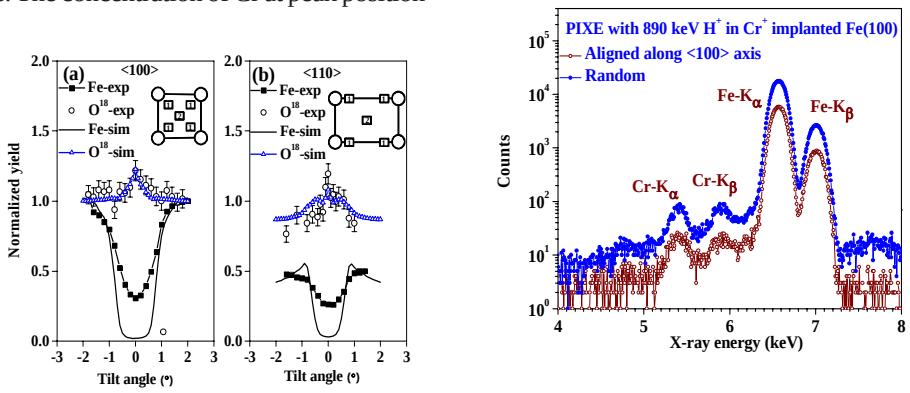

Fig. 12 PIXE spectra of Cr+ ion implanted bcc Fe(100) at random and <100> axial directions.

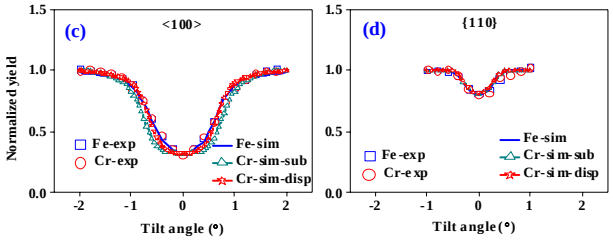

Fig. 13 Tilt angular scans of Fe RBS signal and O^{18} NRA signal measured (a) along <100> axis, (b) along <110> axis, Tilt angular scans Fe and Cr- PIXE signals (c) along <100> axis and (d) along {110} plane of Fe3(O^{18}+Cr@R_p) are shown.

The shape of O^{18} scan is similar to Fe+O^{18} implanted samples, indicating tetrahedral interstitial position, which is also confirmed by FLUX simulation. Shape of Cr-PIXE signal follows the shape of the host Fe-signal, indicating thst Cr is in substitutional position. FLUX simulation shows that Cr atom is displaced by 0.15 Å along <100> from substitutional site, which may be due to interaction with interstitial dislocation loops.

300 keV O^{18} ions are implanted into FeCr crystal with 15% concentration Cr at a fluence of 1×10^{16} ions/cm^2 and annealed *in-situ* in vacuum at 400 °C. This sample is defined as *FeCr(O^{18})*. This sample is introduced with excess vacancies by implanting Fe self ions at twice the depth of projected range of oxygen and this sample is defined as FeCr(O^{18}+Fe@2R_p). Energy dependence of dechanneling probability shows the presence of dislocation loops and positron annihilation spectroscopy shows the presence of excess vacancies [10]. Tilt angular scans taken from these two samples are shown in **Fig. 14**.

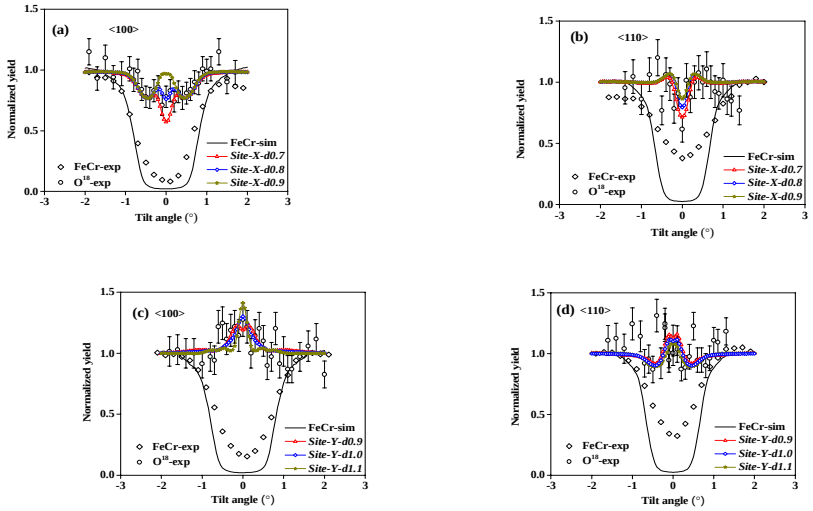

Fig. 14: Experimental and simulated tilt angular scans of Fe+Cr and O^{18} signals along (a) <100>, (b) <110> axes of *FeCr(O^{18})* and along (c) <100>, (d) <110> axes of FeCr(O^{18}+Fe@2Rp)

The best simulated scan for *FeCr(O^{18})* with FLUX7 is obtained by taking O^{18} at *site-X-d0.8* (Figure 15) (displaced 0.8 Å from substitutional to nearest octahedral site in other words displaced 0.63 Å along <100> from octahedral interstitial site) is matching with experimental scan tilt angular scans. The error in measurement is ±0.1 Å. By fitting the experimental scans of FeCr(O^{18}+Fe@2R_p) within error bar the lattice location of O^{18} is found to be at *site-Y-d1.0* (Figure 15) which is displaced 1.0±0.1 Å along <110> from octahedral interstitial site.

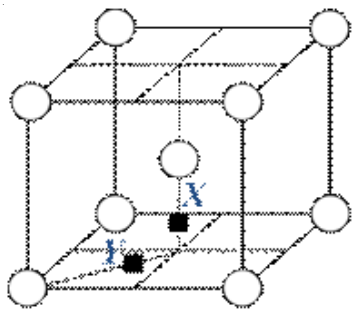

Fig. 15: Lattice location of site X and site Y in bcc system.

O and Cr interactions with vacancy defects are studied by DFT calculations and lattice locations of O^{18} in various configurations are compared with experiment. The resultant defect structure is identified and results are discussed in the context of effect high Cr concentration on O-defect clusters formed in Fe and FeCr alloy. The configuration of O^{18} displaced by 0.37 Å towards octahedral from tetrahedral for the interaction of O with interstitial dislocation loop is closer to the experimental value in *Fe3(O^{18}+Cr@R_p)*. O^{18} is displaced by 0.46 Å along <100> from substitutional site for O interaction with <100> vacancy dislocation loops in *FeCr(O^{18})* [30]. DFT calculations predict that Cr is more attractive to interstitial dislocation loop (binding energy 0.5 eV - 0.7 eV) when compared to vacancy dislocation loops (binding energy ~0.15 eV). The experimental and DFT results show a substantial effect of Cr segregation on O interaction with both interstitial and vacancy dislocation loops in FeCr alloy. The O is trapped in Cr-segregated vacancy dislocation loops although the Cr-segregated interstitial dislocation loops are dominant at O^{18} depth in FeCr alloy. There is substantial evidence of competing interactions between defects and

solutes in Fe and FeCr alloy and the strong influence of Cr concentration on defect evolution under radiation damage.

Conclusion

The interactions of solute atoms with vacancy and interstitial clusters is an important factor affecting the microstructural changes in the structural materials used in high radiation environment. Ion channeling is a suitable technique for studying impurity-defect interactions together with DFT calculations. Lattice site of oxygen is studied with channeling and DFT calculations in the presence of excess vacancies or interstitials in bcc Fe and FeCr alloy. O^{18} is found to be closer to tetrahedral interstitial site in Fe and FeCr upon interaction with interstitial dislocation loops, while it is closer to octahedral interstitial site upon interaction with vacancy dislocation loops. Cr segregation is found to affect the trapping of oxygen at vacancy and interstitial dislocation loops. These studies show strong evidence of competing interactions between solutes and defects in Fe based alloys.

References

[1] W. K. Chu, J. W. Mayer and M. A. Nicolet, Backscattering Spectrometry, (Academic Press New York, 1978).

[2] L. C. Feldman, J. W. Mayer and S. T. Picraux, Materials Analysis by Ion Channeling (Academic Press, New York, 1982).

[3] B. Sundaravel, Amal K. Das, S. K. Ghose, K. Sekar and B. N. Dev, Applied Surface Science, 137, (1999) 11.

[4] K. Takahiro, S. Nagata, and S. Yamaguchi, Appl. Phys. Lett. 69 (1996) 2828.

[5] P. V. Satyam, B. Sundaravel, S. K. Ghose, B. Rout, K. Sekar, D. P. Mahapatra and B. N. Dev, Indian J. Phys. 70A, (1996) 783.

[6] S. Dhamodaran, N. Sathish, A.P. Pathak, D.K. Avasthi, R. Muralidharan, B. Sundaravel, K.G.M. Nair, D.V. Sridhara Rao, K. Muraleedharan and D. Emfietzoglou, Nucl. Instru. and Meth. B254 (2007) 283.

[7] B. Sundaravel, et al., Nucl. Instr. and Meth. B188 (2002) 84.

[8] B. Sundaravel, Christopher David, A. K. Balamurugan, S. Rajagopalan, A. K. Tyagi, B. K. Panigrahi, K. G. M. Nair and B. Viswanathan, Phys. Rev. A 73 (2006) 42902.

[9] B. Daudin, J. L. Rouvière, and M. Arlery, Appl. Phys. Lett. 69 (1996) 2480.

[10] B. Sundaravel, E. Z. Luo, J. B. Xu, I. H. Wilson, W. K. Fong, L. S. Wong and C. Surya, J. of Appl. Phys. 87 (2000) 955.

[11] R. P. Sharma, L. E. Rehn, P. M. Baldo, and J. Z. Liu, Phys. Rev. B38 (1988) 9287.

[12] H.-J. Gossmann and L. C. Feldman, Phys. Rev. B 32 (1985) 6.

[13] J.W.M. Frenken, J.F. vander Veen, Phys. Rev. Lett. 54 (1985) 134.

[14] K.Suresh, B.Sundaravel, B.K.Panigrahi, K.G.M Nair, B.Viswanathan, Rev. of Scientific Instruments, 75 (2004) 4891.

[15] B. Sundaravel, K. Saravanan, B.K. Panigrahi, and K.G.M. Nair, AIP Conf. Proc. 1349 (2011) 499.

[16] Flux, http://www.pjms.nl/flux.html

[17] L.K. Mansur, J. Nucl. Mater. 216 (1994) 97.

[18] A.A.F. Tavassoli, J. Nucl. Mater. 302 (2002) 73.

[19] S. L. Dudarev, Annu. Rev. Mater. Res. 43 (2013) 35.

[20] Y.de. Carlan, J.L. Bechade, P. Dubuisson, J.L. Seran, P. Billot, A. Bougault, T. Cozzika, S. Doriot, D. Hamon, J. Henry, M. Ratti, N. Lochet, D. Nunes, P. Olier, T. Leblond, M. H. Mathon, J. Nucl. Mater. 386–388 (2009) 430.

[21] Z.F. Ziegler, J.P. Biersack, U. Littmark, Stopping and Range of Ions in Solids. Pergamon Press, New York (1985).

[22] Georges. Amsel, and David. Samuel, Anal. Chem. 39 (14) (1967) 1689.

[23] Vairavel Mathayan, Sundaravel Balakrishnan, Binaykumar Panigrahi, Nucl. Instr. and Meth B 383 (2016) 47.

[24] Hiroshi Kudo, Phys. Rev. B, 18 (1978) 5995.

[25] Vairavel Mathayan, Saravanan Kothalamuthu, Jaiganesh Gnanasekaran, Sundaravel Balakrishnan, and Binaykumar Panigrahi, Nucl. Inst. and Meth. B 414 (2018) 141.

[26] C. David, B. Sundaravel, T.R. Ravindran, K.G.M. Nair, B.K. Panigrahi, H.P. Lenka, B. Joseph, D.P. Mahapatra, Appl. Phys. A, 88 (2007) 397.

[27] Vairavel Mathayan, et al., Acta Mate. 143 (2018) 198.

[28] Vairavel Mathayan, et al., J. of Nucl. Mater., 532 (2020) 152032.

Dr. B. Sundaravel*joined IGCAR, Kalpakkam in November 2001after completing his Ph.D from Institute of Physics, Bhubaneswar and postdoctoral work at Chinese University of Hong Kong, HongKong. He visted Tamkang Univerisity, Taipei, Taiwan in 2008 as a postdoctoral fellow and as a Forchungzentum Dresden-Rossendorf, Dresden, Germany as a Guest Scientist in September 2009. His area of interest includes ion beam analysis, ion beam modification of materials and epitaxial growth. He has published several papers in various peer-reviewed internationaljournalsand conferences.*

Ion Beam Analysis: A Literature Survey

V Sharma[1], Sk Wasim Raja[1], S.K. Samanta[1], Y. Sunitha[2], K B Dasari[3], R Acharya[1]

[1]Radiochemistry Division, BARC, Trombay Mumbai-400085
[2]National Centre of Compositional Characterization of Materials, BARC, ECIL Post, Hyderabad- 500062
[3]Korea Atomic Energy Research Institute, Daejeon, South Korea

Abstract : This article gives a literature survey on IBA techniques. It deals with the summary of the research work carried out related to the chemical characterization of diverse matrices including various R&D contributions utilizing low energy proton beam from tandem accelerator.

Applications of IBA techniques: A literature survey

PIGE applications range from geological and archaeological samples, ceramic samples, steel samples, dust and aerosol samples to biomedical samples.

Material Science: Pierce et al **[1]** used energetic beam of deuterons for carbon determination in steel samples. In 1967, Moller and Starfelt applied the same technique for studying fluorine contamination of zircaloy cladding for reactor fuel **[2]**. Pierce et al **[3]** quantified Si in different kind of steels by using 4 MeV proton beam. J. Raisanen and R. Hanninen analyzed hafnium plate by bombarding with 10 mC of 2.4 MeV protons. They determined the following elements/isotopes: O (495 keV from 16O and 871 keV from 17O) (150 mg kg-1), 23Na (440 keV, 0.3 mg kg-1), 27Al (844, 1014 keV, 30 mg kg-1) and 31P (1266 keV, 5 mg kg-1) including heavier elements /isotopes 92Zr (657, 1083 and 1208 keV, 2.8%), Fe (1378 and 1920 keV, 100 mg kg-1) and Cu (992 keV, < 50 mg kg-1) **[4]**. Van Ijzendoorn et al **[5]** used the PIGE technique to quantify thin layers of SiF*x* that were a result of reactive ion etching of Si wafers with CF4 plasma. The quantification is important to understand the etching process. The $^{19}F(p,p'\tilde{a})^{19}F$ reaction was used to determine F on the Si wafer using proton beam of 2.78 MeV. The energy was so chosen to suppress a Si reaction and thus to limit the Compton background.

Application toward environmental: The PIGE technique was utilized for determination of O, C, N, Si and S in coal samples using 9.5 MeV proton beam. Macias et al reported the accuracy of method ~5% of the concentration of each element and a precision of ~ 4% for elements constituting 1% of coal by weight **[6]**. Volfinger et al determined Li, Be, B and F in the individual grains of micas using alpha particle beam of energy 1-3 MeV. The reported 20 mg kg-1 limit of detection is reached for Be, 25 mg kg-1 for Li, 900 mg kg-1 for B and 450 mg kg-1 for F in the granite samples **[7]**. Smectite Swy-1 clay samples were analyzed by Savidou et al using 4 MeV proton beam and they reported the concentrations of Li, B, F, Na, Mg, Al, Si and P in their work **[8]**. Macias Edward et al analyzed aerosol samples for environmental studies using PIGE for the determination of low Z elements **[9]**. Different samples of geological importance and environmental reference materials have been analyzed by Valkovic et al using PIGE methods **[10]**. Roelandts used PIGE technique for analysis of five coal samples of reference materials (Roelandts *et al.*, 1996) [11]. Macias et al reported the accuracy of the PIGE techniques, ~5% of the concentration of each element and precision of ~4% for elements constituting 1% of coal by weight which is quite good if considered to other techniques(Macias and Barker, 1978)[12].Groundwater samples were also analysed by Kaur *et al.* using PIGE method to assess water quality from Punjab region of India(Kaur *et al.*, 2012) [13]. As solid samples are are difficult to dissolve due to its complex matrix and prone to increase the error during analysis as no of steps increased. This gave us opportunity to analyse the source samples like soil and sediment which release fluoride in water and cause fluoride toxicity (Dhorge *et al.*, 2017, Dhorge *et al.*, 2020) [14-15].

Nuclear Physics applications: Pierce et al. also studied the nuclear reactions for different low Z elements starting from Li to Cl using 0.5 MeV proton beam **[16]**. Use of Ge based detectors in 1970 onwards, revolutionized the field of gamma-ray spectrometry. The Ge based detectors (Ge(Li) and HPGe) with better energy resolution than NaI(Tl) helped PIGE to quantify multi-elements simultaneously in a sample. Since then, studies have been carried out with both light (like p and d) and heavy (like t, ?and 3He) projectiles. G. Deconninck at LARN, Belgium and other researchers (Boulton and Ewan) studied (p, p'?), (p, ?) and (p,n?) nuclear reactions for different elements like Li, B, F, Na, Al, P, Cr, Mn, Se, Rh, Pt and Au using proton beam of energy up to 3 MeV and reported the respective detection limits **[17-20]**. By increasing the beam energy, the excitation function also improves for a thick target which leads to increase in cumulative cross-section of a particular nuclear process and hence improved sensitivity of method with better detection limit can be achieved. In view of this it is important to have an idea of gamma-ray yield of most intense gamma-ray emitted during a nuclear process from the isotope of interest. Therefore, the gamma-ray yields were measured using proton beams of energy from 2 to 10 MeV **[21]**. In accelerator-based experiments beam current or fluence normalizations is an important aspect of the experiment. If beam current or fluence variation is experienced during irradiation, than that can be normalized by measuring the current directly from the sample if the same is conducting **[22]**, by measuring the beam current using Faraday cup kept just behind the thin target **[23]** or by using RBS method. In RBS approach, backscattered ions from thin foils of high Z metals like Au, Ag and W are measured using a Si based surface barrier detector kept at a fixed backward angle with respect to the ion beam **[24]**. The beam current/fluence normalized count rates were utilized in relative PIGE methods for determining the concentrations of analytes in various samples. Relative PIGE method is more popular and simple to use over absolute PIGE method for concentration

determination. Thus PIGE is a promising analytical tool for chemical characterization of materials (particularly for low Z elements) and when it combines with PIXE, complete compositional characterization of materials is feasible **[25]**. Beam current is being an important parameter while IBA analysis has been carried out for the quantitative analysis. Various methodology have been adopted for monitoring the beam current for their normalization during the analysis. Like samples are either wrapped with thin aluminum foil or the exit window is coated with Ag/Au and variation in the beam current is monitored from the variation in the count rate of Al or the Ag/Au layer on the exit window [26-27] J.-O. Lill (1999) carried out indirect measurement of beam current using N2 molecules or Ar gas present in the air [28-29].

Geological Samples

In 1960, Sippel and Glover **[22]** for the first time showed that gamma-rays emitted by using energetic protons of the order of MeV could be used for determining low Z elements like Li, Be, C, N, O, F, Na, Mg Al and P in geological samples. They discussed about the general outline of PIGE method and experimental details comprehensively. Roelandts used PIGE method for determination of fluorine in eighty international geochemical reference samples (GRS) including rocks, soils, sediments, minerals and ores.(Roelandts *et al.*, 1985)after that PIGE method has been extensively used for fluorine determination in geological materials [30]. Przybylowicz used PIGE method for analysis of fluorine in serpentinite rocks from Lower Silesia of South-West Poland(Przyby³owicz, Szymczyk and Kajfosz, 1986)[31]. Measured fluorine concentrations varied from 140 to 300 ppm, Roelandts estimated fluorine by the same technique inmetamorphiccharnockitic rocks from Rogaland(South-West Norway). They analysed more than 200 specimens and found an average crustal abundance of fluorine is 625 ppm. PIGE method has been previously applied for geological samples as it containsa high amount of fluorine and is difficult to analyse by other conventional wet chemical and spectroscopic techniques. Advantage of this method over other techniques is, it can use direct solid samples without pre-treatment(Roelandts *et al.*, 1987) [32].

Biological Samples

G.E. Coote, in 1992 reviewed specifically the nuclear reactions for PIGE analysis of F and other low Z elements in different materials including biological (like teeth, bone and fish scales), archaeological and atmospheric samples. In the same review, brief description about the experimental part of PIGE method is discussed including excitation function and interferences **[33]**. Nsouli et al analyzed F concentration in a drug as a part of chemical quality control exercise using proton beam for the first time **[34]**. Boulton and Ewan determined boron in a bean leaf using PIGE, which is an essential nutrient to plants in trace quantities and poisonous in large quantities. The boron concentration reported in this sample was 600 mg kg-1 **[5]**. Yosnda et.al determined the F concentrations in teeth **[35]** samples using proton beam. Saarela et.al showed that PIGE can be used for determination of Na, Mg, Al, P and Mn in plant samples using 3 MeV proton beam in external PIGE set-up. They also showed that the elemental concentrations to detection limit ratios were enhanced greatly by dry ashing of biological samples **[36]**. first time in 1992, Farooqi has applied this method for detecting fluorine in diet samples. This was the time when researchers started utilizing this technique for geological as well as biological samples(Farooqi *et al.*, 1992)[37]. PIGE technique was also used to determine the fluorine concentrations in teeth samples using proton beam(Salah and Arab, 2007) [38]. Carvalho used PIGE method for fluorine determination of healthy and carious teeth to understand the mechanism/impact of fluoride toxicity. The two groups are exposed to different levels of fluoride in drinking water (all other parameters like dietary habits, occupation, and age of donors are same). They concluded that student t-test did not confirm that increased levels of fluoride concentration in drinking water are significantly correlated with an increased concentration of fluorine in the dentine region(Carvalho *et al.*, 2001) [39].Lavielle*et al.* determined fluorinated traces in tissue by using $^{19}F(p,p2\tilde{a})^{19}F$ nuclear reaction which was first attempt to organic fluorine imaging (Lavielle *et al.*, 2011) Along with dentine samples, ivory samples of elephant, mammoth, aquatic (walrus, pot whale, narwhal, hippopotamus) and archaeological ivory were also analysed for fluorine concentration determination, and it found to vary in the range of 55 mg $kg^{-1}$to 2.3 %. This type of study was specifically important as it has the potential to serve as a marker in identifying different types of ivory(Sastri *et al.*, 2013) [40-41].

Application of IBA towards Art and Archaeology

Ancient art and archaeology objects are often valuable and unique piecesthat representing the ancient culture and contain invaluable information. To reveal the hiddeninformation, sophisticated scientific methods are necessary. Moreover, most of these objects are extremely inhomogeneous through individual pieces. The analysis of these objects requires specific characteristics such as large or whole objects and non-destructive to reveal the precise information of objects [42]. The ion beam analysis (IBA) is a unique technique for investigation of chemical and physical properties of art and archaeology objects. The first IBA technique was developed in 1972for characterisation of obsidian [43]. The IBA technique solves many archaeological problems such as authentication of objects, identification of composition [44]. Since implementation of this technique, it has been improved as per the challenges in art and archaeology. The development of external beam setup, making this technique fully non-invasive, has considerable strengthened the popularity of IBA in this filed [45]. Among the IBA techniques, particle induced X-ray emission (PIXE) and particle induced gamma ray emission (PIGE) has up-to now been mostly applied to art and archaeology objects.The major advantages of these techniques are high sensitivity, low detection limit and easy implementation at atmosphericpressure [46].

Several articles, reviews and reports on application of IBA to art and archaeologyhave been published [42-52]. These studies were distinguished into three categories. The first one is archaeometrythat deals with ancient objective creation, usages and provenance studies. The second one is conservation science that deals with preservation of cultural

heritage in archaeology sites and museums. The third one is authentication of objects or art works identifications that deals with distinguish the object belong to modern or ancient periods.

Archaeometry

In these studies, on chemical composition of objects helps to identify mainly (a) ancient source or origin for production of ceramics, (b) trade and (c) cultural activities of ancient people. Provenance study is the evaluation of chronology of ownership or location of an archaeological object/artifact. Archaeologists are interested in provenance studies based on the data obtained using both physical and chemical analysis of artifacts using various analytical methods included IBA. They are useful to know whether they are of same or different origin of archaeological objects under investigation as well as to identify their source or production centers. Even if the artifact is brought by migrating population/society, these studies are important to identify the source and also the source of the raw materials used, which are important for provenance studies [42, 47-48]. Archaeological artifacts such as clay potteries, bricks, glass, stones, paintings, tiles, coins, bones, and documents (paper and ink) are often studied [42]. These artifacts are expected to possess information on the source materials, preparation technology, activities including trade of ancient people. Among these artifacts, ceramics like clay pottery was first synthetic material, frequently available in the archaeological sites and has been of major focus of archaeological studies [47-49]. The chemical composition of clay potteries is strongly related to the sources of clay and recipe for making them. Ceramic samples once produced retain the characteristic properties of the source materials using key elemental composition (Al, Ce, Co, Cr, Cs, Eu, Hf, La, Lu, Sc, Si, Sm, Tb, Th, Yb, and Zn) of clay potteries. The key elements remain unchanged for years. It is an important source for archaeological studies on art and archaeology [48].

Conservation Science: In archaeological science, conservation and restoration of archaeological monuments/ remains are important. Scientific studies present a necessary complement for cultural heritage conservation, preservation and investigation of similar objects. Ancient monuments are regularly affected during weathering. Ancient monuments are affected due to environmental: aerial, terrestrial and under water changes. Therefore, determination of physical and chemical characteristics of this environment (aerosol, soil and water samples) is of interest to establish the causes of the damage exhibited on the object [48]. These environmental samples contain toxic element and high acid content (SO_2, NOx) that may influence the ancient monuments. IBA is suitable for environmental samples (aerosols) analysis for toxic elements (Ca, Fe, S etc.,) and light elemental (Al, Si, Na, Cl, S) quantification [49].

Authentication

Authentication of archaeological artifacts constitutes a great challenge and often requires fully a nondestructive and noninvasive analytical technique is mandatory. To confirm whether the selected object is genuine or fake, several criteria are followed such style, manufacture, date and chemical composition. The results are compared with genuine objects previously studied [45]. Chemical composition of art and archaeological objects are greatly usefulness for Pigment identification on manuscripts, paintings, ceramics and papyri is critical in finding solutions to problems of restoration, conservation, dating and authentication in the art world [52].The external IBA techniques are highly helpful for authentication of art and archaeology objects [46].

Application of IBA towards glass analysis for cultural heritage, Art and Forensic Science

Dran et al (2004) has compiled the 14 year IBA work for the analysis of art and archaeological work at the request from museum curators in addition to research and development work in Louvre. Their aim is to get the elemental mapping in addition to complete elemental information with the combination of PIGE-PIXE-NRA and ERDA methods [53]. They Sokaras et al (2011) was first to utilized their external micro beam facility for the analysis Greek paintings for document and pigment analysis by using 5.5MV VDG Tandem accelerator [54]. Bouquillon et l (2002) have studied the kinetics of the materials by real time analysis using micro PIXE. They have utilized the approach for studying the kinetics of Pb in solution during the aqueous dissolution of lead containing glasses [55]. Zucchiatti and Agullo-Lopez (2012) have done the critical assessment of the consequences of IBA on the cultural heritages objects for archaeometric applications [56]. Kanngieber et al (2012) have extended the capabilities of the PIXE setup from micrometer level to some extent by doing modification of confocal geometry for the application toward cultural heritage (CH) objects [57]. Corregidor et al (2011) have utilized the external proton beam for the characterizing the mercury gilded art objects and Hg and Au/Ag ratio have been utilized for the dating purposes [58]. Vilaigues et al (2011) have utilized the external micro beam PIGE/PIXE for the characterization of 15^{th} and 16^{th} century stained glasses. The study resultd into the important conclusion that corrosion has been taken place due the reaction of moisture and atmospheric CO2 with the oxalic acid secreted by micro-organisms nor because of acid rain [59]. Bugoi et al (2011) have been carried out the ion beam analysis of glass bracelets from 18-19 century and found that the all the fragements had different recipes indicating their manufactures were different and can utilized for the provenance studies of the archeometric objects [60]. Further, in 2013, authors have also characterized the twenty more glass bracelet fragments from Byzyntine site from 10^{th} -13^{th} century AD by utilizing external PIGE/PIXE methods and identified these fragments as "mixed natron plant ash" based soda-lime glasses which are found to contain Co, Mn, Cu and Fe as chromophores [61]. The work has been extended to analyse more glass bracelets (78 in nos) fragments and glass making recipe and raw materials were also identified and pigment used for the decoration of the external surfaces was identified as lead stannate and gold alloy. Results were also confirmed that bracelets wer prepared by recycling the different coloured glasses in local market [62]. Mando et al (2011) have proved the importance of the small particle accelerator in the field of cultural heritages (for material analysis and dating) and also highlighted the capabilities of

accelerator mass spectrometric methods [63]. Mader and Neelmeijer (2004) have utilized the combination of three IBA methods namely PIGE, PIXE and RBS for evaluating the chemical stability of glass objects those are valuable for artistic and cultural heritage purposes using external proton beam at Rossendorf [64]. A number of glass samples of archaeological importance have been studied using PIGE-PIXE combination. The elements reported by PIGE using proton beam were Na, Mg, Al and Si **[65]**. Sharma et al. (2020) have been utilized the PIGE techniques using low energy proton beam (4 MeV) from tandem accelerator and INAA using reactor neutron for characterizing the real automobile windshield glass and laboratory based synthetic soda-lime glass samples. Results were really helpful in distinguishing the automobile windshield glass from the synthetic soda-lime glass samples by concentration ratios like La/Ce and total REEs (La, Ce, Sm, Yb and Eu) obtained from INAA results. These finding could be utilized for the forensic application to discriminate the various glass [66]. Recently, our group also set up the external PIGE facility at FOTIA, BARC using low energy proton beam from6MV VDG tandem accelerator. The present facility was successfully utilized for the analysis of various geological, environmental and department samples important for the nuclear energy program having non standard geometry also. Sharma et al (2021) have utilized this facility for the chemical characterization of sodalime/automobile windshield glasses and borosilicates using external PIGE facility and analytical results have showed that the class of glasses can easily be confirmed. Al was found as the one of the discriminating elements for distinguishing the glass samples among the similar type for the possible forensic applications [67]. Dhara et al. (2021) have been quantified the phosphorous in the alkali based borosilicate glasses along with Si, Na, B using external (in-air) PIGE facility, FOTIA, BARC. Direct sample pellets were irradiated with the proton beam (energy =3.5MeV on the target) from low energy Tandem accelerator and emitted prompt gamma-rays were measured with HPGe detector and quantification of the P in glass was carried out using 2233 keV gamma line for $^{31}P(p,p')^{31}P$ using *in situ* current normalized PIGE method[117].

Ion beam analysis in the characterization of energy materials

Ion beam analysis (IBA) refers to surface analytical techniques that utilize energetic ion beams obtained from a particle accelerator as probes [68-70]. Classified into nuclear reaction analysis (NRA), Rutherford backscattering spectrometry (RBS), particle induced g-ray emission (PIGE) etc., on the nature of the interaction of the ion beams with the atom / nucleus, IBA techniques possess attractive analytical features that are complementary in nature. Simultaneous multielement detection, sensitivity to a wide range of elements and non-destructive depth profiling capability are some of the distinguishing features of IBA techniques [71-76]. Consequently, materials development has benefitted considerably from IBA. One particular area where IBA holds much promise for futuristic development is energy materials. Energy security is very important for the sustenance and further progress of modern civilization. Amongst the various sources of energy deemed as the substitutes of the conventional sources of energy and endowed with a potential to provide succour from the environmental issues, hydrogen energy, solar cells and lithium ion batteries occupy the most important positions [77-81]. It is important to note that materials, bulk or thin films, lie at the core of these technologies. The ability of IBA to analyze thin films and also deeper regions of bulk materials make it suitable for investigating materials useful for a wide range of energy technologies. The usefulness of IBA for these applications is further buttressed by its sensitivity to low z elements as most of the energy technologies utilize materials that have one or more low z elements as major constituents [79-83].

Hydrogen energy exploits the energy released on the combustion of hydrogen in oxygen. Hydrogen storage is an important component of hydrogen energy. Nuclear resonance reaction analysis is eminently suitable for the detection and depth profiling of hydrogen in materials. A review by Lanford gives an excellent account of different nuclear resonance reactions generally employed for depth profiling hydrogen [84]. In one of their numerous applications, $^{1}H(^{19}F, ag)^{16}O$ nuclear reaction, that exhibits a resonance at 6.4 MeV and emits 6.1, 6.9 and 7.1 MeV characteristic g-rays has been utilized to find out conditions optimum for the storage of hydrogen in Mg films and nano-crystalline powders of the element by shedding light on the mechanism and kinetics of sorption. $^{25}Mg(p,p'g)^{25}Mg$ nuclear resonance reaction also proved crucial in ascertaining and standardizing the different aspects of sorption by facilitating the determination and depth profiling of Mg in materials [85]. It is important to note that light elements such as Li, Mg and Al are the most suitable materials for storing hydrogen and these elements can be easily determined and depth profiled by NRRA. Apart from NRRA, RBS has also proved to be very effective in developing materials for hydrogen storage by providing information on interfacial mixing and phase formation during hydrogenation or dehydrogenation process [86-89]. Phase formation between the catalyst and active material has a negative impact of the storage capacity and cyclic stability of the material. These aspects have been comprehensively investigated in a study on Pd/Mg/Si films [90]. **Fig.1** shows the hydrogen depth profiling by NRRA in Pd/Mg/glass films during hydrogenation and dehydrogenation.

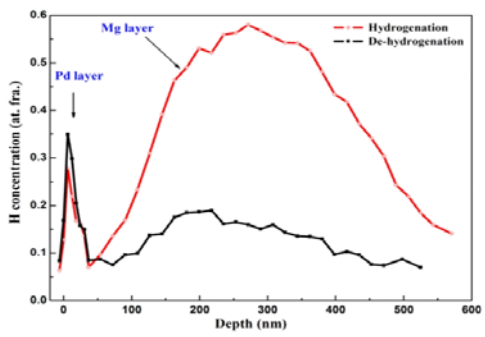

Fig.1 Hydrogen depth profiles showing hydrogenation-dehydrogenation behaviour of Pd(40nm)/Mg(250nm)/glass films. Hydrogenation was carried out in 0.15 MPa hydrogen pressure at 348K for 4 hours while dehydrogenation at 373 K in three hours under dynamic vacuum

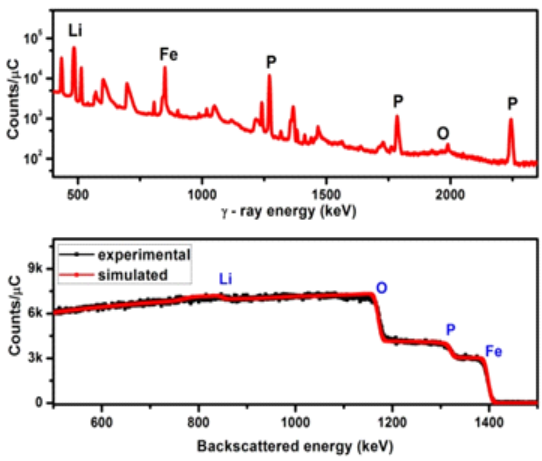

Fig.2 Analysis of LiFePO4: (a) a PIGE spectrum and (b) a proton backscattered spectrum recorded with 4.0 and 1.5 MeV protons respectively

Thin film photovoltaics is yet another non-conventional source of energy that works by directly converting solar or light energy into electrical energy. IBA can play an important role in the fabrication of the devices and also in troubleshooting. Thin film solar cell has a multilayered structure with each layer serving a specific objective. Information on the functionality of the different layers and the respective suitable materials can be obtained from excellent reviews in literature [91-92]. For example, the device can have an absorber layer of I(Cu)-III(In)-VI_2 (S,Se) or $I(Cu)_2$-II(Zn)-IV(Sn)-$VI(S,Se)_4$ compound semiconductor. The films of these materials are prepared by a thin film deposition method. However, the preparation is not trivial and often requires the optimisation of different deposition parameters to obtain films of the desired stoichiometry [93-94]. The techniques of RBS and NRRA have proved to be very useful in identifying conditions for the deposition of stoichiometric films of varying thicknesses. An example in the case is the deposition of $CuInS_2$ films by thermal evaporation with a mixture of chemically synthesised powders of copper sulphide and indium sulphide serving as the evaporant [93-94]. The techniques can also be employed to obtain information on any interfacial reaction during thermal annealing which is often required to bring about phase formation and to introduce crystallinity. Specific mention should be made of the $^{32}S(p,pg)^{32}S$ nuclear resonance reaction which can be employed for depth profiling sulphur across large depths in the devices with good depth resolution [95].

Lithium ion battery (LIB) is one of the most widely used portable energy storage devices. It is a kind of electrochemical cell. In a typical configuration, graphite is used as an anode, $LiCoO_2$ as a cathode and $LiPF_6$ as an electrolyte in a lithium ion battery. $LiMn_2O_4$ and $LiFePO_4$ are other common cathode materials [76, 96-97]**.** The working principle of LIB involves the transport of Li ions from cathode to anode during charging and back again to cathode from anode during discharging. Li forms intercalated compound namely, C_6Li with graphite. Apparently the content of residual Li in anode or corresponding deficiency of Li in cathode is of immense significance. Also, the capacity of LIB has been found to be closely related to solid electrolyte interphase (SEI) existing at the boundary of the anode and electrolyte. Hence it is essential to determine the concentration of Li in both cathode and anode as a function of depth from their respective surfaces.

Ion beam analysis (IBA) techniques such as proton induced g-ray emission (PIGE) employing $^7Li(p,p¢g)^7Li$ (Eg=478 keV) reaction can be utilised for determining bulk Li in the precursors of cathode and electrolyte materials, while proton elastic backscattering spectrometry (p-EBS) is useful for the compositional analysis of Li-bearing films [98-99]. The simultaneous multi-element detection capability of PIGE and backscattering spectrometry enables the determination of other elements (P, Fe,O, C etc) constituting the electrode materials [86]. The PIGE and p-RBS spectra of $LiFePO_4$ (C) in Fig.2, demonstrates the capability of the techniques in the determination of overall composition.

Similarly, a nuclear reaction analysis (NRA) method involving $^7Li(p,a)^4He$ reaction and PIGE method involving $^7Li(p,g)^8Be$, a proton capture reaction that displays a resonance at E_p = 441 keV, are recommended for depth profiling of lithium [100]. These methods with a probing depth of more than 20 microns can serve as suitable alternatives to neutron depth profiling (NDP) which till date is the most widely used method for depth profiling Li in lithium ion batteries [101-102].

In conclusion, IBA endowed with multiple attractive features can be effectively utilised for the compositional analysis of energy materials. It's capability to depth profile elements non-destructively is the unique among the surface analytical techniques, which can be employed to determine the thickness of the films, the depth profile distribution of dopants and can also provide information on interfacial mixing and the formation of new / additional phases, which can affect the functionalities of the energy devices.

Characterization of Reactor Materials by Particle Induced Gamma-ray Emission (PIGE)

Particle Induced Gamma-ray Emission (PIGE) method is a powerful technique for characterization of reactor materials by quantifying low Z elements and this technique has been successfully used since its discovery by Sippel and Glover **[**22**]** in the early 1960's to determine the composition of reactor materials [103]. In 1967, Moller and Starfelt applied this method for studying fluorine contamination of zircaloy cladding for reactor fuel [2]. Pierce et al. [3] quantified Si in different kind of steels by using 4 MeV proton beam. Incorporation of better energy resolution Ge based detectors (Ge(Li) and later HPGe) from 1970 onwards, revolutionized the field of gamma-ray spectrometry and it helped PIGE to quantify multi-elements simultaneously in a sample. Raisanen and Hanninen [4] analyzed hafnium plate by bombarding with 10 mC of 2.4 MeV protons. *In-situ* current normalized PIGE using 4 and 5 MeV proton beam from FOTIA, BARC has been successfully standardized for simultaneous total B mass fraction determination as well as isotopic composition of boron (IC, $^{10}B/^{11}B$ atom ratio) in boron based compounds like B_4C (natural and enriched with respect to ^{10}B), boron composites, transition metal diborides and rare earth metal

hexaborideshaving complex matrices which are difficult to be analyzed by conventional analytical methods due to difficulty in dissolution of the ceramic/refractory materials[104-107].As the mass fraction as well as isotopic composition of B are very crucial parameter for practical purposes like to operate reactor effectively, to assess the thermo-physical/mechanical properties and to ascertain the nature of compound, whether it has natural B or enriched with respect to ^{10}B, it is necessary to determine accurately total boron mass fraction as well as its isotopic composition in the finished product as a part of Chemical Quality Control (CQC) purpose [106-108]. Among the nuclear analytical techniques based on detection of X-ray/gamma rays, PIGE has been proved as a suitable method for simultaneous determination of total B mass fraction and IC and it is competitive to conventional mass spectrometry based techniques[105]. *In-situ*current normalized PIGE has also been applied in barium borosilicate glasses, which is a promising matrix for nuclear waste vitrification, to examine the retention or loss of F during vitrification at high temperature [109-110]. This method was extended for the composition determination of lithium and other low Z elements in the tritium breeder blanket materials in proposed D-T based fusion reactor under ITER programme [111-112] as a part of CQC in sol-gel synthesized lithium titanate [111], lithium aluminate [112], and Li doped neodymium titanate as they are difficult to be analyzed using wet chemical methods. 4 MeV proton beam was used for the determination of Li,Al and Ti and O was determined using 8 MeV proton beam by PIGE method [113].Though elements like Li, F, Na, B and Al have good sensitivity at 4 MeV proton beams, elements like C, N, O, and Z>20 have better sensitivities at higher proton beam energies (above 6 MeV) because of their higher thick target gamma-ray yields. Systematic study on thick target gamma ray yields at higher proton beam energies (7 to 9 MeV) to achieve better sensitivities with lower detection limits of elements beyond Z>20 in the reactor materials could be measured as presently very few literatures are available above 4 MeV proton beam energy [4,21]. PIGE using low energy proton beam (below 4 MeV) is most common and there are few studies using projectiles like d, $^{3,4}He$ etc.. Pierce et al. [3] used energetic deuteron beams for carbon determination in steel samples. Compared to conventional in beam vacuum chamber PIGE, external PIGE (beam extracted in atmospheric air) has been developed in different accelerator facilities across the globe for analysis of non-standard geometry samples [29]. External nuclear reaction analysis (NRA) was used to determine the deuterium depth profile and to measure the D content by $D(^3He,p)^4He$ reaction. In-air $D(^3He,p)^4He$ nuclear reaction analysis (NRA) using external ^3He ion beams is now routinely used to characterize deuterium in both fusion and fission reactor materials [114].Ex-vacuo nuclear reaction analysis based on the $D(^3He,p)^4He$ reaction is routinely used at Sandia National Laboratories for multidimensional characterization of deuterium profiles in fusion reactor materials[115]. It facilitates direct nondestructive analysis of the typically rather large components comprising the tokamak plasma limiter and first wall with a significant improvement in analysis convenience and throughput, which would otherwise have to be sectioned mechanically for analysis using vacuum chambers. In addition to in-beam PIGE, external PIGE (beam in air) keeps promise for analysis of many solid (direct powder) and non-standard geometry samples of importance including archaeological samples/ceramics [116].An external (in air) PIGE method using tantalum as window material was standardized at FOTIA, BARC for rapid compositional characterization of "as-received" glass samples [67]. 135 or 165 keV from tantalum window (^{181}Ta) was used as the external current normalizer. This method was found to be a rapid non-destructive method for both qualitative and quantitative discrimination of glasses which is important for forensic applications.

References:

1. T.B. Pierce, P.F. Peck, W.M. Henry, **1965**, *Analyst*, 90, p.339–345.
2. E. Moller, N. Starfelt, 1967, *Nucl. Instrum. Methods*, 50, p.225-228.
3. T.B. Pierce, P.F. Peck, D.R.A. Cuff, **1965**, *Anal. Chim. Acta*, 39, p.433–436.
4. J. Raisanen, R. Hanninen, **1983**, *Nucl. Instrum. Methods*, 205, p.259–268.
5. E.S. Macias and J.H. Barker, **1978**, *J. Radioanal. Chem.* 45, p.387-394.
6. M. Volfinger, J.L. Robert, **1994**, *J. Radioanal. Nucl. Chem.* 185, p.273–291.
7. Savidou, X. Aslanoglou, T. Paradellis, M. Pilakouta, **1999**, *Nucl. Instrum. Methods B*, 152, p.12-18.
8. S.S. Macias Edward, C. Radcliffe, R. David, W. Lewis Charles, R. Sawicki Carole, **1978**, *Anal. Chem.* 50, p.1120–1124
9. O. Valkovic, M. Jaksic, S. Fazinic, V. Valkovic, G. Moschini, E. Menapace, **1995**, *Nucl. Instrum. Meth. B*, 99, p.372–375.
10. T.B. Pierce, P.F. Peck, D.R.A. Cuff, **1967**, *The Analyst*, 92, p.143-150.
11. Roelandts, I. *et al.* (1996) 'Determination of total fluorine in five coal reference materials by proton-induced gamma-ray emission spectrometry.', *Talanta*, 43, pp. 439–449. doi: 10.1016/0039-9140(95)01765-8.
12. Macias, E. S. and Barker, J. H., *Journal of Radioanalytical Chemistry*. Springer, 45(2) (1987) pp. 387–394.
13. Kaur, R. *et al.* (2012) 'ELEMENTAL ANALYSIS OF GROUND WATER USING PIXE AND PIGE TECHNIQUES', *International Journal of PIXE &*, 22(4), pp. 259–269. doi: 10.1142/S0129083512400359.
14. Dhorge, P. S. *et al.* (2017) *J. Radioanal.Nucl. Chem.* 311(3) (2017)1803–1809
15. Pooja S. Dhorge, Priya S. Girkar, Anoubam D. Sharma, Tirumalesh Keesari, N.S. Rajurkar, R. Acharya, P.K. Pujari, *Geochemistry*. Elsevier, 80(4) (2020), 125551

16. G. Deconninck, **1972**, *J. Radioanal. Chem.*, 12, p.157–169.

17. L.J. van IJzendoorn, M. Haverlag, A. Verbeek, J. Politiek, M.J.A. de Voigt, **1996**, *Nucl. Instrum. Methods B*, 113, p.411–414.

18. I.S. Giles, M. Peisach, **1979**, *J. Radioanal. Chem.*, 50, p.307–360.

19. B. Borderie, J.N. Barrandon, **1978**, *Nucl. Instrum. Methods*, 156, p.483–492.

20. R.B. Boulton, G.T. Ewan, **1977**, *Anal. Chem.*, 49, p.1297–1304.

21. J. Raisanen, T. Witting, J. Keinonen, **1987**, *Nucl. Instrum. Meth. B*, 28, p.199-204.

22. R.F. Sippel, E.D. Glover, **1960**, *Nucl. Instrum.Methods*, 9, p.37–48.

23. J. Raisanen, R. Lapatto, **1990**,*Nucl. Instrum. Meth. B*, 30, p.90-93.

24. R. Tripathi, S. Sodaye, B.S. Tomar, **2004**, *Nucl. Instrum. Meth. A*, 533, p.282–286.

25. Z. Smit, P. Pelicon, H. Hole, M. Kos, **2002**, *Nucl. Instrum. Meth. B*, 189, p.344-349

26. J. Raisanen, Int. J. PIXE, 1992, 02, 339–350.

27. L. Beck, L. Pichon, B. Moignard, T. Guillou and P. Walter, Nucl. Instrum. Methods Phys. Res., Sect. B, 2011, 269, 2999–3005.

28. J.-O. Lill, Nucl. Instrum. Methods Phys. Res., Sect. B, 1999, 150, 114–117.

29. L. Giuntini, Anal. Bioanal. Chem., 2011, 401(3), 785–793.

30. Roelandts, I. *et al. Geostandards Newsletter*, 9(2) (1985) 191–197.

31. Przyby³owicz, W., Szymczyk, S. and Kajfosz, J. *Nuclear Instruments and Methods in Physics Research Section B: Beam Interactions with Materials and Atoms*. Elsevier, 15(1–6) (1986) 573–575.

32. Roelandts, I. *et al. Journal of Radioanalytical and Nuclear Chemistry Articles*, 112(2) (1987)453–460.

33. G.E. Coote, **1992**, *Nucl. Instrum. Methods B*, 66. P.191-204.

34. Nsouli, A. Bejjani, S.D. Negra, A. Gardon, J.P. Thomas, **2010**, *Anal. Chem.* 82, p.7309–7318.

35. K.Yosnda, V.H. Hai, M. Nomachi, Y. Sugaya, H. Yamamato, **2007**, *Nucl. Instrum. Meth. B*, 260, p.207–212.

36. K.E. Saarela, L. Harju, J.O. Lill, J. Rajander, A. Lindroos, S.J. Heselius, **2000**, *Talanta*, 51, p.717–725.

37. Farooqi, A. S. *et al.* (1992) 'Fluorine determination in diet samples using cyclic INAA and PIGE analysis', *Journal of Radioanalytical and Nuclear Chemistry Articles*, 161(1), pp. 71–78. doi: 10.1007/BF02034881.

38. H. Salah and N. Arab *Journal of Nuclear and Radiochemical Sciences*, 8(1) (2007) pp. 31–34.

39. Carvalho, M. L. *et al. Nuclear Instruments and Methods in Physics Research, Section B: Beam Interactions with Materials and Atoms*, 179(4) (2001) 561–567.

40. Lavielle, S. *et al. Pharmaceutics*, 3(1) (2011), 88–106.

41. Sastri, C. S. *et al. Journal of Radioanalytical and Nuclear Chemistry*, 298(1) (2013)311–315.

42. IAEA-1501, 2011.Nuclear techniques for cultural heritage research.IAEA publication, Vienna, Austria.

43. Coote, G. E., N. E. Whitehead, and G. J. McCallum. J. Radioanalytical Chem. 12 (1972)491–496.

44. Guerra, M. F., and T. Calligaro. SpectrochimicaActa Part B 60 (2003)1503–1516.

45. Silva T.F., Rodrigues C.L., Added N., RizzuttoM.A., TabacniksM.H., MangiarottiA., CuradoJ.F., Aguirre, AgueroN.F., Allegro P.R.P., CamposP.H.O.V., RestrepoJ.M., TrindadeG.F., AntonioM.R., AssisR.F., Leite A.R., Nucl. Instr. Meth. Phys. Res., Sect. B, 422 (2018), pp. 68-77.

46. Tite, M.S., Archaeometry 50 (2008) 216–231

47. Dasari K.B., Provenance studies of arcaehological artifacts using nuclear analytical techniques, Ph.D. Thesis, GITAM University, 2013.

48. Dasari K.B., Chhillar S., Acharya R., Ray D.K., Behera A., Lakshmana Das N., Pujari P.K., Nucl. Inst. Meth. B 339(2014) 37-41.

49. Calligaro, T., J.-C. Dran, J. Salomon, and Ph. Walter. Nucl. Instrum. Meth. B 226 (2004)29–37.

50. Calligaro, T., J.-C. Dran, J.-P. Poirot, G. Querré, J. Salomon, and J. C. Zwaan. Nuclear Instruments and Methods B 161–163 (2000)769–774.

51. Clark, R. J. H. Comptes Rendus Chimie 5 (2000) 7–20.

52. Jean-ClaudeDran, JosephSalomon, ThomasCalligaro, PhilippeWalter Nuclear Instruments and Methods in Physics Research Section B: **219-20 (2004) 7-15**

53. Sokaras D, LambrosGeorgiou et al Nuclear Instruments and Methods in Physics Research Section B: 269 (5) (2011) 519-527, https://doi.org/10.1016/j.nimb.2011.01.002

54. A. Bouquillon, J.C.Dran, G.Lagarde, P.Martinetto, F.Mathis, B.Moignard, J.Salomon, Ph.Walter Nuclear Instruments and Methods in Physics Research Section B: 188 (2002), 1-4;156-161. https://doi.org/10.1016/S0168-583X(01)01066-7

55. A. Zucchiatti and F. Agulló-Lopez Nuclear Instruments and Methods in Physics Research Section B: 278 (2012) 106-114. https://doi.org/10.1016/j.nimb.2012.02.016

56. B. Kanngießer, W. Malzer, I. Mantouvalou, D. Sokaras and A. G. Karydas Applied Physics A, 106; (2012) 325-338.

57. V. Corregidor, L.C. Alves, N.P. Barradas, M.A. Reis, M.T. Marques, J.A. Ribeiro, Nuclear Instruments and

Methods in Physics Research Section B: 2011, doi:10.1016/ j.nimb.2011.04.070

58. M. Vilarigues, P. Redol, A. Machado, P.A. Rodrigues, L.C. Alves, R.C. da Silva, "Corrosion of 15th and early 16th century stained glass from the monastery of Batalha studied with external ion beam", Materials Characterization 62, 2011, pp. 211217, doi:10.1016/ j.matchar.2010.12.001

59. R. Bugoi, I Poll, GH Manucu-Adamesteanu, T Calligaro, L Pichon, C Neelmeijer, F Eder (2011) Ion beam analysis studies of ancient glass bracelets discovered in Bucharest. Romaninan reports in physics. 63 (4); 912-922.

60. R. Bugoi, I Poll, GH Manucu-Adamesteanu, T Calligaro, L Pichon, C Neelmeijer, F Eder Journal of archeological science, 40(7) (2013); 2881-2891.

61. R. Bugoi, I Poll, GH Manucu-Adamesteanu, T Calligaro, L Pichon, C Pacheco (2016) PIXE PIGE analyses of Byzantine glass bracelets (10^{th} -13^{th} centuries AD) from Isaccea, Romania. J. Radioanal Nucl Chem, 307 (2016); 1021-1036. DOI 10.1007/s10967-015-4240-0

62. P A Mando, M E Fedi and N Grassi (2011) the present role of small particle accelerator for the study of cultural heritage. The European Physical Journal Plus. 126, 11.

63. M Mader and C Neelmeijer (2004) Proton beam examination of flass-an analytical contribution for preventive conservation, Nuclear Instruments and Methods in Physics Research Section B: Beam Interactions with Materials and Atoms, 226 (1-2); 110-118.

64. **M. Mosbah, N. Metrich, P. Massiot, 1991, *Nucl. Instrum. Meth. B,* 58, p.227–231.**

65. Sharma, V., Acharya, R., Samanta, S.K. et al. J Radioanal Nucl Chem 323, (2020) 1451–1457.

66. Sharma V, Acharya R, Bagla H K, Pujari P K, J Anal At. Spectrom 36 (2021) 630-643.

67. Z. B. Alfassi, M. Peisach, Elemental analysis by particle accelerators, CRC Press, Inc, 2000.

68. J.R. Tesmer, M. Nastasi, Handbook of modern Ion beam materials analysis, Materials Research Society, Pittsburgh, 1995.

69. H. R. Verma, Atomic and Nuclear Analytical Methods (2007) Springer

70. W.K. Chu, J.W. Mayer, M. A. Nicolet, Backscattering Spectrometry, Academic Press, 1978.

71. G. Deconnick, Introduction to Radioanalytical Physics, Elsevier Scientific Publishing Co. Amsterdam, 1978.

72. C. Jeynes J. L. Colaux, Analyst, 141 (2016) 5903-6162.

73. S. Lany, Journal of Physics: Condensed Matter, 27 (2015) 283203.

74. L. L. Chopra, P. Paulson, V. Dautta, Progress in photovoltaic research and application, 12 (2004) 69.

75. D. Deng, Energy Science and Engineering, 3 (2015) 385.

76. S. J. Kalita, Nano Sci. Tech., 168 (2008) 219.

77. A. Sawa, Materials Today, 11 (2008) 28.

78. N.P. Barradas, R. Mateus, M. Fonseza et. al, Nucl. Instr. Meth. Phys. Res. Sect. B 268 (2010) 1829-1832.

79. A. Z. Kiss, E. Koltay, B. Nyako et. al, J. Radioanal. Nucl. Chem. 89 (1985) 123-141.

80. B. Wielunska, M. Mayer, T. Schwarz-Selinger, Nucl. Instr. Meth. Phys. Res. Sect. B, 387 (2016) 103.

81. R. Acharya, P. K. Pujari, J. of Radioanal. and Nucl. Chem. 318 (2018), 1727–1735.

82. M. J. Kenny, J. R. Bird, E. Clayton, Nucl. Instr. Meth. 168 (1980) 115-120.

83. W. A. Landford, Nucl. Instr. Methd. B 66 (1992) 65-82.

84. G.L.N. Reddy, Sanjiv Kumar, S. Vikram Kumar et.al, Nucl. Instr. Method, B 266 (2008) 3281-3289.

85. G.L.N. Reddy , Sanjiv Kumar, Int. J. of Hydrogen Energy 43 (2018) 2840-2849.

86. Sanjiv Kumar, G.L.N. Reddy, V.S. Raju, Journal of Alloys and Compounds 476 (2009) 500-506.

87. G.L.N. Reddy, Sanjiv Kumar, Int. J. of Hydrogen Energy 39 (2014) 4421-4426.

88. Devina Rattan Paul, Rishab Sharma, Anshu Sharma et. al, Materialstoday: Proceedings (2020), https://doi.org/10.1016/j.matpr.2020.09.577.

89. Y. Sunitha, Sanjiv Kumar, G.L.N. Reddy, V.S. Raju, Applied Surface Science 256 (2009) 1553-1559.

90. R. Klenk, J. Klaer, Ch. Koble et. al, Solar energy mater. Solar cells 95 (2011) 1441-1445.

91. M. Weber, R. Scheerz, H.J. Lewerenz et. al, J. Electrochem. Soc. 149 (2002) G77.

92. Pritty Rao, Sanjiv Kumar, N.K. Sahoo, Materials Research Bulletin 48 (2013) 2915-2921.

93. Pritty Rao, Sanjiv Kumar, Naina Raje et.al, Materials Research Bulletin 79 (2016) 105-114.

94. Pritty Rao, Sanjiv Kumar, S. Vikram kumar, V.S. Raju, Nucl. Instr. Method, B 269 (2011) 2557-2562.

95. J. B. Goodenough, Journal of Solid State Electrochemistry, 16 (2012) 2019–2029

96. M. S. Whittingham, Chem. Rev. 104 (2004) 4271–4302

97. H. B-Moudden, G. Blondiaux, P. Vinatier, A. Levasseur, Thin Solid Films 333 (1998) 16-19.

98. Y. Sunitha, Sanjiv Kumar, J. of Radioanal. and Nucl. Chem. 314 (2017), 1803-1812.

99. Y. Sunitha, Sanjiv Kumar, Nucl. Instr. Method, B 400 (2017) 22-30.

100. R. G. Downing, G. P. Lamaze S. T. Hwang, J. Res. Natl. Inst. Stand. Technol. 98 (1993) 109-126.

101. G.P. Lamaze, H.H. Chen-Mayer, D.A. Becker et.al, Journal of Power Sources 119–121 (2003) 680–685.

102. P. Dimitrioua,H.-W. Beckerb, I. Bogdanovic-Radovicc, M. Chiarid, A. Goncharove, A.P. Jesusf, O. Kakueeg, A.Z. Kissh, A. Lagoyannisi, J. Räisänenj, D. Strivayk, A. Zucchiatti Nucl. Instrum. Methods 371 (2016) 33-36.

103. S. Chhillar, R. Acharya, S. Sodaye, P. K. Pujari Anal Chem 8 (2014) 11167-11173.

104. R. Acharya, Wasim Raja Sk, Sumit Chhillar, J. Gupta, J.K. Sonber, T.S.R. Ch. Murthy, K. Sasi Bhushan, Radhika M. Rao, S. Majumdar, P. K. Pujari J Anal At Spectrom. 33 (2018) 784-791.

105. R. Acharya, P.K. Pujari J Radioanal. Nucl. Chem. 318 (2018) 1727-1735.

106. S.W. Raja, R. Acharya, P.K.Pujari J Radioanal. Nucl. Chem. 323 (2020) 1359-1366.

107. S.W. Raja, S.K. Samanta, V. Sharma, R. Acharya, P.K.Pujari J Radioanal. Nucl. Chem. 325 (2020) 933-940.

108. Chhillar S, Acharya R, Sodaye S, Sudarshan K, Santra S, Mishra RK, Kaushik CP, Choudhury RK, Pujari PK, J Radioanal Nucl Chem 294 (2012) 115-119.

109. Chhillar S, Acharya R, Mishra RK, Kaushik CP, Pujari, PK, J Radioanal Nucl Chem. 312 (2017) 567-576.

110. Chhillar S, Acharya R, Vittal Rao TV, Bamankar YR, Mukerjee SK, Pujari PK, Aggarwal SK, J Radioanal Nucl Chem 298 (2013) 1597-1603.

111. Modi KB, Acharya R, Munot Samyak, Parida SC, Pujari, PK, J Radioanal Nucl Chem 314 (2017)1113-1120.

112. Chhillar S, Acharya R, Triptahi R, Sodaye S, Sudarshan K, Rout PC, Mukerjee SK, Pujari PK, J Radioanal Nucl Chem 305 (2015)463-467.

113. Laursen T, Leger M, Xin-Pei MA, Macarthur JD, Palmer GR, Whitton JL, Nucl. Instrum. Methods Phys. Res., Sect. B 165 (1989) 156-163.

114. Walsh DS, Knox JM, Doyle BL, Nucl. Instrum. Methods Phys. Res., Sect. B 45 (1990) 62-65.

115. Samanta SK, Raja SW, Sharma V, Girkar PS, Acharya R, Pujari PK J Radioanal Nucl Chem. 325 (3) (2020) 923-931.

116. Amrita Dhara Prakash, R. K. Mishra, T. P. Valsala, V. Sharma, R. Acharya, A. K. Tyagi, P.K. Pujari, C. P. Kaushik, J Radioanal Nucl Chem, 328 (2) (2021) 519.

Vishal Sharma is a CSIR sponsored Senior Research Fellow (SRF) at K.C. College, Mumbai and working at in collaboration with RCD, BARC since 2018. He is working on a forensic science project and pursuing his PhD work under University of Mumbai utilizing conventional and Nuclear Analytical Techniques like ED-XRF, PIGE and INAA. He has about 10 Journal publications to his credit.

Sk Wasim Raja joined Radiochemistry Division, BARC in 2016 after successfully completing one year training course from 10th batch of IGCAR Training School. He has completed his masters in Chemistry from University of Calcutta and he is now pursuing Ph.D. in Chemistry from Homi Bhabha National Institute. His present research interest is development of Particle Induced Gamma-ray Emission methods for characterization of reactor materials using low and medium energy proton beams from particle accelerators. He has published more than 10 journal papers.

S.K. Samanta is working at Radiochemistry Division, BARC, Mumbai as a Scientific Officer since 2018 after completion of BARC training School at IGCAR in Chemistry Discipline & he was awarded overall topper of the Batch. He is working in the field of Nuclear Analytical Chemistry utilizing PIGE, INAA and PGNAA for chemical characterization of Energy/Nuclear Energy Materials. He has published four peer reviewed international journal papers and about 10 conference presentations to his credit.

Dr. Y. Sunitha graduated from 49 th batch (Chemistry) of B.A.R.C. Training School. She completed her M.Sc. from Osmania University and Ph.D. in Chemistry from HBNI, Mumbai. Dr. Y. Sunitha specializes in surface analysis of materials by ion beam analysis (IBA). The development of materials for renewable energy is her key research area. She is currently working in the Surface and Profile Measurement Section at National Centre of Compositional Characterization of Materials, BARC, Hyderabad.

Dr. Kishore B. Dasari is working as Research Scientist at Korea Atomic Energy Research Institute (KAERI), Daejeon, South Korea (Biodata is given in previous article on PIXE).

Dr. R. Acharya is working in the field of Nuclear Analytical Chemistry at Radiochemistry Division, BARC, Mumbai (Biodata is given in previous article on PIGE).

Folded Tandem Ion Accelerator at BARC

Folded Tandem Ion Accelerator (FOTIA) is an indigenously built DC particle accelerator operational at BARC since year 2000. The first beam of ions was delivered from it at 9:30 p.m. on Friday, April 21, 2000. The beam was of 12C ions at 12.5 MeV beam energy.It was characterized by performing the Rutherford Back Scattering (RBS) on Gold, Tin, and Iron target nuclei. The accelerator has the capability of delivering heavy ion beams upto A» 40 and beam energy upto 66 MeV with a maximum terminal voltage of 6 MV.

SNICS Ion Source at FOTIA

Analysing Magnet of FOTIA

These beams are used for research in basic and applied sciences in the field of nuclear physics, astrophysics, material science, accelerator mass spectrometry, atomic spectroscopy, etc.

In FOTIA the components in the high voltage areas are subjected to electric field gradients of hundreds of kV/cm and therefore this region is enclosed inside a pressure vessel filled with SF6 insulating gas at 90 psig.

High Voltage Column of FOTIA

Inside view of High Voltage terminal

The name folded comes from the fact that the ion beam is folded by 180° using a Folding magnet after one stage of acceleration and then gets reaccelerated in 2nd stage through another accelerating tube placed by the side of the first one (see figure 1).

The source for the charged particles is located at the ground floor, which generates negative ions that are initially accelerated to low energies in a short horizontal section. These low energy negative ions are then bent through 90° using a 70° injector magnet followed by a 20° electrostatic deflector into the vertical accelerating column. In the first stage, the negative ions are accelerated towards the positively charged high voltage terminal situated at the top of the accelerator. The high electric potential at the terminal is achieved by continuous transfer of charge to the terminal by means of the pellet chain system. Inside the terminal, the ions pass through a stripper in the form of a thin carbon foil or a small volume of gas. The fast moving ions lose electrons while passing through the stripper and acquire positive charges. The average positive charge of the ion depends upon the type of the ion and its energy. The resulting positive ions now get bent through 180° by the magnet placed inside the terminal and then enter the second or high energy stage of acceleration where the high positive voltage of the terminal acts repulsively on the positive ions. The final energy of the ions which have acquired a positive charge of n units will be (n+1)eV, where V is the terminal voltage. Typical final energies at the maximum terminal voltage are 12 MeV for protons, 18 MeV for alpha particles, and 66 MeV for Calcium ions of the 10^+ charge state.

Table 1

Specifications:	
Type of accelerator	Electrostatic DC
Terminal Voltage Range	1-6 MV
Voltage Stability	± 2 kV
Pre-acceleration Energy	80 keV
Type of Ions	Protons to Calcium
Beam Intensity	
(a) Proton	200 nA
(b) Heavy Ions	50 nA

APPLICATIONS

1. ***Nuclear Physics :*** To study the reactions at energy near and below the Coulomb barrier relating to:

1.1. Enhancement in fusion cross section

1.2. Broadening of spin distribution

1.3. Threshold anomaly

1.4. Abnormally large value of fission fragment anisotropy,

1.5. · Deep subbarrier large fission cross sections: ^{232}Th, ^{235}U and ^{238}U,

1.6. · Nucleon and cluster transfer reactions at sub-barrier energies (to understand the mechanism and importance of nuclear cluster aspects of reaction)

2. ***Nuclear Astrophysics :*** To measure nuclear cross sections at low energies (E/V_{Coul} ~ 0.1-1.0), for studying the elemental abundance in the universe (nucleosynthesis)

3. ***Atomic Physics Research:*** To investigate atomic collisions and study

3.1. X-ray emission probabilities

3.2. Spectroscopy of multi-ionised ions(Beam Foil Spectroscopy)

3.3. Low energy heavy ion clusters.

4. Applied Research

4.1. Materials characterisation and modifications

4.2. Analytical applications (Surface profiling, Charged particle activation)

4.3. Ion implantation (modification)

4.4. Trace element analysis using PIXE, RBS and NRA (Biological, environmental and Medical)

5. Accelerator Based Mass Spectrometry

5.1. Catering to different applications involving Radioactive species

6. ***Characterisation of Detectors:*** Evaluate the performance parameters such as

6.1. Efficiency and energy resolution of Large area gamma-detectors including BaF2 & NaI

6.2. Calibration and response to high energy gamma- rays.

6.3. Charged particle detectors (NaI, plastic, CsI) using monoenergetic p and ? particles

EXPERIMENTAL BEAMLINE FOTIA:

At present three beam lines are operational at FOTIA whereas forth beam line is being installed.

- Zero degree beam line is used for Rutherford back scattering, material irradiation and radiation biology experiments.
- ***25° degree HS beam line:***

  In 2018, the 25° degree Hill Side (HS) beam-line has exclusively been developed for the research program of measuring the prompt fission neutron and gamma spectra, neutron and gamma multiplicity distributions, fission fragment mass, charge and kinetic energy distributions produced in the fast neutron induced fission of Actinides and Minor Actinides relevant to Gen-IV reactor systems and ADS. Quasi-monoenergetic neutrons produced by the ^{7}Li(p,n) reaction are used for these measurements. Research activities on this beam-

line are in full-swing and recently the measurements of prompt fission neutrons and gamma rays spectra have been carried out in the fast neutron induced fission of ^{232}Th at an average neutron energy of 2.6 MeV (S. De et al, Eur. Phys. J. A 56 (2020) 116). For high precision experimental data on the fast neutron induced fission, the research team is currently developing a forward-focused secondary neutron beam using inverse kinematics at this beam-line.

- ***50^{o} degree HS beam line:***

  The 50^{o} degree HS beam line is currently under development for high-resolution x-ray studies using the crystal spectrometer. The characteristic x-rays originating due to ion-atom collisions will be measured and different inner-shell atomic processes, namely relative intensity of x-rays lines, satellite lines, fluorescence yield etc, will be studied.

  25 degree-hill side beam line is used for fast forward focussed neutron experiments.

- 25 degree-sea side beam line is dedicated for PIXE and PIGE.

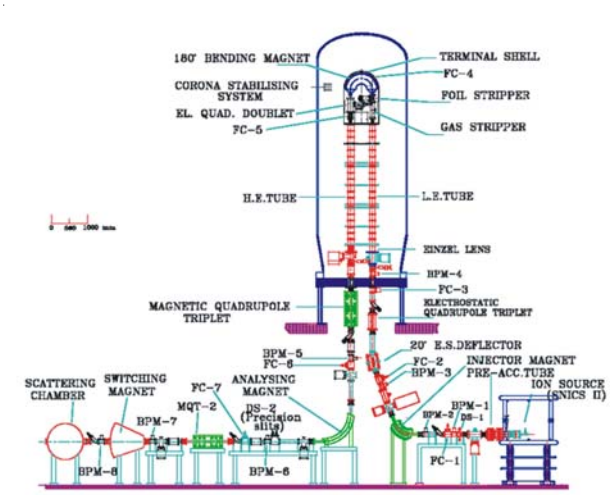

Fig. 2: FOTIA schematic drawing

User Community:

Bhabha Atomic Research Center (Mumbai)
Variable Energy Cyclotron Center (Kolkata)
University of Mumbai (Mumbai)
ISRO Satellite centre, Banglore
Indian Institute of Technology (Bombay)
Panjab University (Chandigarh)
University of Dharwad
Manipal University
UM-DAE Centre for excellence in basic science, Mumbai
MS University, Baroda

Contact Persons

S Krishnagopal Head, IADD, BARCTel: (22)-2559 3787(O), Email: krishnas@barc.gov.in

Arun Agarwal Officer-in-Charge, FOTIAIADD, BARCTel: 022-25593787Email:aarun@barc.gov.inFOTIA Control room :022-25592759

Author information

Arun Agarwal is Officer in charge of Folded Tandem Ion Accelerator, IADD, BARC. He joined BARC as scientific officer in 1994 after completing one year training course from 37th batch of training school of BARC. He was involved in development and installation of Folded Tandem Ion Accelerator at Van-de-Graaff.

3 MV Tandetron Facility at NCCCM, BARC, Hyderabad

A 3 MV Tandetron accelerator at the Surface and Profile Measurement Laboratory of NCCCM, BARC, Hyderabad is operational since 1995. The objective of this facility is to provide materials characterisation by ion beam analysis at surface and near surface regions of the materials. This accelerator has been procured from High Voltage Engineering Europa (HVEE), Netherlands. This facility is the first in Indian accelerators to be accorded the ISO 17025 accreditation for the measurement of thickness of films. A schematic of 3 MV Tandentron facility with different experimental end stations and the ion sources is given in figure 1.

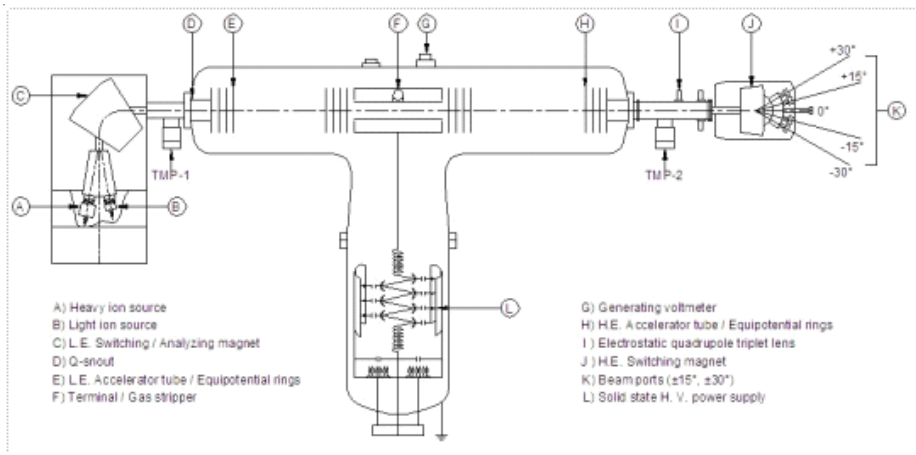

Fig. 1. A schematic view of 3 MV Tandetron

The basic Tandetron system consists of the following main subsystems viz:

- Injector system with ion sources and analysing magnet as shown in figure 2
- Accelerator system with low and high energy accelerating tubes and a central +ve high voltage terminal with a stripper canal
- A switching high energy magnet system for beam deflection.

Two ion source

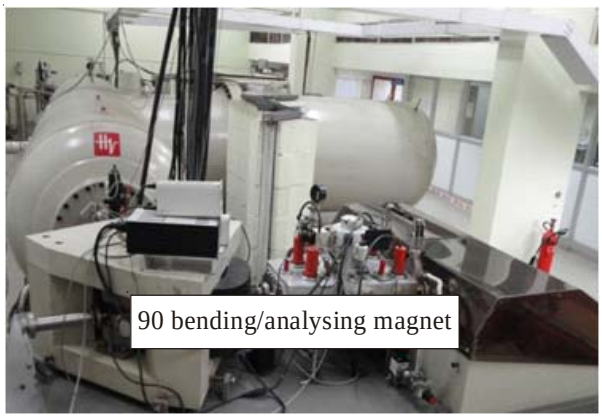
90 bending/analysing magnet

There are two ion sources, a 358 model duoplasmatron ion source for protons and a-particles and a 860C model universal cesium sputter type ion source to generate negative ions e.g. C^-,F^-,Si^- ,Au^-etc. from solids.

Negative ions generated by ion sources and pre-accelerated by a Q-snout are injected into the accelerating tubes and are stripped at the terminal to become positive ions after acquiring an energy equivalent to terminal potential. These +ve ions are further accelerated to ground potential, leading to second stage of acceleration of the ions to generate an energy equal to double or multiples of terminal voltage depending on charge states of the +ve ions. Particles emerging from accelerator are +vely charged and are mono-energetic having an energy equal to $(n + 1)\mathbf{V}$ keV, where n is the charge state of the beam and **V** is the terminal voltage(kilo *Volts*).

The low and high energy accelerator tubes are embedded in high voltage columns on either side of terminal. While the ion path regions are evacuated to high vacuum

using turbo-molecular pumping systems, the high voltage columns and the terminal are enclosed in a steel tank filled with insulating SF_6 gas (7 bar**),** with leak proof assemblies and protection systems. The accelerator has only a few moving parts such as the generating voltmeter, the stripper gas control, and the terminal pumping system.

The energetic charged particles coming out of the accelerator are selected for mass and energy by a switching magnet and guided into any of the 4 beam lines located at $\pm 15^{o}$ and $\pm 30^{o}$ (Figure 3). All along the path of ion trajectory, a clean high vacuum of 2×10^{-6} mbar is maintained. The ions are steered and focussed by several electrical and magnetic beam handling devices to provide a fine collimated spot of ~0.5mm or higher on target.

Fig 3. Experimental end-stations

These energetic charged particles with energies in 300 keV-8 MeV range are used for carrying out ion bam analysis. Ion beam analysis (IBA) referes to multitude of techniques viz Rutherford Backscattering Spectrometry (RBS/EBS), Elastic Recoil Detection Analysis (ERDA), Particle Induced g-Ray Emission Spectroscopy (PIGE), Nuclear Resonance Reaction Analysis (NRRA), Particle Induced X-Ray Emission Spectroscopy (PIXE). Using these IBA techniques we carry out depth profiling of light elements (H, C, N, O, F, Al, Mg, S, etc), compositional analysis, thickness determination, interfacial reaction and diffusion, defect analysis and micro-area elemental distribution in various solid materials.

Contact persons:

1. Dr. Sanjiv Kumar, Head, NCCCM (sanjukumar@barc.gov.in)
2. Dr. G.L.N. Reddy, SO/G (glnreddy@barc.gov.in
3. Dr. J.V. Ramana, SO/G (ramana@barc.gov.in)

Ion Beam Facility of Institute of Physics Bhubaneswar

Institute of Physics Bhubaneswar is engaged in research programs both in theoretical and experimental areas in the fields of high energy, condensed matter, and nuclear physics. The Ion Beam Facility (IBL) and other associated research facilities from the mainstay of the experimental research in the institute. The IBL houses a 3 MV tandem Pelletron accelerator (9SDH-2,National Electrostatic Corporation (NEC), USA make), which is being used for a variety of research in condensed matter, materials science, nuclear physics, and other applied inter-disciplinary areas. The IBL national facility (FIG. 1) also caters to the research need of a large number of external user from Universities and other Research Institutions. The main programs being undertaken using the ion beams available from the Pelletron are Rutherford Backscattering (RBS), Particle Induced X-Ray Emission(PIXE), External-Proton Induced X-Ray Emission(E-PIXE), Proton Induced Gamma-Ray Emission (PIGE), Accelerator Mass Spectrometry (AMS), Nuclear Reaction Analysis (NRA), Elastic Recoil Detection Analysis (ERDA), High-Energy Energy Dispersive X-Ray Fluorescence(HE-EDXRF) Spectroscopy, Ion Implantation, Channeling, Surface Physics, and Microbeam Analysis.

Fig. 1 The 3 MV tandem Pelletron accelerator of IOP Bhubaneswar

[* File contains invalid data | In-line.JPG *]At present, there are 5 beam lines equipped with various gadgets to carry out several experiments. The scientific parameters of each beam lines are as follows:

1. Rutherford Backscattering (RBS) Beam Line (+45˜^{0})

Facility For:	Rutherford
Backscattering (RBS)	Ion channeling
	Elastic Recoil Detection Analysis(ERDA)
Experimental chamber:	20" X12"
	63 CF Ports (3)
	35 CF Ports (1)
Sample Holder :	30 samples at a time
Vacuum :	10^{-6} mbar (turbo)
Detectors :	Surface Barrier Sodium Iodide

Fig.2 RBS Beam line facility Si(Li)

2. Nuclear Physics and External Beam Line (0^0)

Facility For	: Nuclear Physics and External PIXE Experimental chamber: 80 cm (dia)
Special features	: Graphite Collimator Kapton foil (8 micro metre)
Vacuum	: 10-7 mbar (diffusion pump)
Detectors	: Si(Li) (active area 30 mm2),
Resolution	: 165eV at 5.9 keV

Fig.3 Nuclear Beam line facility

Data Acquisition: Multi-parameter data acquisition System AMPS version 1.0

Fig. 4 External Beam line facility

3. Implantation Beam Line(-15^0)

Facility For	: Implaantation / irradiation of solid targets
Common Ions	: Au, Si, Ni, Sb, C, O, N, H

Experimental chamber : 12" X17"

Sample Holder : 20 samples of 1 cm2 (single load)

Vacuum : 10^{-7} mbar (turbo)

Fig. 5 Implantation Beam line facility

4. Pulse laser based growth Beam Line (-30^0)

Facility For: Epitaxial growth of complex perovskites, metal oxide.

Pulse laser deposition system

Special features: RHEED growth analyzer, It has a future provision of in-situ ion irradiation during crystal growth

Sample Holder :

3 axes movement with angular adjustment Heating up to 1000k

Fig.6 : PLD Beam line facility

Vacuum : ~10^{-8} mbar
(Ion plus Ti-sublimation)

5.Ion Micro-Beam Line(-45^0)

Facility For : Micro PIXE, Micro RBS

Beam size : ~100 microns

Resolution : 4ìm

Sample Hnadling : chamber on X-Y stpper table

Detectors : Surface Barrier Si(Li)
Aluminized plastic scintillator

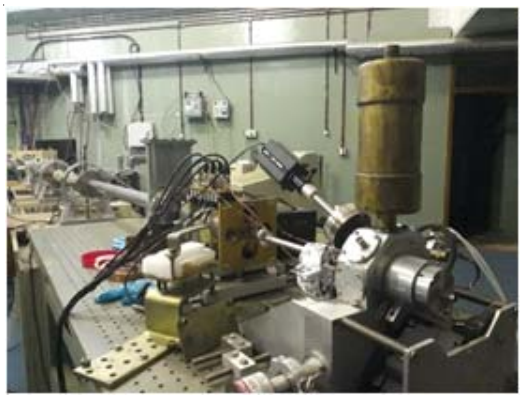

Fig.7 Micro Beam line facility

How to Apply for the Beam Time:-

OPEN: - https://www.iopb.res.in/

CLICK: - Beam Time Request to use Accelerator Facilities (3.0 MV and 40 kV) at IOP

CLICK: - Click here for BTR

Fill up the form and Submit

Write an e-mail to : Prof. Satyaprakash Sahoo, Prof-In-Charge , IBL

For

3.0 MV Pelletron Accelerator (NEC-make) – MCSNICS ion source iopaf@iopb.res.in
Ion Beam Laboratory: Beam lines for RBS/Channeling, ERDA, PIXE, Implantation, and AMS sahoo@iopb.res.in

50 keV Low Energy Ion implanter – SNICS ion source iopaf@iopb.res.in
sahoo@iopb.res.in

BARC-TIFR Pelletron Linac Facility, TIFR, Mumbai

The Pelletron-Linac facility, set up as a collaborative project between BARC and TIFR, located at TIFR campus, Mumbai, has been a major centre for the heavy ion accelerator based research in India. The accelerator facility consists of a 14UD Pelletron with LINAC booster. The Pelletron accelerator was formally inaugurated on 30th December 1988 and marked an important milestone in nuclear physics research in India. The Pelletron accelerator has been operating round-the-clock delivering more than 45 different ion species from proton to Iodine. The accelerator is mainly used for basic research in the fields of nuclear, atomic and condensed matter physics as well as material science. Over the years, a number of developmental activities have been initiated resulting in enhancement of overall performance and uptime of the accelerator and also enabling variety of application oriented programmes including, accelerator based mass spectrometry, production of large-scale track-etch membranes, radioisotopes production, low flux Protons irradiation damage studies and secondary neutron production for cross section measurement etc. The developmental activities involve, replacement of voltage grading based on corona needles by resistances, installation of a new terminal potential stabilizer, introduction of recirculation terminal gas stripper system, development of negative ion beams for a wide range of ion species, a double harmonic drift buncher in the low energy injection path and integration of Linux based control & monitoring system. The facility was augmented with the indigenously developed superconducting LINAC booster to enhance the energy of the beams available from Pelletron accelerator. The phase I of LINAC booster was commissioned on 22nd September 2002 and the facility was dedicated to users on 28th November 2007 after the completion of the phase II. The LINAC booster consists of seven liquid helium cryostat modules, each housing four lead coated (2 micrometer) copper quarter wave resonators (QWR). The cavities are designed to operate at 150 MHz with an optimum acceptance at a velocity corresponding to beta=0.1. Most of the critical components of the LINAC booster have been designed, developed and fabricated indigenously. A variety of state-of-the-art experimental facilities have been developed at this centre to pursue frontier research in nuclear, atomic, condensed matter and multidisciplinary areas. Experimental facilities are attached to dedicated beam lines installed in Cascade beam hall for Pelletron energies and two Linac beam halls I & II for both Pelletron and Linac boosted energies. While a majority of the researchers at this facility are from BARC and TIFR, the experimental community includes scientists and students from other research centers and universities within India and abroad. About 125 Ph.D. theses and 725 publications in international referred journals have resulted from the research activities at the PLF. These include more than 25 publications in Letter journals.

A Schematic layout of 14MV Pelletron accelerator and LINAC

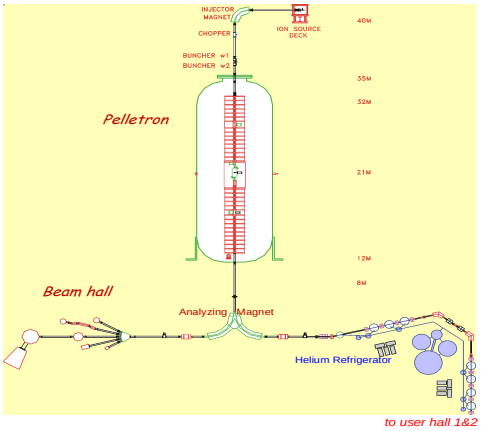

Technical Specifications:

Pelletron Accelerator

Type of Machine	DC Electrostatic Tandem Accelerator
Max Terminal Voltage	14 Million Volt
Type of Beams	Proton to Heavy Ion
Max Mass	^{127}I (accelerated so far)
Voltage Stability	+/- 1 kV
Proton Energy Range	8.0 MeV to 28 MeV
Alpha Particle Energy Range	12.0 MeV to 42 MeV
Acceptance Test values (Proton Current)	3.0 µA at 8.0 MeV5.0 µA at 28.0 MeV
Acceptance Test Values (Alpha Particle Current)	2 µA at 42.0 MeV
Acceptance Test Values (Chlorine Current)	100 pnA at 14.0 MV Terminal
Applications	Nuclear & Atomic Physics, radiochemistry, Material Science, Accelerator Mass Spectrometry and Industrial applications.
Radiation Type	Instantaneous X-rays, Gamma and Neutrons.

LINAC Booster:

Type of machine	Superconducting RF linear Accelerator
Accelerating Structure	Quarter Wave Resonator
Superconductor	Lead
Operating Temperature	4.2 K
Operating Frequency	150 MHz
Input velocity range(b=v/c)	0.07 – 0.14
Optimal input velocity (b_{opt})	0.1
Mass range accelerated	12 - 80
Design output energy	14 MV per charge state

Main Instrumentation for Nuclear Physics Experiments:

i. Clover Detector Array for discrete gamma ray spectroscopy with auxiliary detectors

ii. 150cm dia Scattering Chamber, with two independently rotatable arms permitting detector rotation and target ladder adjustment from remote without beam interruption using Programmable Logic Controller, for charged particle spectroscopy and fission studies

iii. BaF_2/$LaBr_3$ array for high energy gamma ray studies with BGO/NaI(Tl) multiplicity filter

iv. Charged Particle Array based on Si pad (Delta-E) and CsI(E) detectors

v. Neutron Detectors Array of 18 Liquid Scintillation detectors and Annular parallel plate avalanche counter having 12 segmented signal read out with angular coverage from 5 degree to 11 degree, for Time of Flight Technique based compound nucleus residue tagging

vi. MWPC and Si-strip detectors for angular distribution measurements of particles

vii. 7.0T superconducting magnet for hyperfine interaction studies

viii. Electron spectrometer and X ray detector for atomic physics studies with gas and foil targets

ix. Irradiation setups

x. High current proton and neutron irradiation facility

xi. Low background offline counting facility

Main Fields of Nuclear Research:

i. Nuclear reactions (elastic, inelastic, transfer, fusion and fission reactions)

ii. Nuclear structure & spectroscopy

iii. Nuclear data generation relevant to nuclear reactors as well as IAEA coordinated research programs on advanced nuclear reactors and nuclear astrophysics

iv. Elemental analysis using PIGE (Particle Induced Gamma Emission)

Main Fields of Other Research:

i. Atomic & Cluster physics

ii. Condensed Matter Physics &Material Science

iii. Radiochemical studies

iv. Accelerator mass spectrometry, production of track-etch membranes

v. Low flux secondary neutron production for irradiation studies

vi. Low flux proton irradiation damage studies relevant to space bound devices, materials and yield improvement in wheat & rice seeds

vii. Application of thin layer activation technique for wear and corrosion rate measurement.

Future Developments:

1) High voltage upgrade of Pelletron tandem accelerator to sustain operation up to 14 MV by replacing the existing accelerating tubes with new generation high gradient accelerating tubes in phased manner without significantly affecting user utilization.

2) Fabrication and installation of low beta niobium cavities in the first two modules of Superconducting LINAC Booster to enhance the mass range of accelerated ions. Development of digital LLRF control for the superconducting cavities.

User Community:

Bhabha Atomic Research Center (Mumbai)
Tata Institute of Fundamental Research (Mumbai)
Inter University Accelerator Center (New Delhi)
Variable Energy Cyclotron Center (Kolkata)
Saha Institute of Nuclear Physics (Kolkata)
UGC-DAE Consortium for Scientific Research (Kolkata)
University of Mumbai (Mumbai)
University of Calcutta (Kolkata)

Indian Institute of Technology (Roorkee)
Indian Institute of Technology (Bombay)
Indian Institute of Technology (Kharagpur)
Viswabharati University (Santiniketan)
Panjab University (Chandigarh)
Banaras Hindu University (Varanasi)
Delhi University (New Delhi)
Andhra University (Vishkhapatnam)
University of Kashmir (Srinagar)
Guru Ghasidas University (Bilaspur)
Bengal Engineering and Science University (Kolkata)
Center for Excellence in Basic Sciences (Mumbai)
Sambalpur University (Sambalpur)
Institute of Physics (Bhubaneswar)
MS University (Baroda)
Allahabad University (Allahabad)
Guru Nanak Dev University (Amritsar)
Notre Dame University (Notre Dame, USA).

Compiled by: Dr Anit K Gupta, NPD, BARC (anit@tifr.res.in)

Contact Details

TIFR, Homi Bhabha Road, Navy Nagar, Colaba, Mumbai-400005
Tel: +91-22-22782318 (PLF-TIFR Control Room) & +91-22-25593450
E-mail: plfmumbai@gmail.com, maryv@barc.gov.in
Webpage: http://www.tifr.res.in/~pell/pelletron/index.php

C**ontact Person** (User Liaison, PLF):
Dr. Sanjoy Pal
Phone: +91-22-22782454/ +91 -22-22782318
e-mail: plfmumbai@gmail.com, sanjoy.pal@tifr.res.in

Procedure to Apply for Beam time:

The Indian Collaborator or the User Liaison Officer may be contacted for getting relevant information regarding submission of experimental proposal and Beam Time Request (BTR).
e-mail: plfmumbai@gmail.com, sanjoy.pal@tifr.res.in

Accommodation:

Guest rooms at TIFR Guest House

PIGE Facility at VECC, Kolkata

An Upcoming Experimental Set up by RCD BARC

Particle induced gamma-ray emission (PIGE) using low energy proton beam (mainly up to 4 MeV) has been used widely to quantify low Z elements (from Li to S & Ti) in various solid samples. We have standardized and applied PIGE method using low energy proton beams in the range of 2-5 MeV from particle accelerator FOTIA, BARC for characterization of glass, ceramics and alloys by quantifying low Z elements [1, 5]. However, PIGE using medium energy proton beam (above 7 MeV) available at accelerator facilities like BARC-TIFR, Mumbai [6] and VECC, Kolkata [7], can be utilized to determine low as well as medium Z elements with improved sensitivity and detection limit, hence extending the range of elements to be determined by PIGE [8,9]. Medium energy proton beam from these facilities can also be reduced to lower energy, as required, by using beam energy degrader (like Ta) of different thicknesses calculated using SRIM code. Though there will be beam energy straggling, but as we are using relative methods this energy straggling will not be an issue in elemental quantification. The experimental set up shown in Fig. 1 is the recently performed feasibility PIGE experiment using 8 MeV proton beam with 3-5 nA current carried out at Channel 3 beam line of VEC Cyclotron [7]. Target holder containing the samples (as shown in Fig. 2) were placed inside the 3 mm thick SS scattering chamber. A 0.5 cm diameter hole in the lead brick in front of the detector served as a collimator for gamma-rays. The prompt gamma ray spectra were detected using a HPGe detector placed at a distance of 15 cm from the targets, signal processing was done using standard NIM system and data were acquired online in a PC based 4k MCA card during the irradiation of samples.

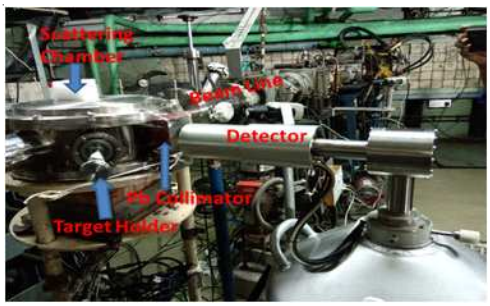

Fig.1: PIGE experimental set up at Channel 3 beam line of VECC cyclotron- feasibility experiment

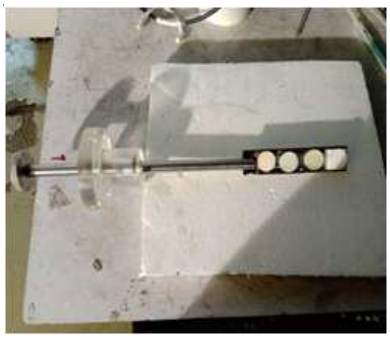

Fig.2: Target pellets (20 mm diameter and 2 mm thick) mounted in the SS sample ladder

Due to attenuation from SS chamber and large target to detector distance (~15 cm) low energy/weakly intense gamma rays were not observed in this feasibility experiment. However, optimization of the experiment is required with respect to energy, current and detection geometry to determine low as well as medium Z elements with improved sensitivity and detection limit at medium energy (about 7 MeV) proton beam. It is needed to have a better sample to detector arrangements with collimated gamma-ray spectrometry and a chamber with Be/ kapton window to obtain desired results of many elements without any attenuation and disturbances. We have well defined plan to measure thick target gamma-ray yields as well as varied applications useful for the Departmental Work program using the medium energy proton beam. Recently a 3MV Tandetron low energy high current accelerator FRENA (Facility for Research in Experimental Nuclear Astrophysics) has been installed at SINP, Kolkata and here also scope is there to do ion beam analysis experiments namely RBS, PIGE/ PIXE using low energy proton beam [10]. Dedicated PIGE facility will be set up in these facilities in near future.

References:

1. S. Chhillar, R. Acharya, S. Sodaye, P. K. Pujari Anal Chem 8 (2014) 11167-11173.
2. R. Acharya, Wasim Raja Sk, Sumit Chhillar, J. Gupta, J.K. Sonber, T.S.R. Ch. Murthy, K. Sasi Bhushan, Radhika M. Rao, S. Majumdar, P. K. Pujari J Anal At Spectrom. 33 (2018) 784-791.
3. R. Acharya, P.K. Pujari J Radioanal. Nucl. Chem. 318 (2018) 1727-1735.
4. S.W. Raja, R. Acharya, P.K.Pujari J Radioanal. Nucl. Chem. 323 (2020) 1359-1366.
5. S.W. Raja, S.K. Samanta, V. Sharma, R. Acharya, P.K.Pujari J Radioanal. Nucl. Chem. 325 (2020) 933-940.
6. Chhillar S, Acharya R, Triptahi R, Sodaye S, Sudarshan K, Rout PC, Mukerjee SK, Pujari PK, J Radioanal Nucl Chem 305 (2015)463-467.
7. Sk Wasim Raja, R. Acharya et al., VECC Annual Progress Report, (2019-20) 67-68.
8. J. Raisanen, T. Witting, J. Keinonnen Nucl. Instrum. Methods Phys. Res., Sect. B 28(1987) 199-204.
9. J. Raisanen, R. Hanninen Nucl. Instrum. Methods Phys. Res., Sect. B 205(1983) 259-268.
10. S. Roy, Proceedings of the DAE Symp. On Nucl. Phys. 63(2018) 53-54.

Compiled by:

Sk WAsim Raja, RCD (BARC) at VECC, Kolkata (email: sw.raja@vecc.gov.in)

For Beam Time Request at Cyclotron of VECC, Kolkata
Directly e-mail your proposals at: beam_time@vecc.gov.in
For details, and updates, please visit: www.vecc.gov.in

Dr. Chandana Bhattacharya. Head, Experimental Nuclear Physics Division, Physics Group, VECC, 1/AF Bidhannagar, Kolkata- 700064 (Email: chandana@vecc.gov.in)

Ion beam Accelerator Facilities at Materials Science Group, IGCAR, Kalpakkam

Dr. Christopher David[1], Dr. P. Gangopadhyay[2], Dr. R. Govindaraj[3]

Materials Physics Division, Materials Science Group,
Indira Gandhi Centre for Atomic Research, Kalpakkam 603102, India
Email: [1]david@igcar.gov.in, [2]pganguly@igcar.gov.in, [3]govind@igcar.gov.in

Abstract : The Particle Irradiation Facility (PIF) forms part of the Materials Science Group, Indira Gandhi Centre for Atomic Research. In the PIF there are three accelerators - the 1.7 MV Tandetron Accelerator, the 400 kV Gaseous Ion Accelerator and the 150 kV Gaseous Ion Accelerator. State of art ion beam experimental facilities like dual ion irradiation facility, in-situ SEM and insitu ionoluminescence, insitu-resistivity, High resolution RBS, General purpose scattering chamber for Ion implantation and Ion beam analysis techniques like RBS, ERDA, PIXE, NRA and ion channeling are built around various beamlines of the accelerators and are in active utilization for materials research.

1.7 MV Tandetron Accelerator

Figure 1 shows the 1.7 MV Tandetron Accelerator. It has replaced an indigenously built 2 MV Pelletron and is in operation since 2002. It has two ion sources, a duoplasmatron ion source for helium ions and a SNICS source for solid targets. Many of the ions of elements in the periodic table can be generated and accelerated. The energy of the ions is given by $V_p+V_T(1-q)$ where V_p is the pre-acceleration voltage, V_T is the terminal voltage of the accelerator which can be varied from 170 kV to 1.7 MV. Accelerated ions can be bent into any of the three beamlines at +30° (1st from left in Figure 1), +10° and -10°. Beam currents on target can be upto a few microAmp.

Figure 1: 1.7 MV tandetron accelerator with its beamlines

-10° beam line is a UHV beamline, coupled to a UHV chamber where ion irradiation can be carried out under UHV at temperatures upto 800°C. This UHV chamber also is coupled with a UHV beam line from a 400 kV accelerator (seen at extreme right of Figure 1), forming the "Dual ion irradiation facility", which is first of its kind in India. The schematic of this set up is shown in Figure 2. Two different ions can be irradiated into a sample simultaneously at high temperature. This facility is mainly used in simulating the radiation damage in clad and wrapper materials for nuclear reactors. Simultaneous irradiation of heavy ions and helium-ions emulate better irradiation conditions of fission and fusion candidate materials for purposes such as material screening and evaluation of basic mechanisms or model calibration.

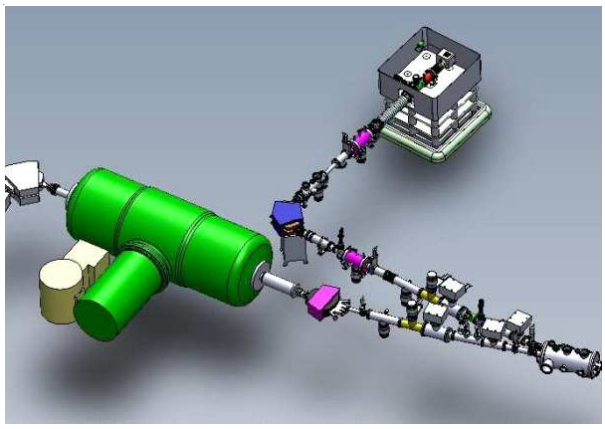

Figure 2: Dual ion irradiation facility

This beamline is extended further and coupled to another chamber for low temperature irradiation experiments upto 20K, by mounting the samples to a closed cycle cryostat.

+10° beamline is coupled with a general purpose chamber. It houses several detectors for ions, x-rays and gamma rays and sample manipulators including a five axis goniometer. Here ion implantation, ion beam analysis techniques like Rutherford backscattering spectrometry (RBS), channeling, elastic recoil detection analysis (ERDA), proton induced x-ray emission (PIXE), nuclear reaction analysis (NRA) can be carried out. Ion beam synthesis of nanoclusters, ion beam modification of materials, characterization of thickness and concentration depth profiles of various materials are being studied. A special holder for insitu-resistivity measurements can be mounted and resistivity can be measured in-situ during irradiation.

+10° beamline is extended after the general purpose chamber and is coupled to a Scanning Electron Microscope (FESEM), which is shown in Figure 3. Ion beam enters into FESEM from right side of Figure 3. The edge welded bellows and various vibration dampeners are incorporated before and after the microscope to reduce the beamline vibration levels. It is possible to perform ion irradiation and monitor the evolving microstructure using the FESEM.

Figure 3: Advanced irradiation cum FESEM imaging Facility.

+30° beamline is coupled to a high resolution RBS facility (Figure 4), which is first of its kind in India. It uses a toroidal electrostatic analyzer (shown in inset), microchannel plates and 1D-position sensitive detector. Energy resolution is 1.6 keV at 400 keV and can give raise to a depth resolution of 2 to 3Å.

Figure 4: High Resoultion RBS Facility.

400 kV Gaseous Ion Accelerator

400 kV Gaseous Ion Accelerator is a single ended accelerator developed indigenously. It is mounted with a RF ion source. Figure 5 shows the high voltage dome (right) and Cockcraft Walton type high voltage stack (left). Gaseous ions of H, He, N, Ar, Kr, etc can be generated. Accelerated ions are bent to a UHV beamline which couples with Dual ion irradiation facility (Figure 2). Beam currents on target can be upto a few tens of microAmp. Electronics and instrumentation to facilitate control and monitoring of the 400kV accelerator and dual ion irradiation facility has been developed in-house.

Figure 5: 400 kV Gaseous Ion Accelerator

150 kV Gaseous Ion Accelerator

150 kV gaseous ion accelerator is a indigenously built accelerator which is in use since 1974. Now it has been refurbished with new vacuum pumps and beamline (Figure 6). It is equipped with a RF ion source inside the high voltage dome (seen in left side of Figure 6). Gaseous ions of elements like H, He, N, Ne, Ar, Kr can be accelerated and bent to a beamline coupled to a implantation chamber. Ion implanation experiments with ion currents upto a few tens of micoAmp. on target can be carried out.

Figure 6: 150kV Gaseous ion accelerator.

The beam line is is extended further to couple with a in-situ ionoluminesence chamber (Figure 7).

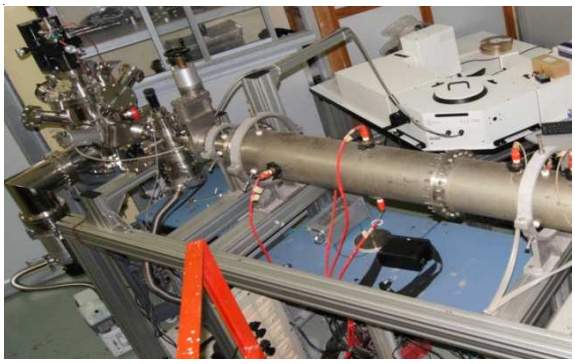

Figure 7: Insitu ionoluminescence Facility.

An optical lens assembly has been fitted in a suitably designed cylindrical stainless steel tube mounted at 30° from the incoming direction of the ion beam. A quartz optical window has been mounted at the chamber port 1 (inset of Figure 7) at the end of the SS pipe tube. The lens assembly is connected to the FLS980 spectrometer (see in top right of Figure 7) via a single-mode optical fiber cable (OFC) bundle. During ion irradiation, ion luminescence, time resolved photoluminescence and optical absorption experiments can be carried out insitu. It is being used for studying defects in insulating materials.

In addition to these facilities at IGCAR, a state of art 200kV ion implanter ions is installed at UGC-DAE-CSR, Kalpakkam Node. It is equipped with a hollow cathode ion source. Ion implantation experiments with gaseous ions and a few metal ions can be carried out. At the Medical Cyclotron Facility in VECC, Kolkatta, a materials science beam line is being built for studying irradiation creep.